Scholars' Mine

Masters Theses   Student Theses and Dissertations

Spring 2012

Field coupled electrostatic discharge sensitivity database

Zhen Li

Recommended Citation

FIELD COUPLED ELECTROSTATIC DISCHARGE SENSITIVITY DATABASE

by

ZHEN LI

A THESIS

Presented to the Faculty of the Graduate School of the

MISSOURI UNIVERSITY OF SCIENCE AND TECHNOLOGY

In Partial Fulfillment of the Requirements for the Degree

MASTER OF SCIENCE IN ELECTRICAL ENGINEERING

2012

Approved by

Dr. David Pommerenke, Advisor
Dr. Jun Fan
Dr. Yaojiang Zhang

ABSTRACT

Electrostatic Discharge (ESD) can disrupt the performance of an electronic system, like an MP3 player either by injected currents or by transient fields. It is possible to predict at least the approximate transient field levels inside a system, but it is difficult to determine the response of ICs subjected to these fields, as no IC specific data is available, and as it is often too involved to measure the sensitivity of every IC possibly used in a product. As deterministic solutions are difficult to achieve, a statistical approach has been selected in this research. The goal of this database for field coupled ESD (Electrostatic Discharge) sensitivity is to give guidance on estimating if soft-error (e.g., resets) problems are likely to occur, for a given ESD scenario. Electric field probes, magnetic field probes, and the $\Sigma\Delta$ probe, which can inject either electrical fields or magnetic fields as desired, are designed as field injection devices for the project. A TEM cell and an IC-stripline, which are designed for high voltage immunity testing, are also developed as injection methods for the purpose of the IC measurements for this database. The measurement setups for the off-shelf electronic products using the probes are shown. Further detailing parameter dependence, a 1.2 mm spacer and a 100 MHz low pass were inserted into the test setups. Observing the crash levels of the ICs under varying conditions allows better insight into the mechanism and the robustness of the database with respect to uncertainties introduced by the field injection methods and their calibrations. In the end, the data from 37 real ICs are analyzed and discussed, and the examples of applications for the database are also discussed.

ACKNOWLEDGMENTS

I would like to express my sincere gratitude to Dr. David Pommerenke, my advisor, for providing me the opportunity to pursue the M. S. degree in EMC Laboratory. I am deeply thankful for his professional guidance, support and warm encouragement on my research work.

I would like to thank Dr. Jun Fan and Dr. Yaojiang Zhang, who served on my committee, for their helpful suggestions and insightful comments on my thesis.

I would also like to express my thanks to Wei Huang, Hongyu Li, Jiang Xiao, Zongyuan Zhou, for their delightful discussions and technical support to my research projects. I also would like to thank Mr. Byong Su Seol, Mr. Jong Sung Lee, and Mr. Jae-Deok Lim with Samsung Electronics Ltd, for their financial support and professional guidance on my thesis project.

I am also grateful to my families and friends, who always believed in me, supported me, and helped me to walk through the difficult times in graduate school.

TABLE OF CONTENTS

LIST OF ILLUSTRATIONS

LIST OF TABLES

1. INTRODUCTION

1.1. ESTIMATION OF IC SOFT ERRORS

Often product designers are faced with the problem of creating a design that will pass ESD testing; however, they have few ways of predicting ESD results. This study links in a methodology that chains multiple approaches for predicting product failure levels. The methodology uses full wave simulation to predict the field strengths and current densities in products using highly simplified models of the product geometry [14], then this database can be used to estimate if a certain field strength is likely to cause ESD problems by direct field coupling into the IC. The study only concentrates on direct coupling into IC, not taking coupling into traces into account. Such situations can occur for example in cell phones, as ESDs may occur very close to the ICs, leading to high field strengths, and due to high layer count and high density no surface traces can be found.

The ESD sensitivity database focuses on soft-error problem caused by ESD. When a system is exposed to an ESD event, a strong electromagnetic field can be coupled through aperture, cables, or slots into the enclosure, and the induced voltages and currents can lead to bit errors, wrong resets or system crash. If a product fails ESD testing by showing soft errors, it is hard to locate the root cause of the ESD soft problem. These are temporary events, leaving no obvious clues about their root cause and location, and the systems can recover themselves by rebooting. In general, ICs are not characterized with respect to their soft-error ESD sensitivity by manufacturers, thus, the user of ICs has little information that can guide the design. Simplified full wave simulations can predict the field strength inside a product or the surface current densities on a PCB if an ESD current is injected to it [1]. However, the simulation will not tell if the product will be disturbed by the ESD injection, as the simulation does not include IC soft-error models. By creating an ESD sensitivity database for "typical" ICs, the distribution of IC disturbance levels can be provided, and then combined with full wave or block level simulations, so as to estimate the risk of soft-errors. With the database statistics, users can estimate the likelihood of soft-errors by calculating the field strength and current density.

1.2. STATE OF THE ART

In system level immunity testing the coupling can either be

- Directly to the IC, if a cable is connected directly to the IC
- Via other cables or via field to the PCB
- Energy can couple to cables that connect PCBs like flex cables
- The energy can couple directly to the PCB, causing current densities on planes that couple to traces and then to the IC
- Or the energy can directly couple, via the field to the IC.

The injection methods of ESD interferences to ICs mainly fall into two groups: one is coupling into component via the IC pins, for example, direct power injection (DPI) [9] which enables the measurement of the susceptibility of an IC by injecting continuous sine wave power with various amplitudes on a wide frequency range [16], bulk current injection method (BCI) [7], Workbench Faraday Cage method [23], etc. These are well defined in the IEC 62132 standard from part 3 to part 5. Also researchers use injection probes excited by very fast TLPs to inject disturbances to IC pins through a capacitor [16].

Many portable devices have hardly any surface traces, as the PCBs are often packed with components on both sides. In these cases, field coupling can be dominant during an ESD event. For the direct coupling to cause IC soft errors it requires relatively large field strengths. Those are usually not reached in tests that use a modulated sine wave signal, such as radiated immunity (IEC 61000-4-3) or conducted immunity (IEC 61000-4-6), only sometimes in high power microwave testing. However, impulse testing, like EFT (IEC 61000-4-4) and especially ESD testing (IEC 61000-4-2) can reach field strengths high enough to cause directly field coupled IC soft errors. A typical scenario is an ESD to a cell phone, which causes momentarily a very large voltage between a battery and a PCB, thus leading to a soft error. Another scenario could be a secondary ESD inside a portable device, an ESD to a floating metallic cover causes a spark between the cover and the metallic frame of the portable device. Due to the small distances inside the cell phone and the high breakdown field strengths of those gaps,

very large field strengths are possible, reaching the range at which direct field coupling becomes a relevant threat.

Regarding disturbance sources for IC immunity testing, researchers use signal generator or VNA with an amplifier [18][21], Transmission line pulsers [10][15][22], ESD generators [14]. Many authors have treated the subject of systems being subjected to strong EM fields, for example researching the reaction to intentional high power microwave [24]. In this case the complete system, often with externally attached cables is subjected to free space electromagnetic waves. Further detailing the coupling investigations that illuminate ICs with attached cables to strong electromagnetic fields have been reported [25] . In this case the main coupling is to cables, not to the IC directly, simply because the loop areas spanned by the cables and the surface areas of the cables are much larger than the loops and surfaces inside the IC. These studies show upset levels of 25 kV/m to 120 kV/m, for logic devices [25].

The objective of the test method is to subject the ICs to a well defined electric or magnetic field. The test methods can be distinguished by either injecting mainly E-field/ H-field, or using a TEM field. And by either requiring a special test board, or allowing to test off the shelf equipment. For the direct injection of fields in ICs two general principles exist: TEM methods and near field scanning.

1.2.1. TEM Methods. The methods are usually realized by using Crawford like TEM cells [4] or other TEM wave guiding structures [13], IC stripline [13]. This thesis further describes to additional TEM structures that are free of higher order resonances up to 2 GHz, or higher. Using TEM cell structures is usually limited by the need to have special test boards, such as they are described in IEC 62132-2 [8]. To test an IC for its immunity against electromagnetic radiation, the standardized, test boards are used to for these methods to guarantee that only the IC is exposed to the electromagnetic field. This method cannot provide information about local sensitivities in the IC, nor can it distinguish between E and H field coupling (although this could be implemented using dual injection techniques). The advantage of the TEM cell method is the ease of use, as only a simple cell is needed. For the purpose of TEM cell injection, the distance between the IC and the septum is usually reduced relative to the classical Crawford cell, such as Fischer's TEM cell. This is done to increase the field strength. At a distance of 4.5 cm

very high voltages would be needed to achieve disturbance causing field strengths. The voltages would be difficult to create and lead to sparking inside the connectors.

1.2.2. Near Field Scanning Methods. Field scanning based methods [10], [11] are also important methods in immunity test, the methods that move a probe above a product to determine the crash level. Field coupled probes like SkateProbe emulator which is designed using two main radiating striplines [18] [19]. Near field scanning methods were not selected for the database for a variety of reasons:

- Scanning many products might have taken too long as an automatic feedback for error detection and reset would have been needed for each product,
- Few people own such test system, a test method that can be reproduced relatively easily to extend the database is desired.
- The additional information obtained, which is the location of the sensitive region of an IC, was not of interest for the purpose of the database.
- The desired field needs to be as homogeneous as possible to illuminate the IC, for example, to allow comparison to TEM data. Also, if a scanning system uses a large probe, thus has only one test point above the IC, then there would be no need to use an automatic scanning system.

Many field probes have been developed for ESD near field scanning [19], [10], but most of them have a relatively small size compared to the ICs, and the field is not homogeneous above the entire IC. For the purpose of this database, the coupling to the traces needs to be minimized, the main reasons are: firstly, the response of the system, if the fields couple to ICs and traces, is strongly dependent on the routing of the traces, ground planes, power planes etc., thus, if we want to obtain IC information we should avoid coupling to traces. Secondly, traces have a much larger surface area than the lead frame or the die; thus, E-field coupling to traces could be much stronger than to the IC, if the probes illuminate the trances and the IC. Thus, subjecting the complete board to strong fields would defy the purpose of the IC field sensitivity database.

In many products, like the cell phones, there are hardly any traces on PCBs. Thus, crashes can be caused by field coupling. Further, the field coupling is enhanced by stacking PCBs and other metallic structures very closely, such that transient voltages

between them will lead to field strengths sufficiently large to cause direct IC coupled crashes. Next, small mobile products often have no shielding, and ESD can discharge to points very close to ICs. In this case again field strengths can reach levels sufficient for direct IC coupling. For this reason, probing to about the size of the IC is needed. Even so it can't perfectly illuminate the IC only, but also some surrounding devices, thus the data base has some uncertainty. However, without having test boards, this is the most suitable approach for achieving this goal. The test boards are defined in and are typically 10x10 cm large, having the IC of interest on one side and all other components on the opposite side of the board. If such a test board and the required operating software are present, then there are plenty of existing, well defined injection methods, such as GTEM, standard TEM cell up to 1 GHz, µTEM, LIHA, and IC-stripline. Previous studies [24][25] have applied up to 50 kV/m field amplitude to the electronic device, and the upset thresholds of the electronics are several kV/m when testing with an open waveguide. The authors also found the breakdown upset thresholds of three PC systems are between 10 kV/m and 20 kV/m when operated in six different program states [25].

1.3. ESD TEST METHOD FOR THE DATABASE

In order to characterize "typical" ICs for the database, many ICs within commercial products have to be tested; standard test boards may not be applicable for most of the cases.

This thesis describes three different types of probes which are customized for E-field and H-field injection. Objective for the E-field and H-field probe design was to create homogenous fields with no resonances over an area which is large enough to cover the IC tested. The entire top surface of the IC under test will see the same field during one injection process. An additional requirement is to hold sufficient voltages of up to 8 kV charge voltage of a transmission line pulser for creating very high field strengths at the location of the IC.

2. FIELD INJECTION HARDWARE

2.1. ELECTRIAL PROBE

The general requirements of the E-field probe in this study are the following:

- Inject an E-field in a frequency range of MHz to a few GHz
- Cover the complete IC
- Have a weak magnetic field
- Provide a clean injection pulse (no resonances, no ringing)
- Couple by 20dB/dec (pure capacitive coupling)
- Have a reverse termination resistance (needed for the transmission line pulser)

Probes previously design at the Missouri S&T EMC lab either have very small area for E-field coupling; or the larger ones showed ringing if the E-field coupling is measured by coupling to a trace. The ringing was caused by reflections of the common mode wave that is injected onto the outside of the driving coax cables. This current allows charge to flow via the TLP, its power connection to the ground of the trace where the E-field is injected to. This current and the displacement current to the DUT form the low and high frequency return path respectively. The disadvantages of the E-field injection devices designed at the EMC lab prior to this research are:

- The size of the injection probe does not match the size of ICs; this is needed as the field is injected mainly to the IC, and expose the complete IC to a more or less homogeneous field

- The ringing of the large probes needed to be reduced.
- A terminative resistor was needed. This provides a termination for the wave coming from the TLP, otherwise, the charge cannot return which inhibits the correct function of the transmission line pulser. This resistor does not have to be 50-Ohm higher values are better, as a 50 Ohm resistor would cut the voltage in half.

2.1.1. Design of the E-field Probe. The lower frequencies return as common mode current on the coax cable of the probe, and then through the grounding of the test equipments and the device under test. A 700 Ω carbon composition resistor is used as

the resistive termination for the probe, which provides a charge return path, and it is also needed for the transmission line pulser, which is used to create fast rise-time pulses. The E-field probe for the database is designed with lossy material around the outer conductor of the coaxial cable to dissipate energy. The photo and the structure are shown in Figure 2.1 and Figure 2.2. The lossy material offers a termination for the high frequency spectral content of the common mode wave. The common mode wave travels on the outside of the coax cable and is initiated by the pulse. The lossy material also couples to the PCB and the surroundings. In this way, it offers a displacement current return path for the high frequency components of the signal .
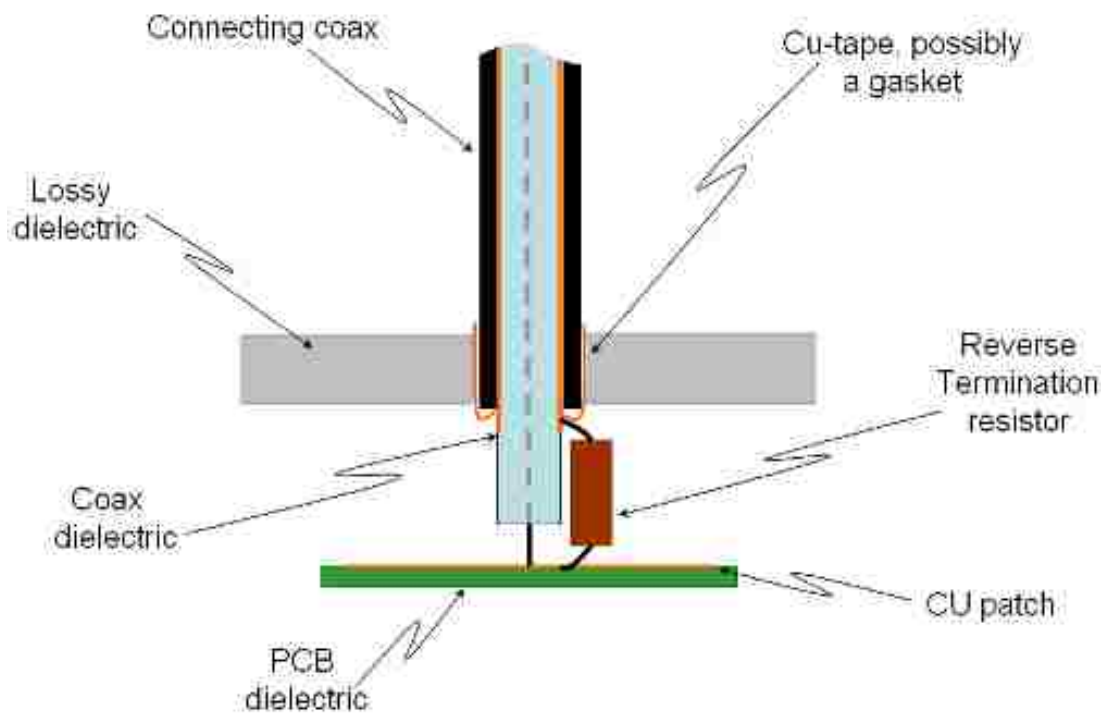
Figure 2.1. Structure of the E-field Probe

Figure 2.2. Photo of the E-field Probe

2.1.2. Measurement Setup. A copper patch on a PCB board is used as the receiver of the electric field. The size of the copper patch is the same as the parallel patch area of the capacitive E-field probe, which is normally the size of the IC under test. Further equipment used is a transmission line pulser which is the injection source, and a digital phosphor oscilloscope. The characterization setup is shown in Figure 2.3. The charge voltage from the TLP is 500 V. The probe model number is ICESD1.
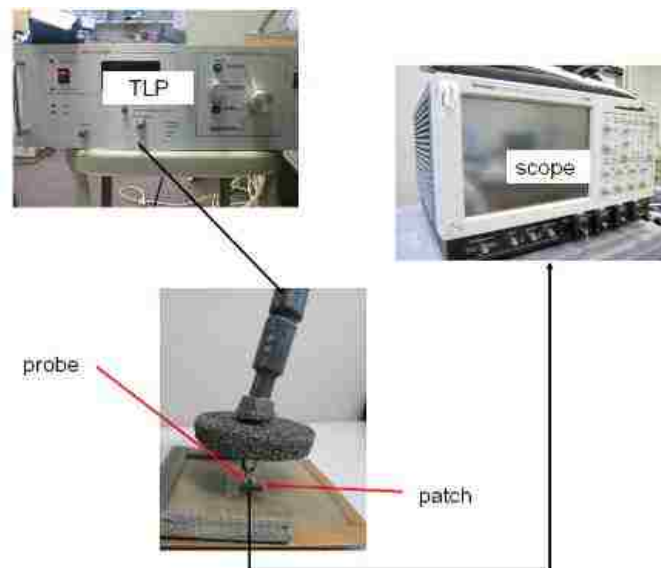
Figure 2.3. Test Setup

2.1.3. Results.   Figure 2.4 shows the pulse induced from probe to the patch. A 40-dB attenuator is used to protect the oscilloscope. One can see a clean pulse without ringing.
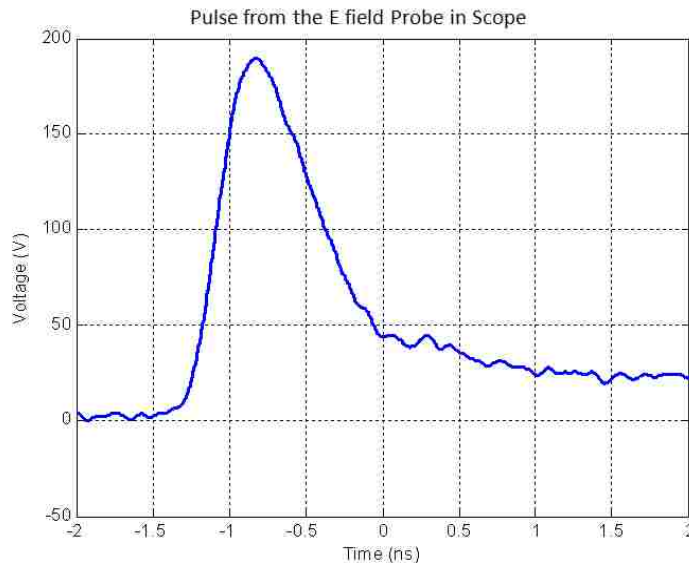
Figure 2.4. Induced Voltage with 500 V Charge Voltage for ICESD1 Probe

2.1.4. Spice Simulation of the E-field Injection. A SPICE model of the E-field injection probe was developed in PSPICE to demonstrate an equivalent circuit of the injection process. First, common mode return impedance is measured to estimate effect of the lossy material, and then the whole process is simulated in SPICE.

2.1.5. Common   Mode   Impedance   Measurement. The   common   mode impedance is the impedance seen between a large metal plane and the outside structure of the probe. The measurement has been performed for two reasons: (1) to create a SPICE model a step by step approach is usually warranted. The common mode impedance can be measured and simulated independent of the coupling patch, (2) the common mode impedance provides the return path for the charge, this way influencing the pulse shape.

A block diagram of the measurement setup is shown in Figure 2.5. The resistor and the copper patch of the probe are removed from the probe in this measurement, as only the common mode impedance is of interest. The cable to the network analyzer is extended to connect the lossy material.
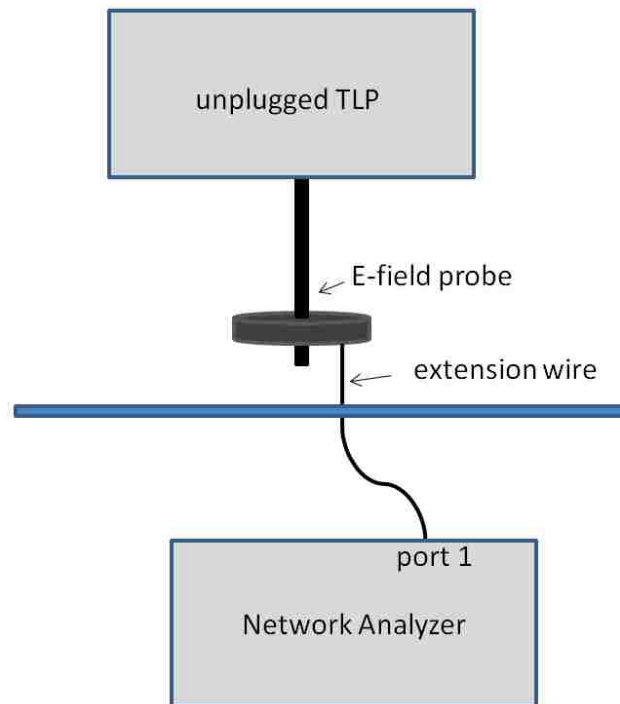
Figure 2.5. Test Setup for Common Mode Impedance

The other end of the probe is connected to an unplugged, but grounded TLP. The functionality of the TLP here is to ensure the probe is grounded, in the same way as it is grounded during testing. The common mode impedance measurement can be used to approximate the effects of lossy material. In the then the impedance is used as bases for creating a model that contains the effect of the loosy material. Then it can further assist in completing the model of the E-Field injection.

2.1.6. PSPICE Model of the Common Mode Impedance. Figure 2.6 shows the PSPICE model for the common mode impedance measurement.
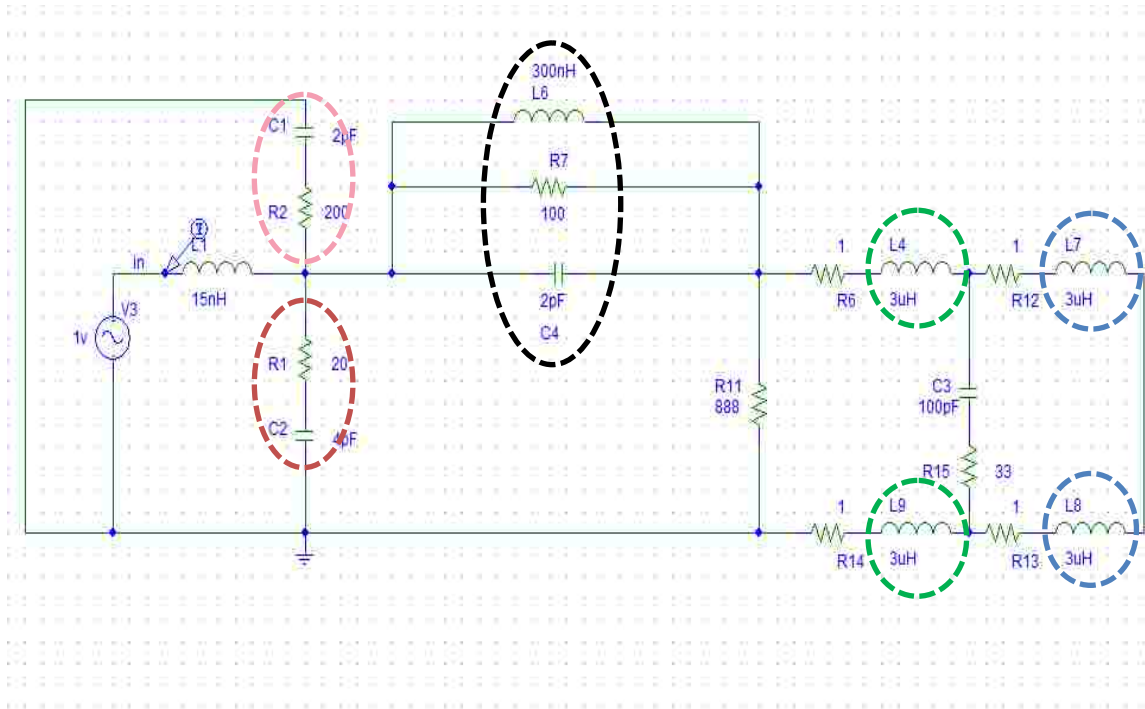
Figure 2.6. Common Mode Impedance Model for the E-field Probe ICESD1

Two pieces of equipment are involved in the test setup. The TLP is placed on the top of a Network Analyzer during the measurement of the common mode impedance. The power cords of the two pieces of equipment are circled in blue, effects caused by the common mode on coax cables are in green, and the model of losses and the capacitance to infinity of the lossy disk are in red circles. Pink circle area is the radiation model. At high frequencies, it provides 200 Ω losses to model radiation. At low frequencies, the capacitance will decouple the resistor, so there is no loss. The black circle highlights a ferrite bead mounted on the probe. Table 2.1 shows physical meanings of these specific components in the model.

Table 2.1. Components in the SPICE Model

Components	Physical meanings

Table 2.1. Components in the SPICE Model (cont.)

C1 R2	Radiation Model
R1	losses of the lossy material
C2	Capacitance between lossy material and infinity
L6 R7 C4	Ferrite beads
L4 L9	Coax cables
L7 L8	Power cords of TLP and network analyzer
R6 R14 R13 R12	Resistors placed to avoid error messages in PSPICE (inductor loop)
R15 C3	Inductance Capacitance and resistance between the TLP and the network analyzer enclosures
L1	Extension wire
V3	Reference voltage source to help us calculate the impedance in PSPICE
R 11	Losses between the inner conductor and outer conductor due to the lossy material

2.1.7. Measurement vs. Simulation Results. As shown in Figure 2.7, the simulation matches the dominating features of the simulation, such as the low frequency inductive impedance the low impedance section around 600 MHz. Differences are mainly in the high impedance region around a few MHz. As a few MHz corresponds to very late in the TLP pulse, and as high impedance mismatch has little effect on the current, so the match shown above is considered to be sufficient shown above as sufficient.
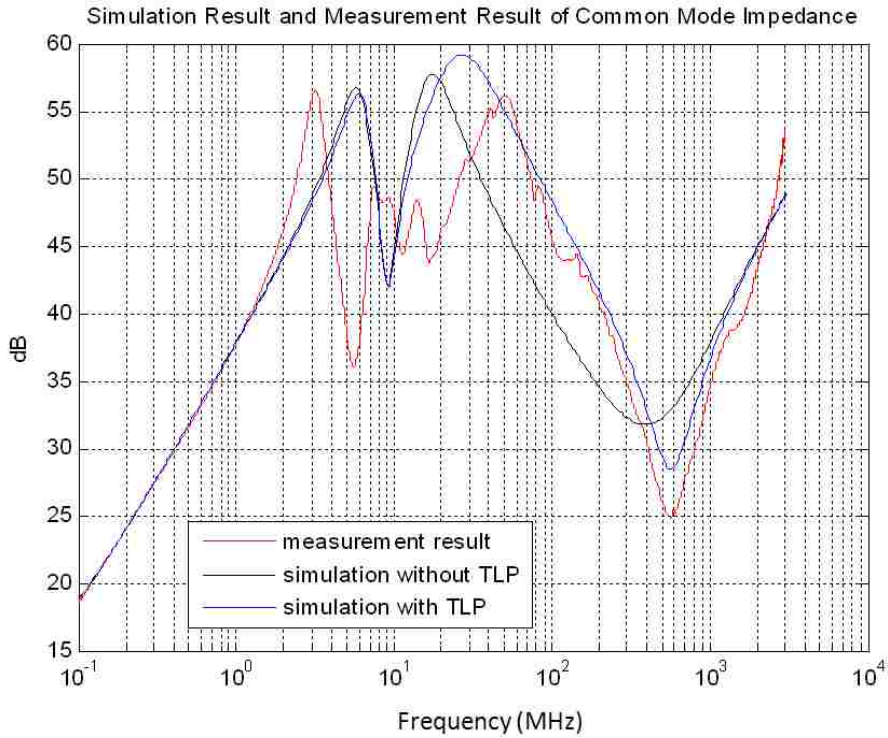
Figure 2.7. Comparison of Simulation Result and the Measurement Result

2.1.8. SPICE Model of the E-field Injection. Figure 2.8 shows the SPICE model of the E-field injection. V1 is the TLP source, C5 is the capacitance between the probe and the patch. R7, C2 and L3 compose the ferrite beads mounted on the probe.

The capacitance between the probe and the patch is about 5 pF, and is calculated as:

$$C = \epsilon_r \epsilon_0 \frac{A}{d}$$

(1)

- C is the capacitance in farads
- A is the area of overlap of the two plates, which is 1.56 cm²
- ε_r is the relative static permittivity, which is 4.5.
- ε0 is the permittivity of free space where $\varepsilon_0 = 8.854 \times 10^{-12}$ F/m
- d is the separation between the plates, which is 1.2 mm.
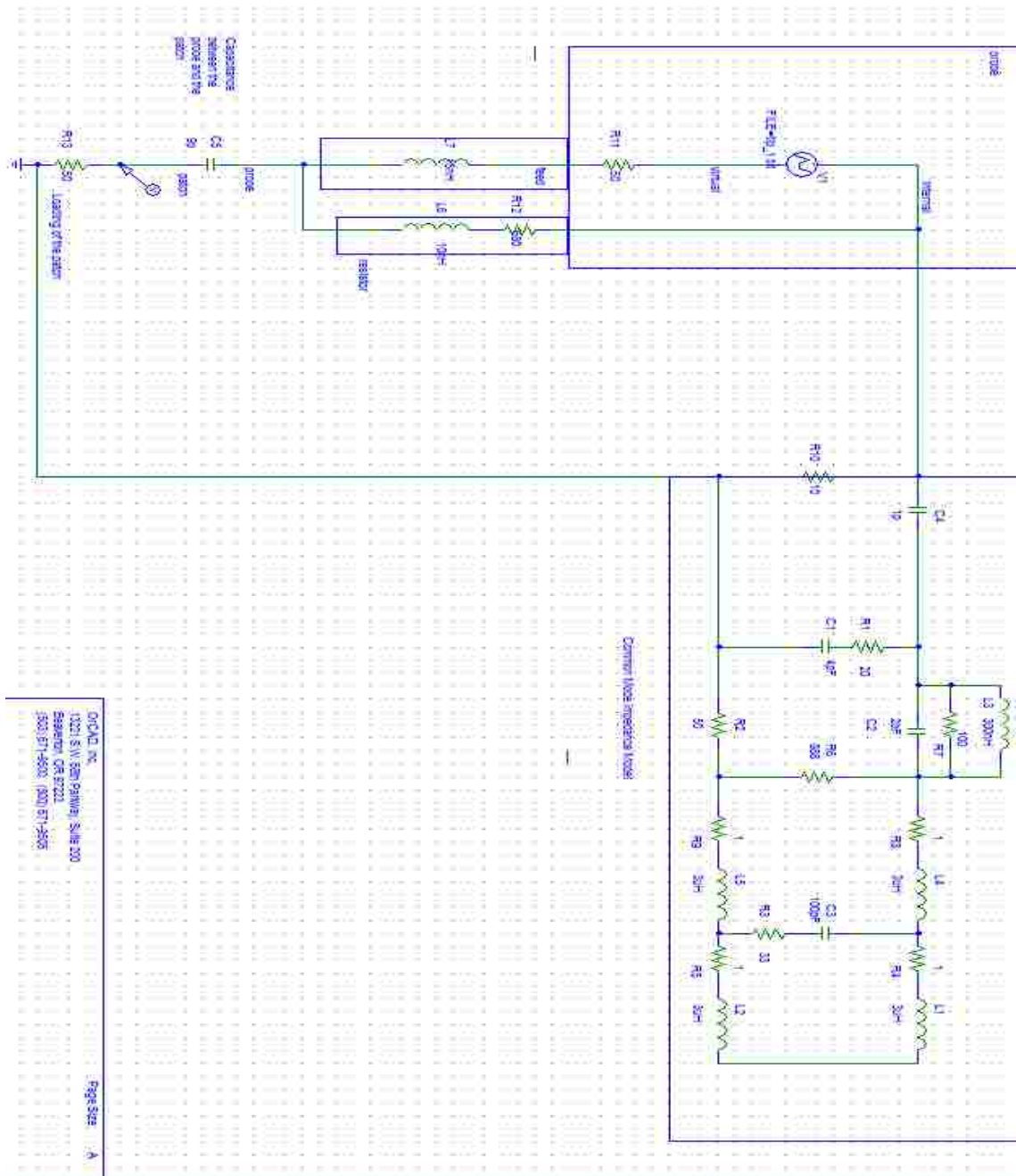
Figure 2.8. SPICE Model for the Probe Calibration

As shown in Figure 2.9, the peak values and rise time of the induce voltage waveform and the simulated signal in SPICE are almost identical.

Voltage induced from E field probe coupling the patch
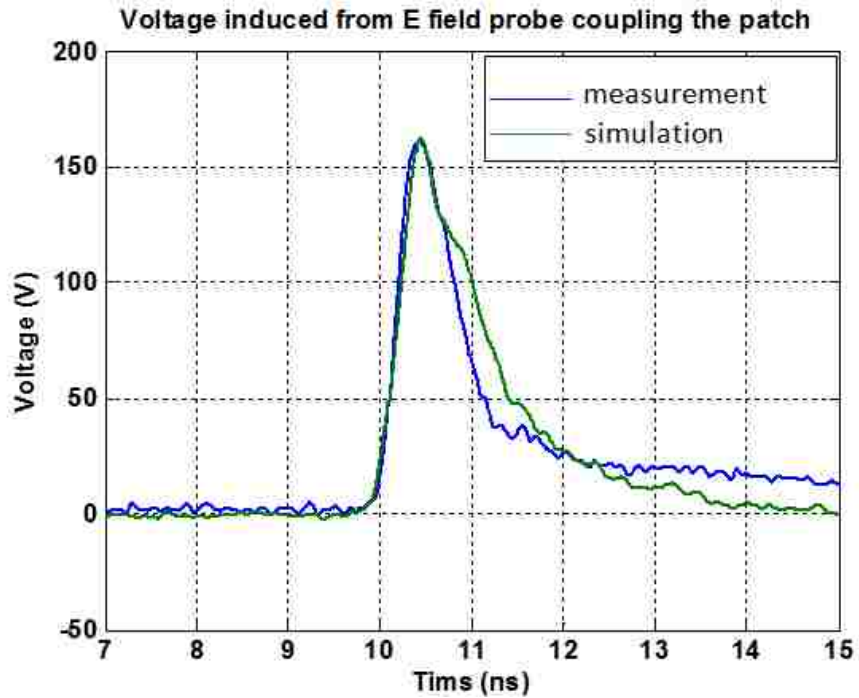
Figure 2.9. Induced Voltage at 500 V Charge Voltages in SPICE Model
and Simulation (Model No.: ICESD1)

2.1.9. CST Full-wave Simulation. The objective of full wave simulation is to estimate the field strength of the E-field probe using a numerical method. The overview of the model is shown in Figure 2.10. The comparison result is shown in Figure 2.11.
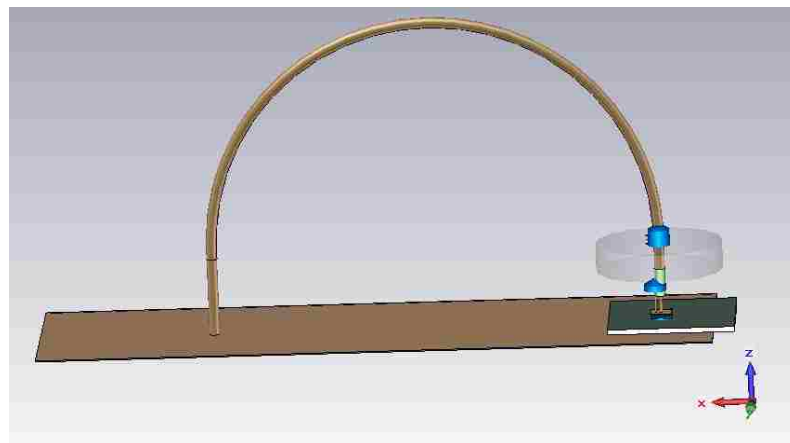
Figure 2.10. Full-wave Model of the ICESD1 E-field Probe
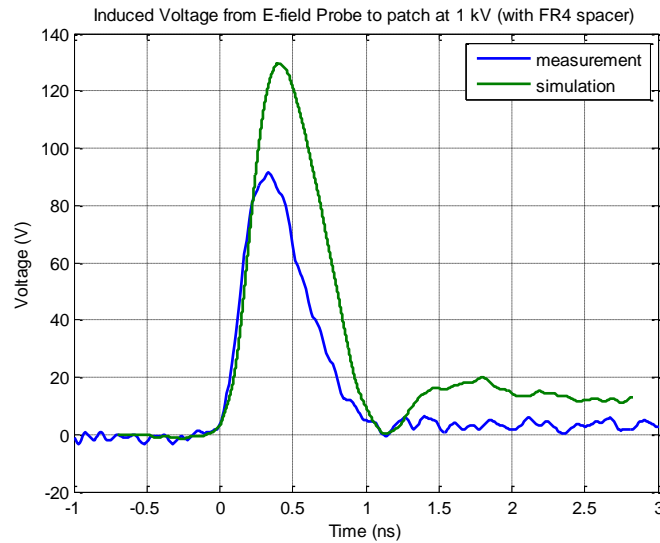
Figure 2.11.Comparison of Measurement and Simulation of the Induced Voltages

In the CST full-wave simulation, the voltage induced by the probe in the patch is simulated, and then compared to the measurement results. The shapes of the two waveforms are nearly the same, but the peak value in simulation is 40% higher than the measurement.

To calculate the field strength, CST E-field probes can be placed in desired locations in the simulation domain (as shown in Figure 2.12). In this case, the field strength would be 40 % larger than the real values

.
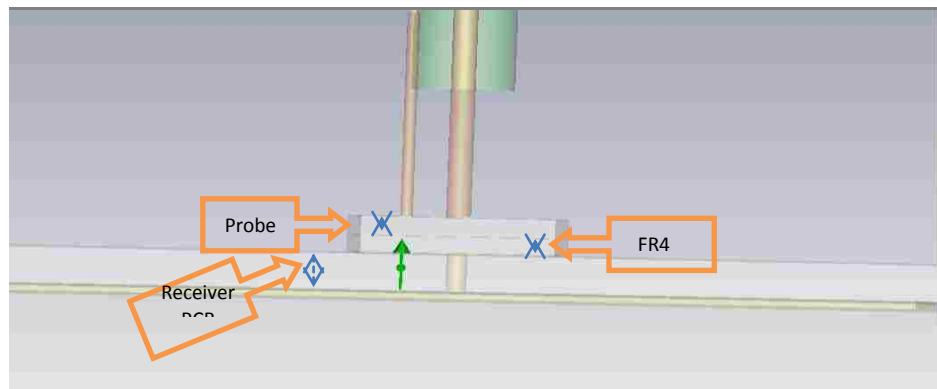
Figure 2.12. CST E-field Probe in the Model

Figure 2.13 shows the calculated field strength when the E-field probe is charged with 1 kV from the TLP. The observation point in CST is 2 mm below the E-field probe PCB. The probe is designed using a square piece of copper, which is adjacent to the patch on the PCB used to detect the signal. Due to the design, which approximates a parallel capacitor, the field strengths within the probe are approximately the same at every location. The result shows that the probe gives about 50 kV/m field strength when the TLP is set at 1 kV, which equals to about 50 V/m for every volt from the TLP system.
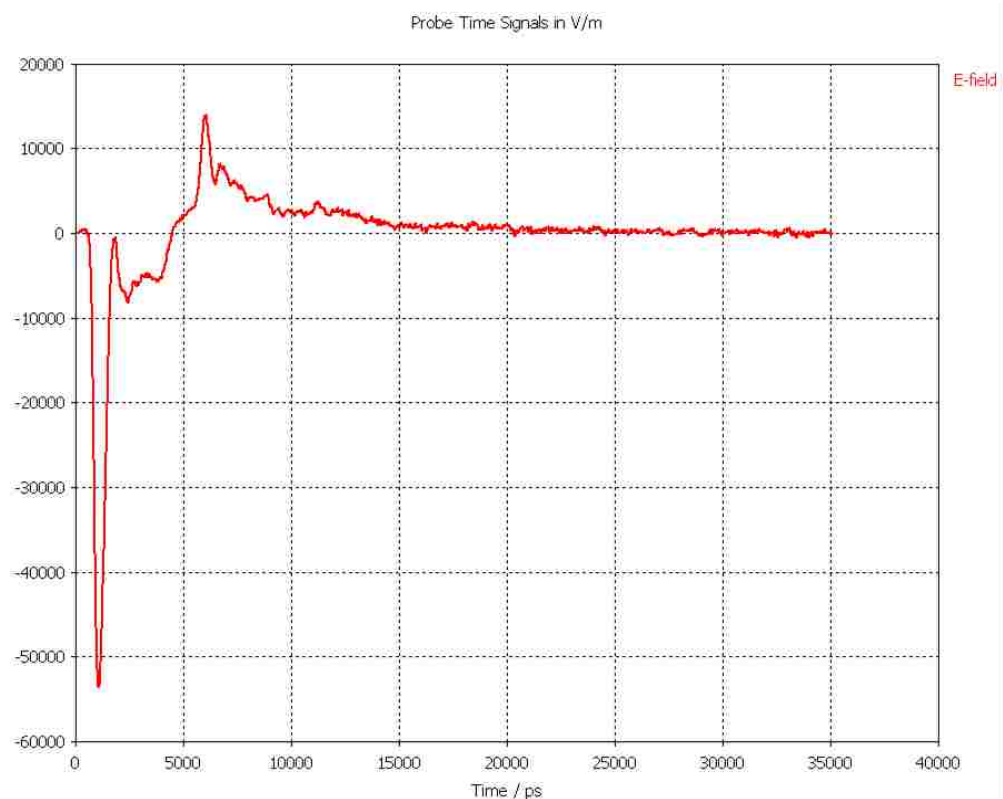
Figure 2.13. Field Strength Calculated in CST (1 kV from TLP)

2.2. MAGNETIC FIELD PROBE

2.2.1. Introduction. The general requirements of the H-field probe in this study are the following:

- Inject a H-field in a frequency range of MHz to a few GHz

- Cover the complete IC

- Have a weak Electric field

- Provide a constant H-Field over an area of a couple of cm².

- Couple by 20dB/dec (pure inductive coupling)

H-field probes previously designed in the EMC lab either had a very limited area for H-field coupling, or H-Field created was not sufficiently homogeneous and constant.

2.2.2. Design of the Magnetic Field Probe. To solve the above limitations, a magnetic field probe was designed according to the requirements of the project.

Figure 2.14 and Figure 2.15 show the side views of the four layers of the H-field probe. The largest via in the center (blue lines in Figure 2.15) is where a SMA connector is mounted. The signal passes through this via to the sensor on the third layer, and then to the ground. The shielding layer, which is indicated by a red line in Figure 2.15, shields the E-field. The area of the sensor can vary according to the size of the test ICs. Figure 2.16 shows the photo of the H-field probes.
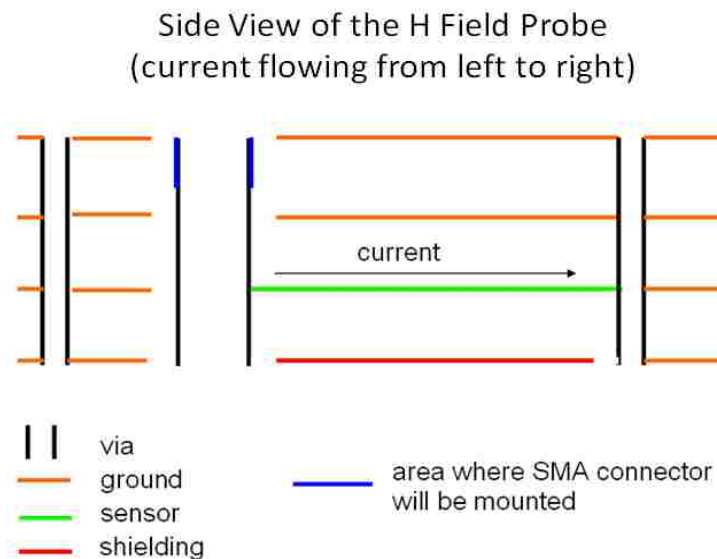
Figure 2.14.Cross-sectional View of the PCB Board

Side View of the H Probe
(current flowing into/out of the screen)
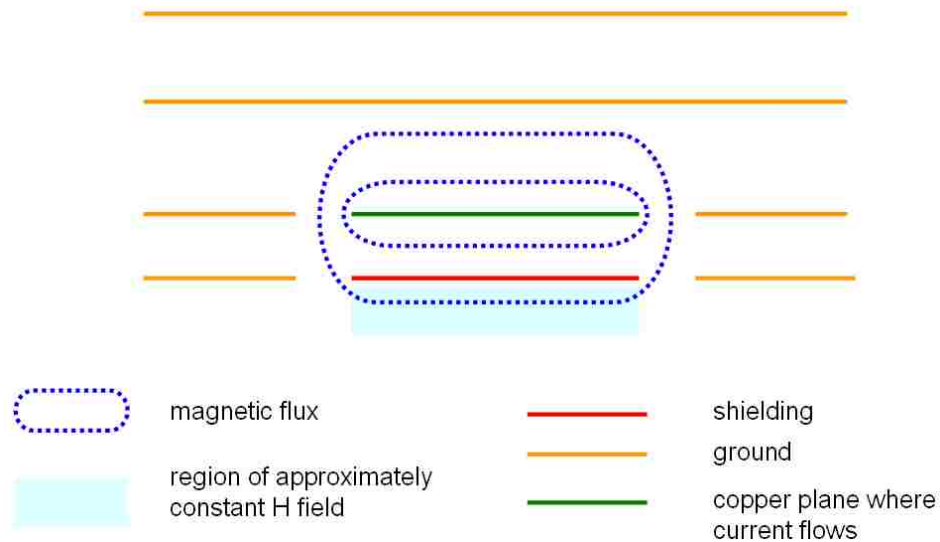
Figure 2.15. Principle View of the H-field Generated by the Probe

2.2.3. Characterization of the H-field Probe. The following subsection explains the characterization of the H-field probe. The main purpose of the measurement is to determine how homogeneous the field distribution is underneath the probe. Figure 2.16 shows a photo of one of the H-field probes tested; further Figure 2.17 depicts the trace used during the characterization measurements. An automatic scanning system has been used to move the probe accurately and measure S21 above the trace at three different heights: 0 mm, 0.5 mm, and 1mm. Objective was to test how homogeneous the field is in X and Y direction and in the height direction Z. For each height, 400 data points on a 2×2 cm² area above the trace are measured.

The length of the trace is 8 mm, and its width is 0.38 mm. During test, the trace is soldered to a large ground plane as shown in Figure 2.17.

Figure 2.16. The Photo of the H-field Probes

Figure 2.17. Photo of the Trace

Figure 2.18 illustrates the test setup. One 180 degree hybrid is used to create a signal which is the difference of both trace outputs.
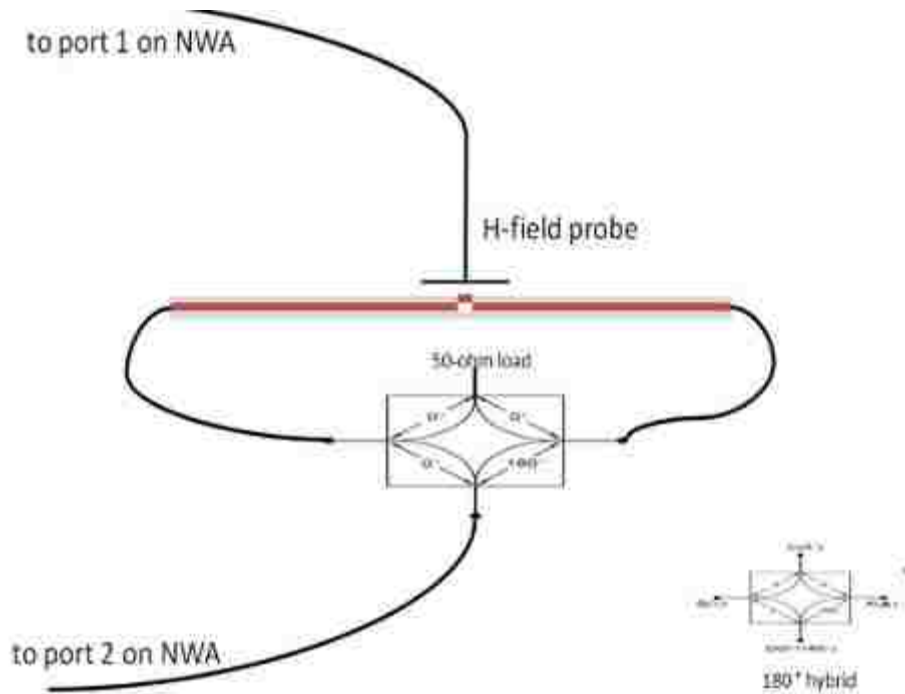
Figure 2.18. Test Setup for Measuring the Coupling
between the H-field Probe and a Short Trace

The output of the hybrid and the probe are connected to the two ports of the Network Analyzer. S21 values are measured for the 400 points in the scanning region. The step size between each point is 1 mm. During the test, the probe board is placed in parallel with the trace, and the wider side of sensor is toward the right side of the trace.

2.2.4. Results and Discussion. The following figures present the S21 results. From the following figures, S21 values are compared for a constant X value or Y value in a coordinate system. The point at x= 365.31mm and y=167.86 mm is the center of the trace. Either X or Y value is fixed, the E-Field strength along this fixed X or Y value can be compared and analyzed at a fixed frequency value. Figure 2.19 & Figure 2.21 are the illustrations showing how the probe moves during the measurement. Figure 2.20 is the S21 along the X axis at Y= 167.87 mm, and Figure 2.22 is the S21 along the Y axis at X= 365.31 mm from 10 MHz to 3 GHz at 0 distance between the probe and trace.
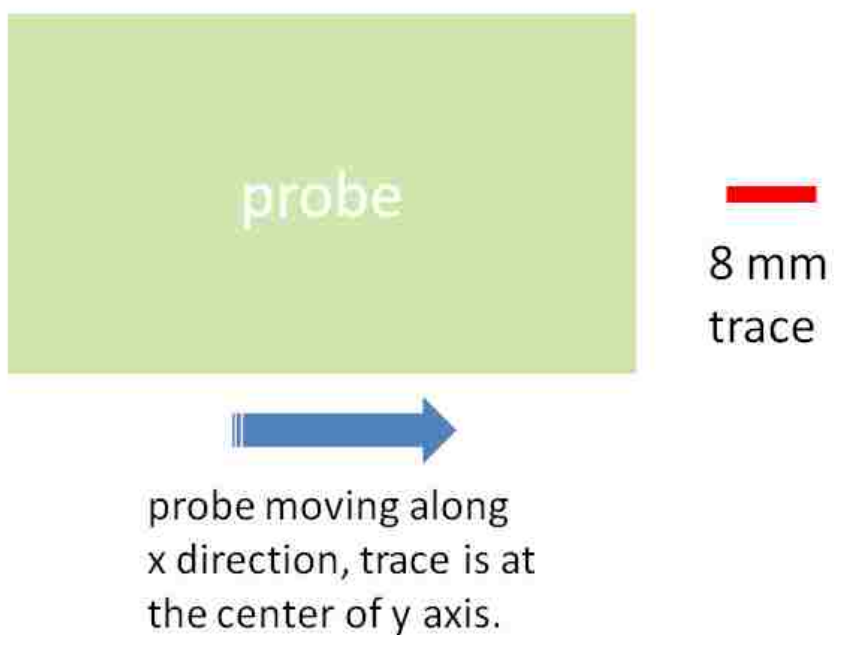
Figure 2.19. Probe Moving Along the X Axis with a Constant Y Position
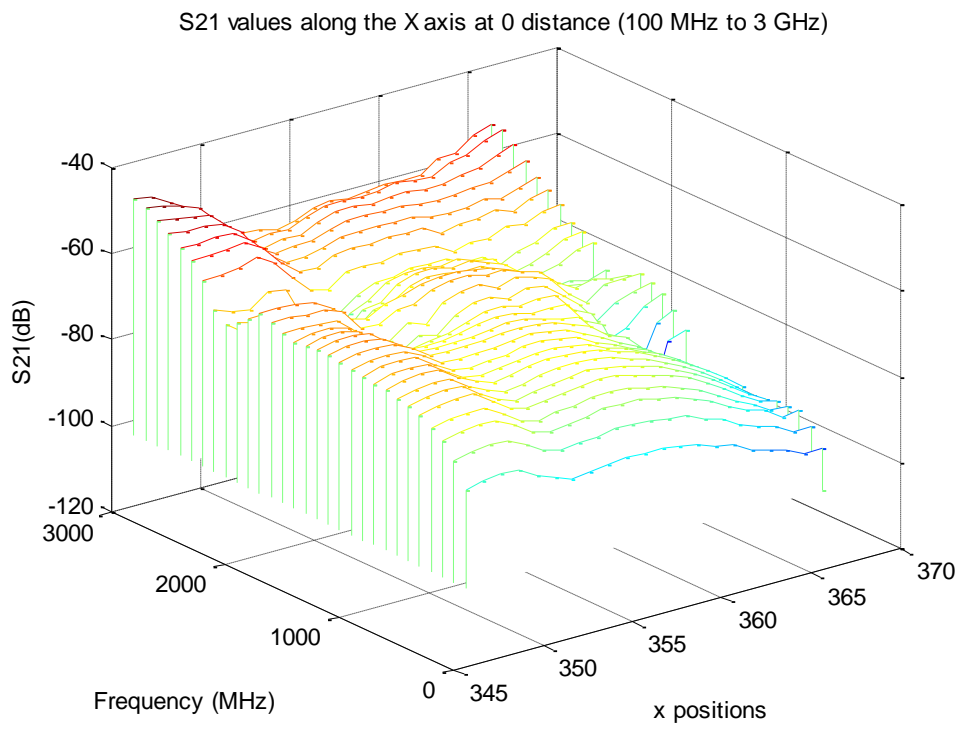
Figure 2.20. S21 Values Along the X Axis with a Constant Y Position
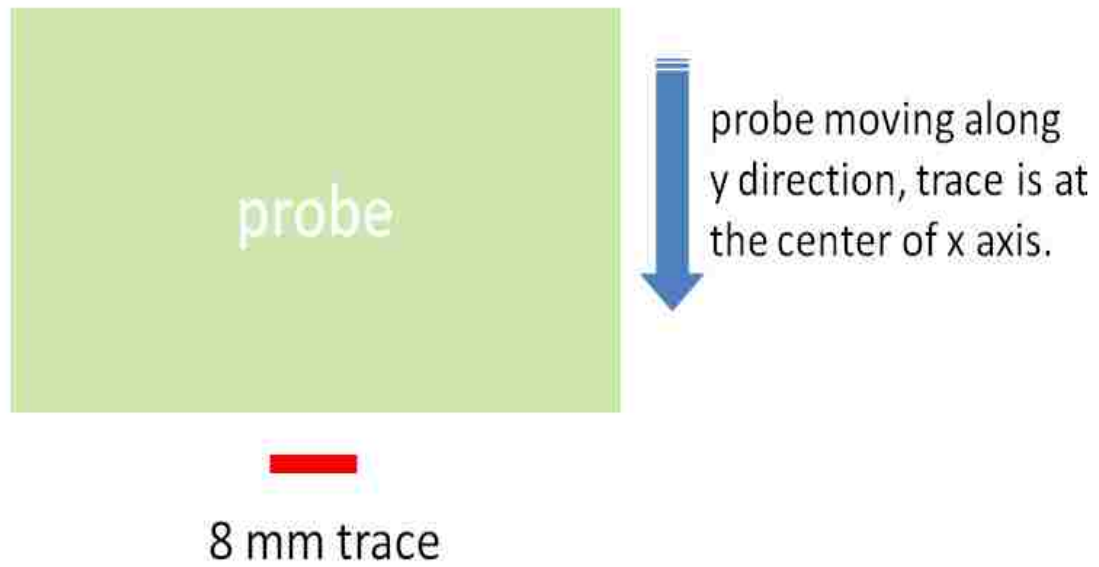
Figure 2.21. Probe Moving Along the X Axis with a Constant Y Position

One of the design goals of the magnetic field probe is that the magnetic field should be homogeneous underneath the probe, and it should show little distance dependence. For a wide current carrying trace the fields above the trace are not a strong function of distance as long as the point of observation is close to the trace (close relative to the width of the trace), and as long one is not close to the edge of the trace. The results above indicate that the designed probe behaves in such a way. Figure 2.22 shows the three curves showing the S21 values at 500 MHz for the three distances between probe and trace. The waveforms are identical to each other in the center region (-5 mm to 5 mm). The peak values are also close in the center region; there is only a 2 dB difference when the height is increased from 0 to 1 mm.
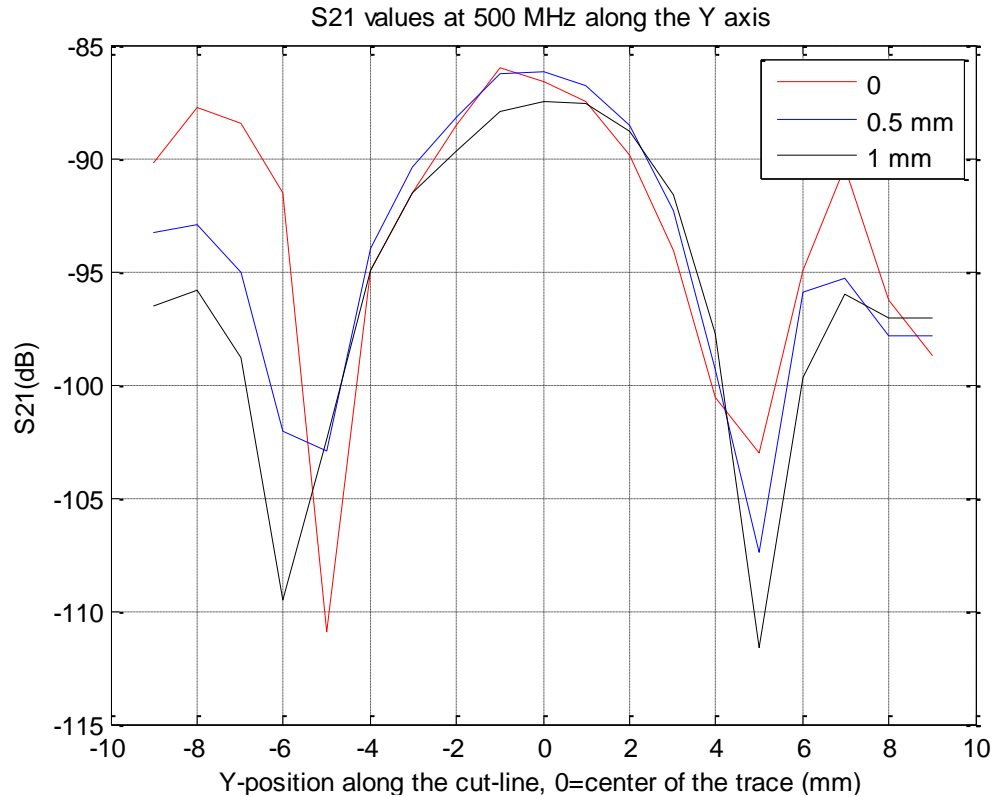
Figure 2.22. S21 Values at 500 MHz along the Y Axis
for 3 Different Heights above the Probe

2.2.5. HFSS Simulation for the Magnetic Field Probes. To further understand the H-Field distribution of the probe, and to identify the strong fields at the side of the current carrying trace, a simulation using HFSS was performed. The simulation in HFSS can also be used to quantify the unwanted E-Field generated by the H-filed probe. Figure 2.23 shows a global view of the H-Field probe model used in the HFSS simulation. The ground vias are modeled with PEC connecting all the layers on the sides for simplification.
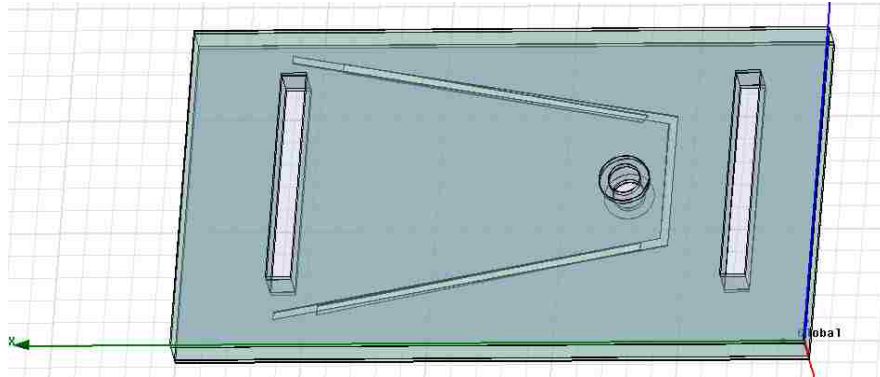
Figure 2.23. H-Field Probe in HFSS Simulation

Figure 2.24 shows the lumped excitation port in the HFSS simulation model, it is a circle on the anti-pad of the SMA connector via on the first layer of the probe. The excitation source energy is 1 Watt.
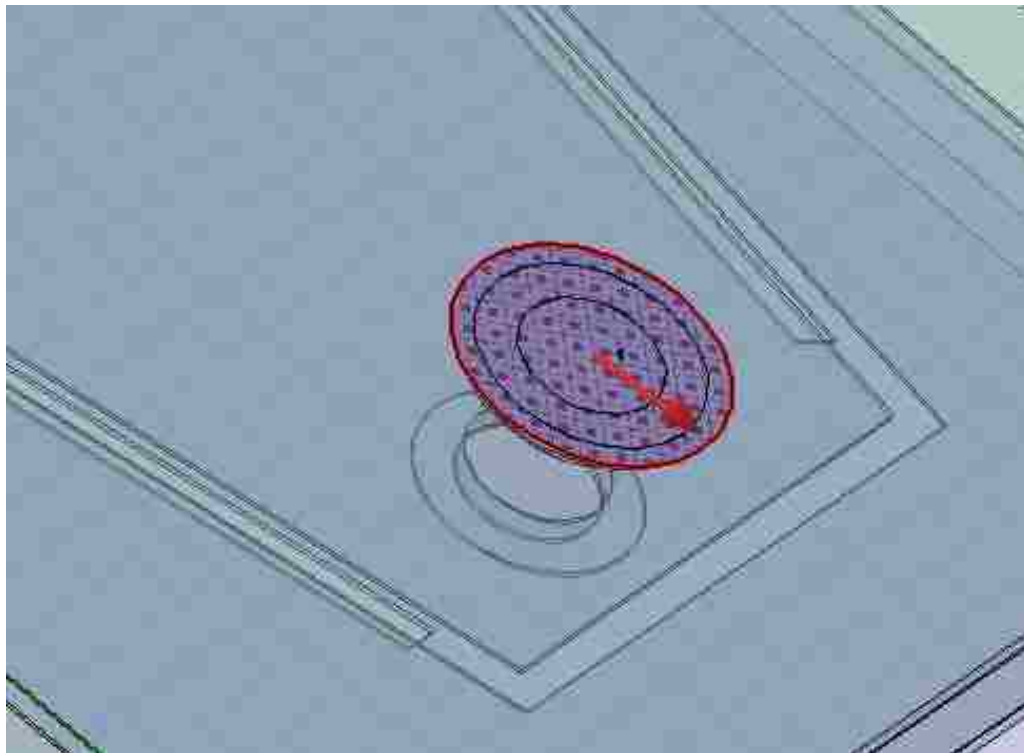
Figure 2.24. Excitation Port in the HFSS Simulation

Figure 2.25 compares the S11 of the H-field probe in simulation and measurement, the objective of this comparison is to check the accuracy of HFSS simulation. The two results are very close, indicating that no structural error is present in the model.
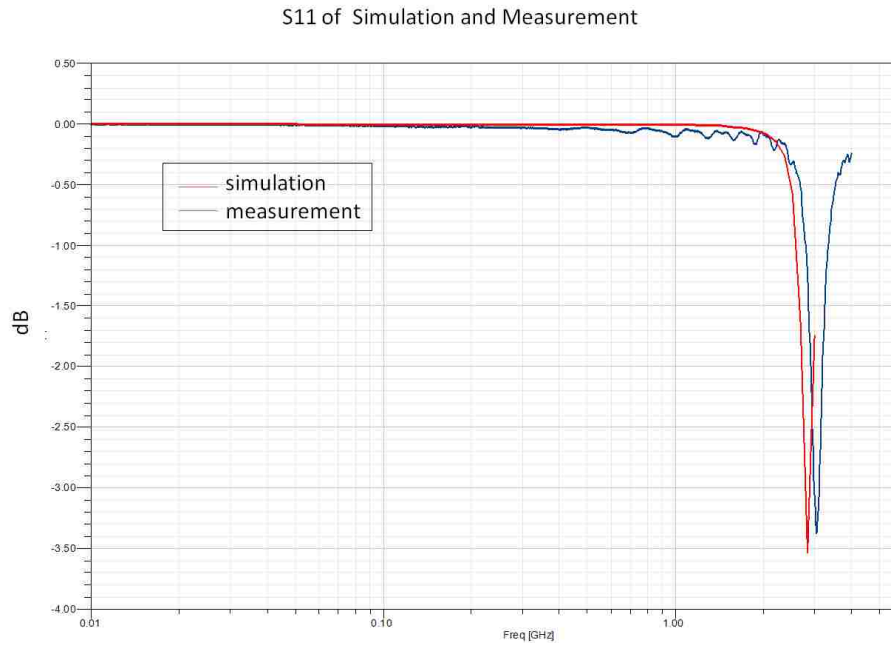
Figure 2.25. Simulation and Measurement of S11

Figure 2.26 shows the H-Field generated by the probe along the X axis cutline. One can easily see that, besides the center region, there are also strong field near the SMA connector. This simulation result can explain the strong field on the left of the X axis in our measurement results. And Figure 2.27 shows the H-Field generated by the probe along the Y axis cutline. Besides the center region, there are also strong field from the two slots on the fourth layer (shielding layer). The distance between the two slots is 6mm to 10 mm from one end to another. In our measurement results, the strongest fields on the two side regions along the Y axis are 6 to 8 mm away from the center region.
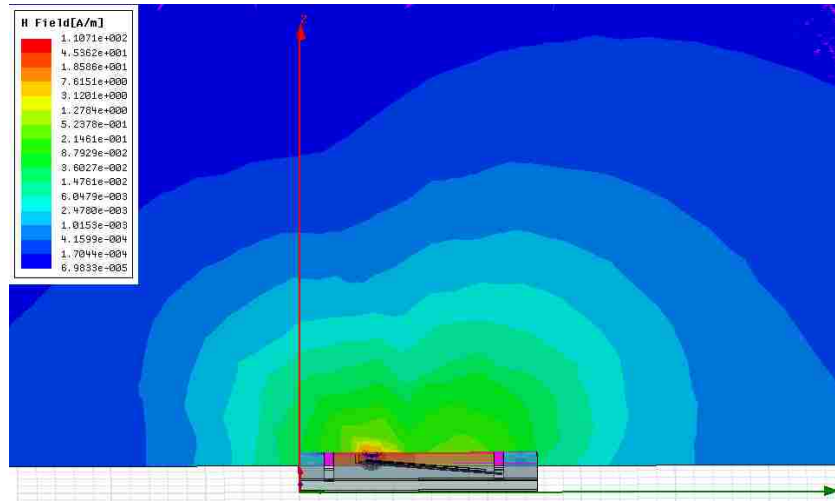
Figure 2.26. Side View of the Probe along the X Axis (Magnetic Field)
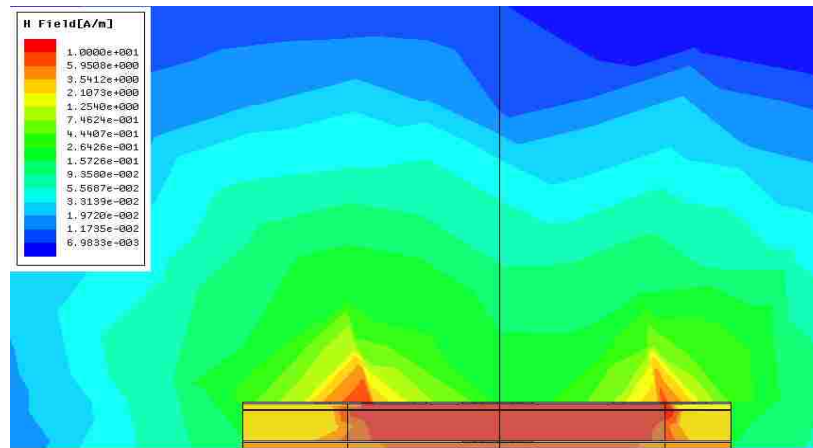
Figure 2.27. Side View of the Probe along Y Axis Cut Line (Magnetic Field)

Figure 2.28 and Figure 2.29 are results for E-field and H-field at 1 GHz. Figure 2.30 shows the ratio of the E-Field and H-Field of the sensor region from 10 MHz to 3 GHz. E-Field is much smaller at frequencies below 2.5 GHz.
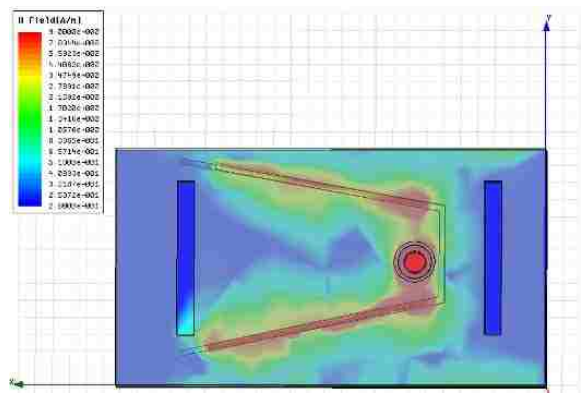
Figure 2.28. H-Field at 1 GHz (0 mm height above the probe)
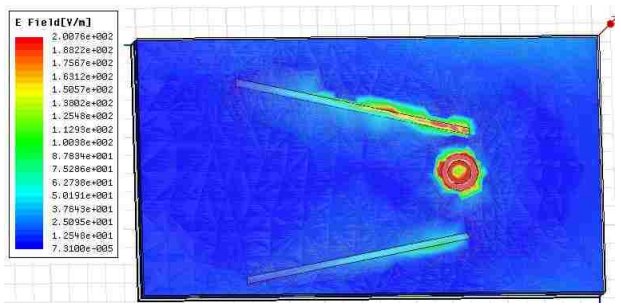
Figure 2.29. E-Field at 1 GHz (0 mm height above the probe)
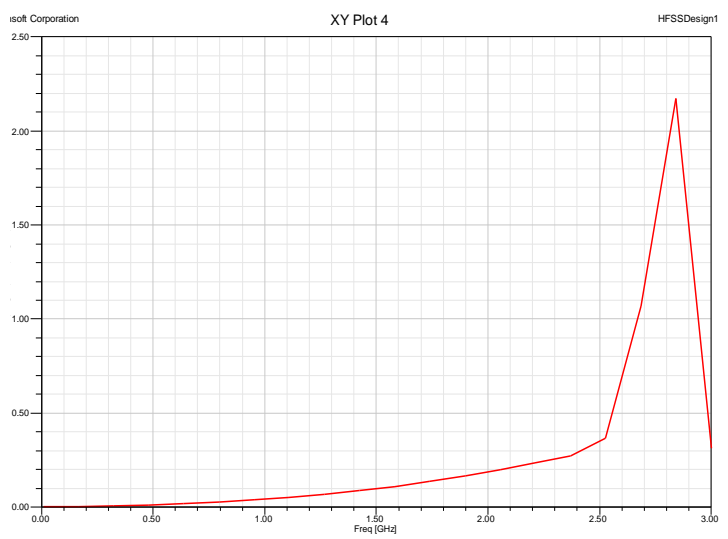
Figure 2.30. The Ratio of E-Field and H-Field from 10 MHz to
3 GHz (0.5 mm above the probe)

Figure 2.31 and Figure 2.32 show the magnetic field lines and current density of the probe at 1 GHz. In general, the area around the SMA connector and along the two slots obtain stronger field. This explains why there are strong couplings when the probe is moved away from the probe at about 6 to 8 mm.

To compare the simulation results and the measurement results, the following assumption is made: The trace is short enough to be considered as a point. This is because the interested frequency is 1 GHz, in which case the wavelength is much longer than the trace. The simulation results are in terms of field strengths at a certain point above the probe. Then one point on the probe in our simulation can be compared to the point that is directly on the top of the trace.

Normalization is needed since the two groups of data are on different scales and with different units. The probe factor of the H-Field probe at one particular frequency is assumed to be a constant, so the E-Field strength or S21 is a linear function of the other.
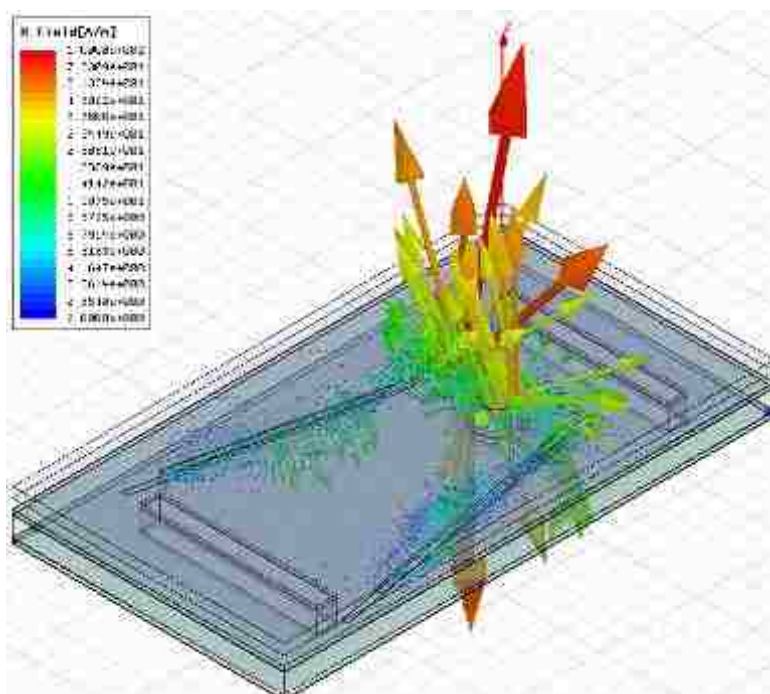
Figure 2.31. H-Field Lines at 1 GHz
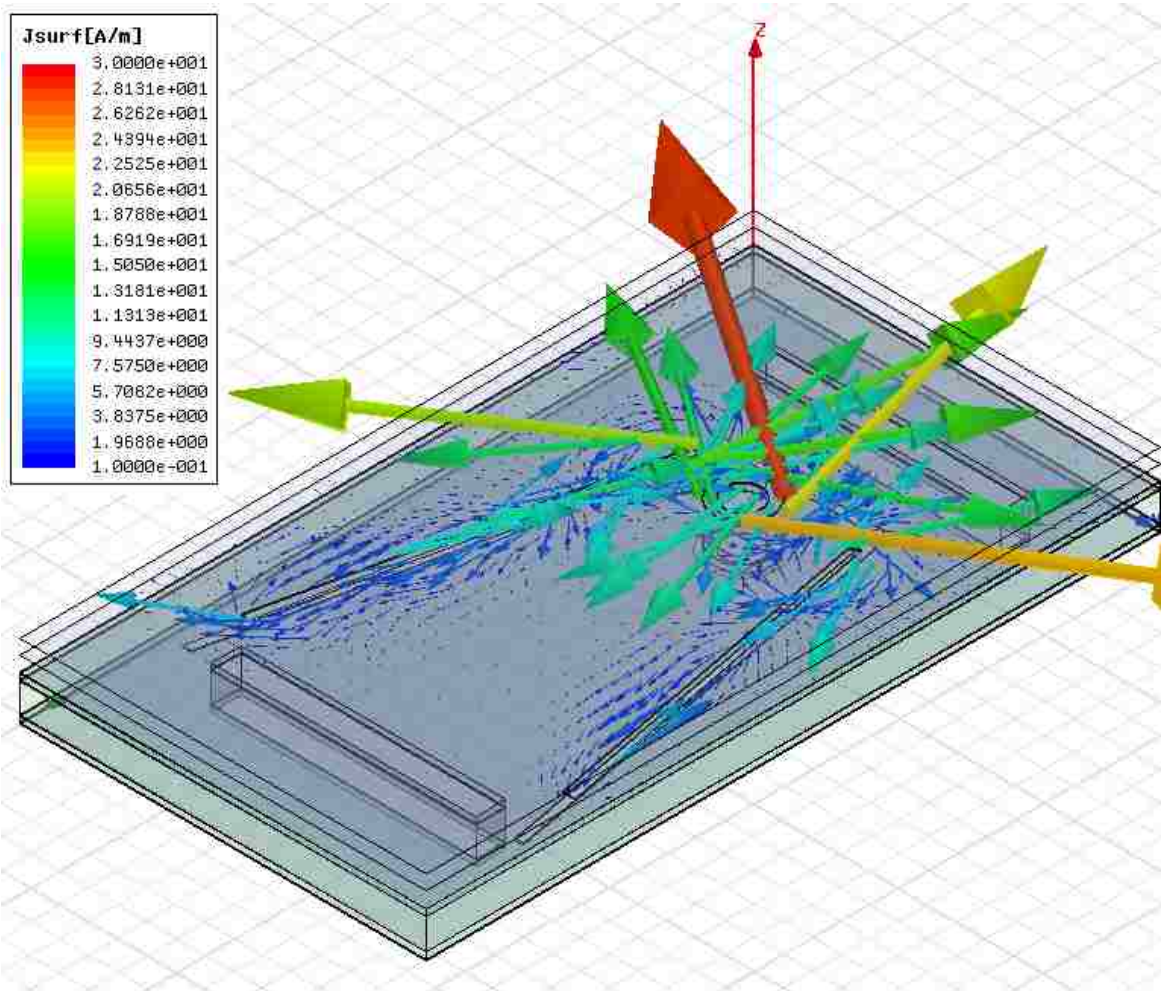
Figure 2.32. Current Density at 1 GHz

2.2.6. Result. Figure 2.33 shows the measurement result, and Figure 2.34 shows the simulation result. The simulation result contour describes the E-Field strengths over a larger area. The simulation shows the E-Field strengths over the entire probe surface. In both figures, one can find that over the sensor region, the E-Field is relatively symmetric and constant; the strongest field coupling is around the SMA connector. However, the difference between values from region to region is very large in the simulation results, further investigation will be needed to find out the reason.
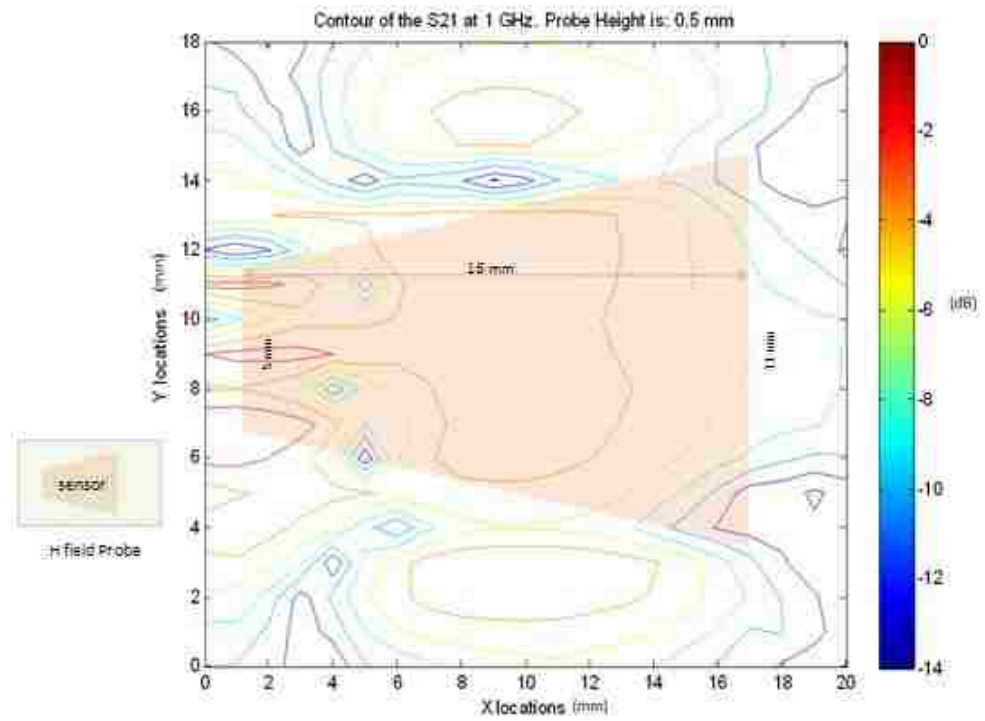
Figure 2.33. Contour of S21 at 1 GHz in Measurement, Probe Height is 0.5 mm
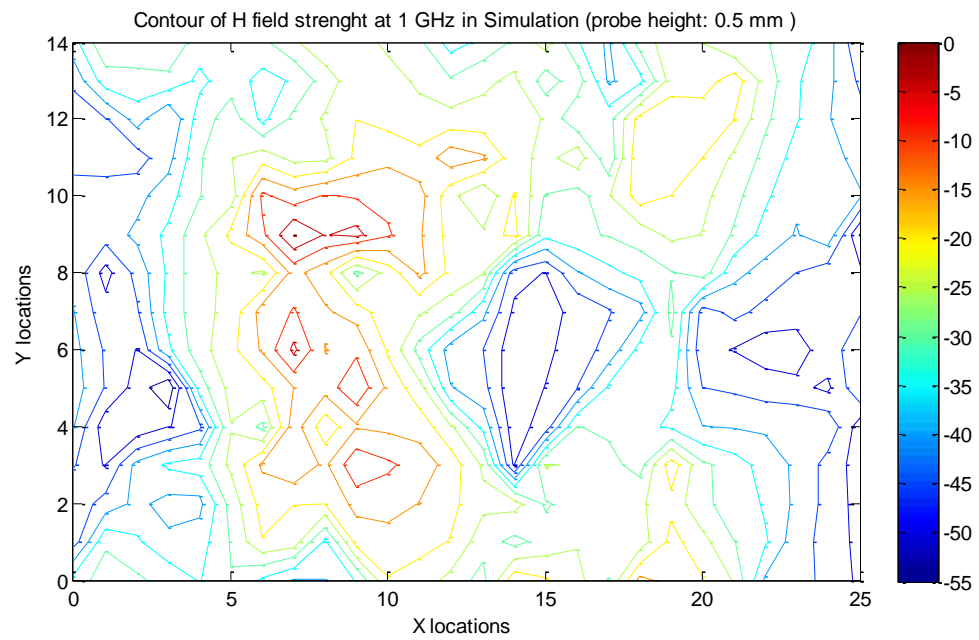
Figure 2.34. The Contour of Field Strength at 1 GHz with 0.5 mm Distance

2.2.7. Characterization for Magnetic Field Probes. The objective of the calibration is to scale the induced voltages of the crash level to field strength and field strength. Then one can use the results scaled in field and field derivative, and compare it to the block level simulations. The test objects are the four H-field probes.

One shielded H-field probe is selected as the reference probe, and its effective area is calculated using TEM cell. The photo of the reference probe is shown in Figure 2.35. And the test setup is shown in Figure 2.36. The first step is to determine the effective area of the reference probe, and the second step is to determine the field strength of the H-field probes using the reference probe as a receiver.

Figure 2.35. Photo of the Reference H-field Probe
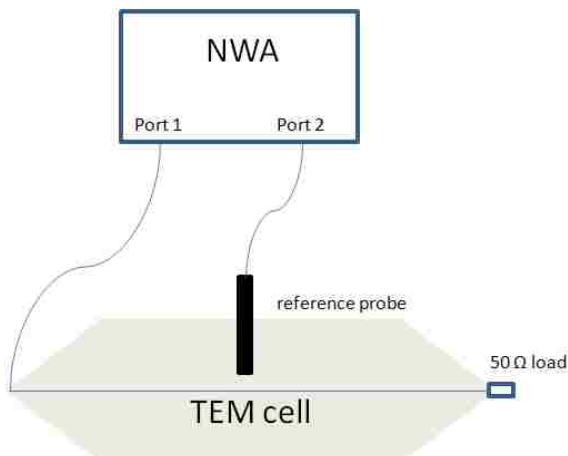
Figure 2.36. Test Setup

In the test setup shown in Figure 2.36, TEM cell is used to excite the reference probe. The loop size of the probe is 1 mm². The vertical H-field components are measured by the reference loop probe. During the measurement, a 10 cm ×10 cm board with a slot is used to cover the top wall of the cell, and the probe is inserted into the cell through the slot. The excitation from the Network Analyzer is set to 10 dBm.

Then the effective area of the probe can be calculated using the following equations:

$$V_2 = A\mu\frac{dH}{dt} = A\mu jwH$$

$$E = \frac{V_1}{h}$$

$$H = \frac{E}{377}$$

$$A = \frac{377hS_{21}}{2\pi f\mu} \qquad (2)$$

In the equations above, h is the height between the probe and the septum of the TEM cell which is approximately 45 mm.

Figure 2.37 is the measurement S21 result using the test setup shown above. And Figure 2.38 is the calculated effective area of the reference using the equation.
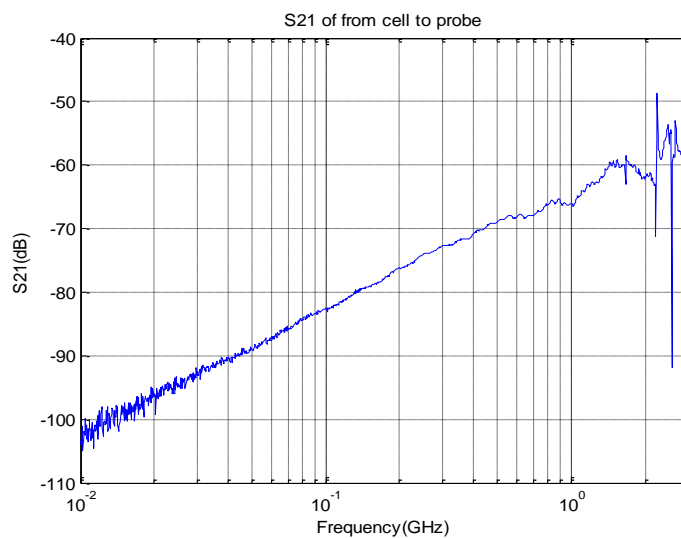
Figure 2.37. S21 from the Cell to the Reference Probe
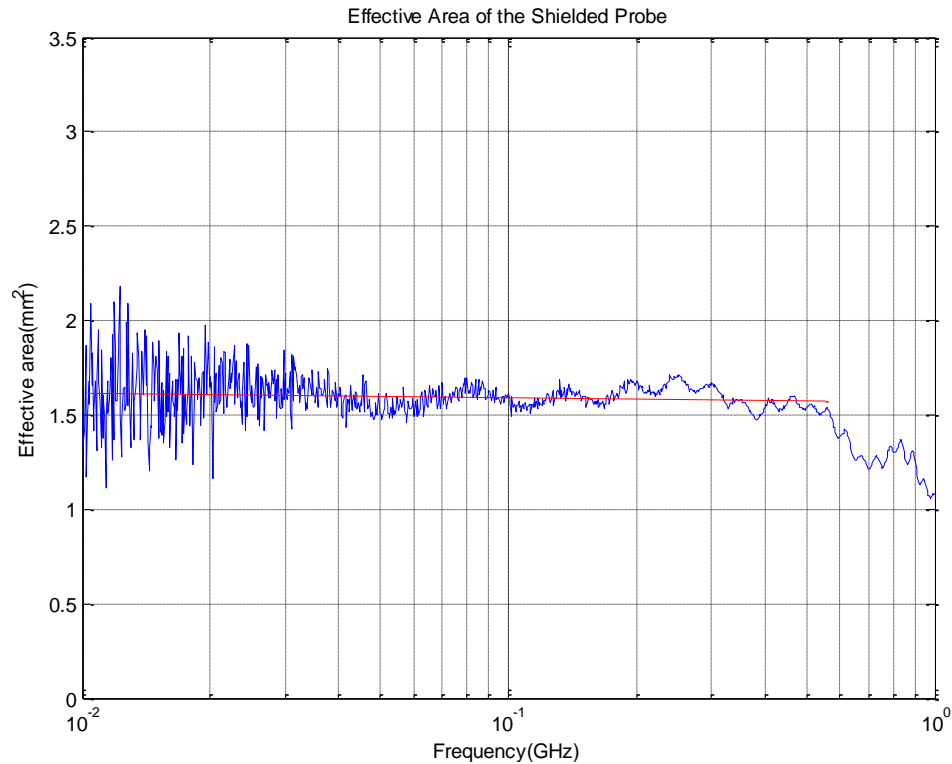
Figure 2.38. Effective Area of the Reference Probe

From the above equations, the calculated effective area of the reference loop probe is about 1.59 mm².

The test setup of step 2 is shown in Figure 2.39. A TLP is used as the source to inject pulse to the H-field probes (waveform shown in Figure 2.40). The charge voltage of the TLP is 200 V during the measurement. And the reference probe is placed vertically to the reference probe to measure the field generated by the H-field probes. Two distances between the probes are selected during the test, one is 0, and the other is 1 mm. a piece of foam which has a thickness of 1 mm is used as the spacer between the two probes.
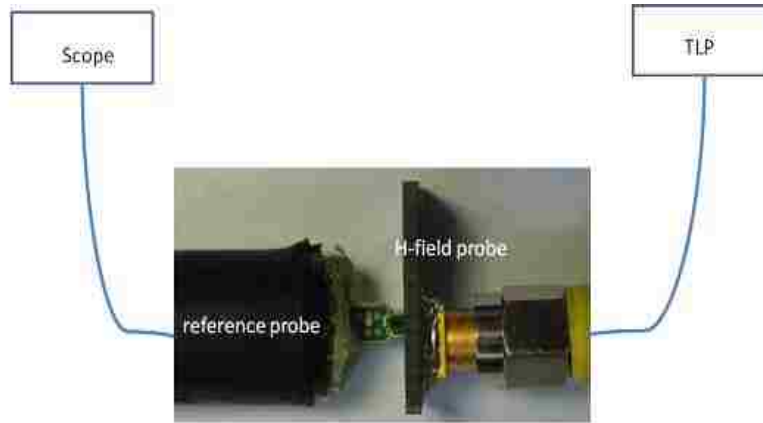
Figure 2.39. Test Setup

The equation we used is to calculate the field strength and field strength derivative is:

$$V = A\mu \frac{dH}{dt}$$

(3)

Figure 2.40 shows the output voltage of the TLP we used in our measurement at 200 V charge voltage. The output voltage from TLP is calculated as:

$$V_{out} = 0.5 V_{ch\,arg\,e} - V_{spark}$$

(4)
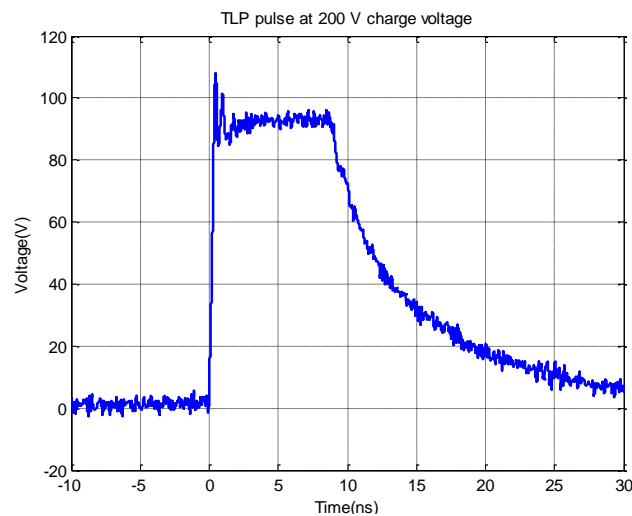
Figure 2.40. TLP Output Voltage at 200 V

Figure 2.41 & Figure 2.42 are the measured waveforms of induced voltages at two different distances for the H-field probes.
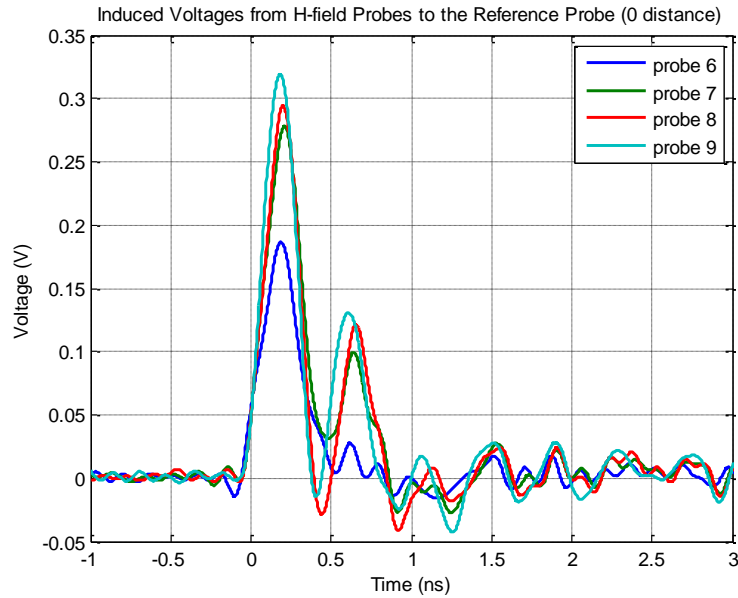
Figure 2.41. Induced Voltages from H-field Probes to the Reference Probe at 0 mm
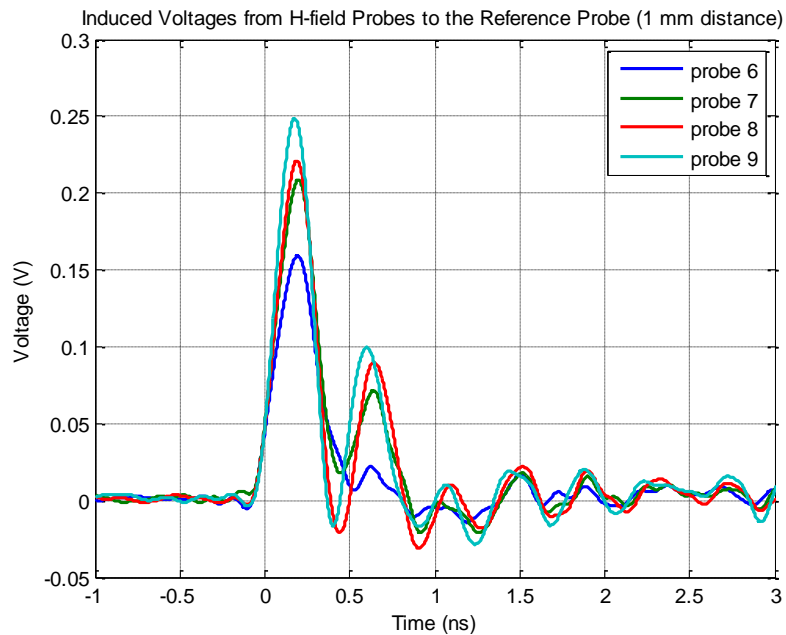
Figure 2.42. Induced Voltages from H-field Probes to the Reference Probe at 1 mm

From induced voltage results, the field derivative can be calculated by equation:

$$\frac{dH}{dt} = \frac{V}{A\mu}$$

(5)

And the calculated waveforms of field derivatives are shown in Figure 2.43 & Figure 2.44. The integrated field strength results are shown in Figure 2.45 & Figure 2.46.
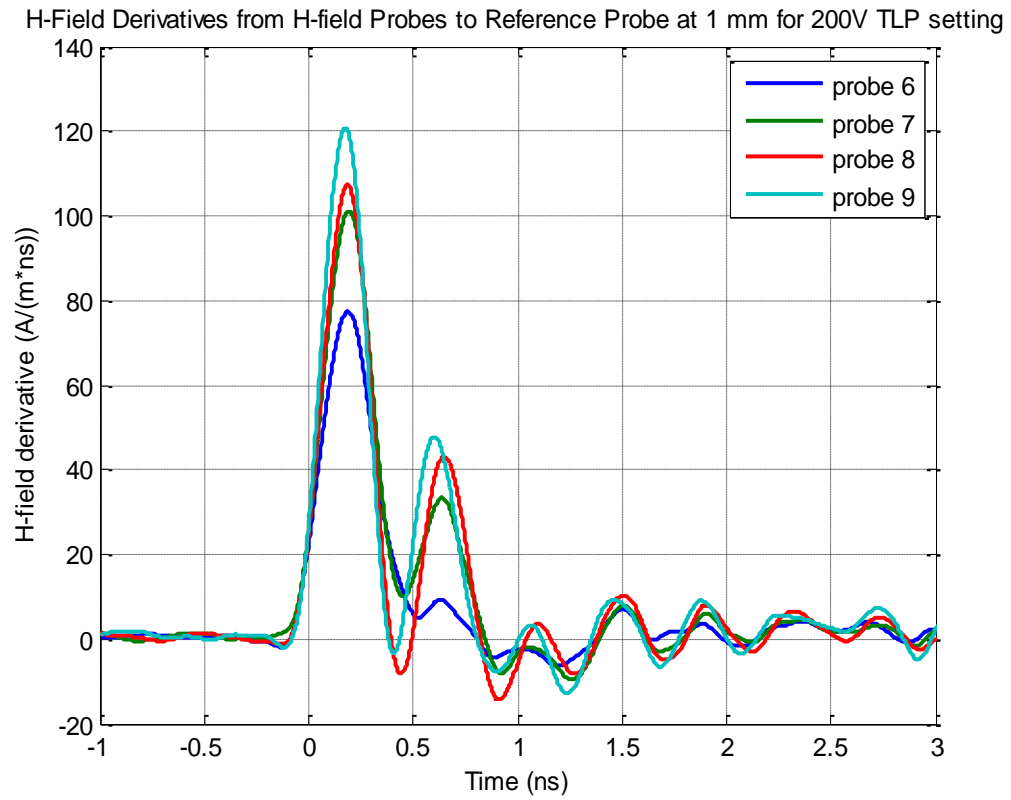
Figure 2.43. Field Derivative of the H-field Probes at 1 mm
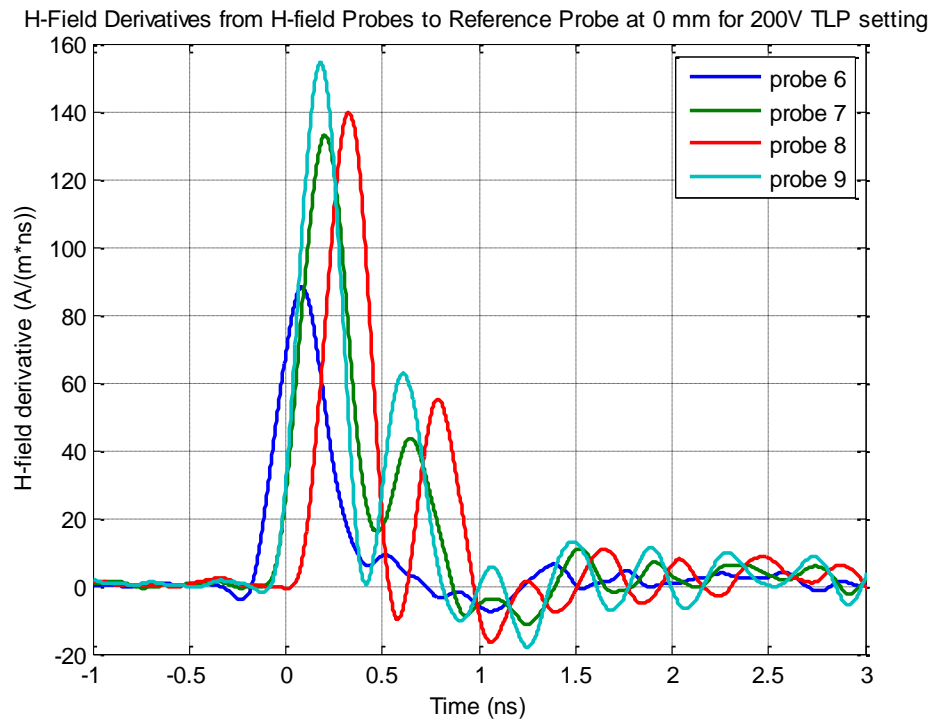
Figure 2.44. Field Derivative of the H-field Probes at 0 mm
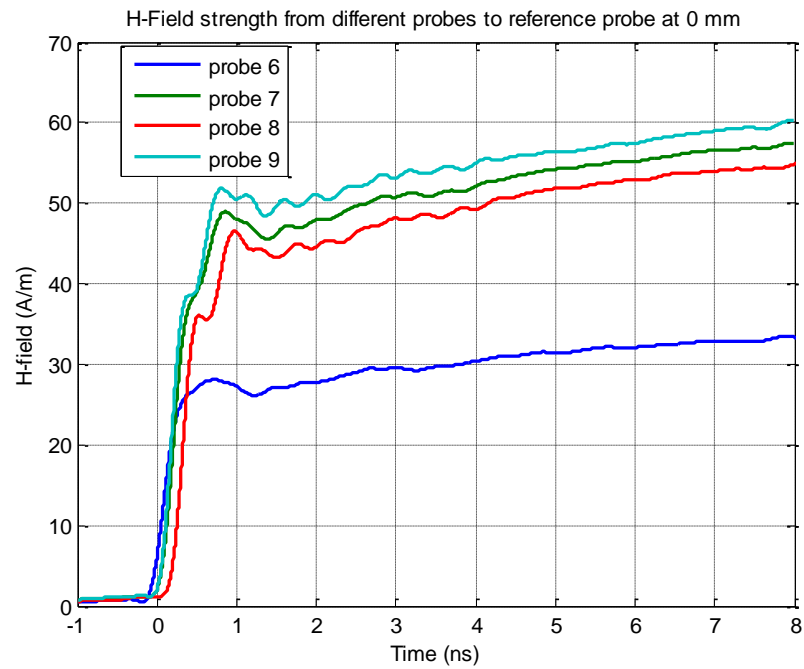
Figure 2.45. Magnetic Field Strength at 0 mm for H-field Probes
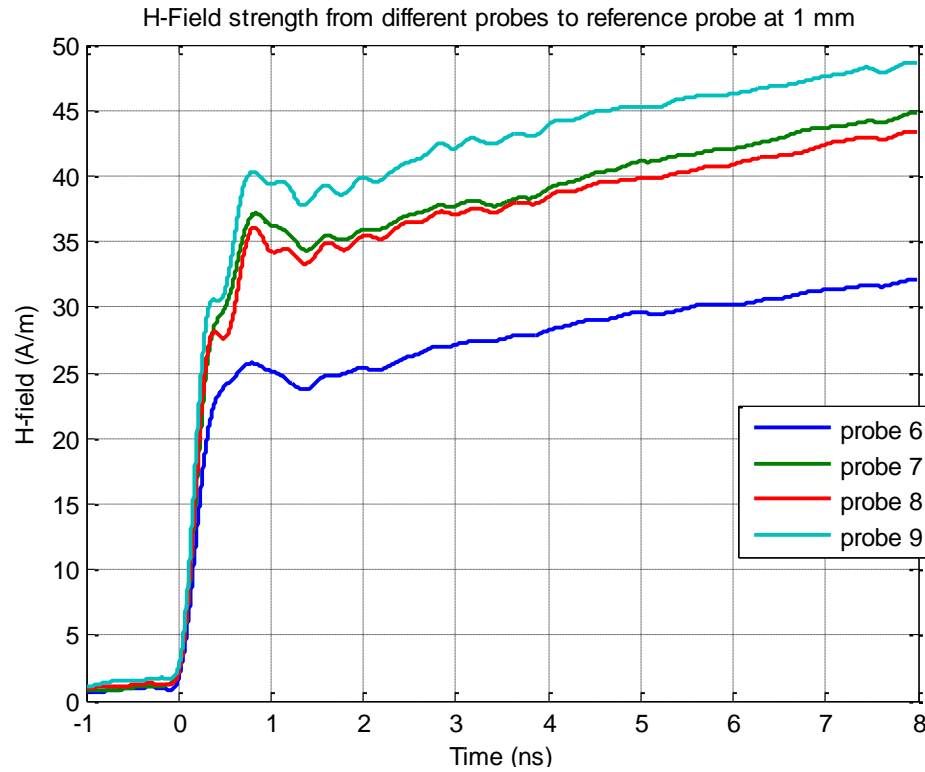
Figure 2.46. Magnetic Field Strength at 1 mm for H-field Probes

Table 2.2 is a table showing the conversion factor for the H-field probes for 1 V charge voltage from the TLP.

Table 2.2. Field Strength of the Probes at 0 mm and 1 mm for 1 V from TLP (V/m)

	0 mm	1 mm
H-field Probe 6	0.1672	0.1605
H-field Probe 7	0.2875	0.2241
H-field Probe 8	0.2751	0.2171
H-field Probe 9	0.3014	0.2432
$\Sigma\Delta$ probe	0.0263	0.0248

2.3. HIGH VOLTAGE ∑Δ PROBE

2.3.1. Design of the $\Sigma\Delta$ Probe. This probe is called ∑Δ probe as it uses the sum of two signals to create a strong E-field and the difference of two signals for creating a strong magnetic field. Thus, it requires two in phase or out of phase drive signals. At lower voltages it would be easy to create those signals using a 0 deg / 180 deg hybrid. However, the hybrids available are either not broadband or cannot handle the voltages needed. For that reason a new design was implemented. It uses:

- A resistive power splitter having 0 deg split
- A pulse inverter

The signal coming out of TLP will be spitted into two separate coax cables by a splitter, and the polarity of the signal of one of the two signals can be changed by an inverter. By easily changing the test set up, the probe can inject E-field and H-field as desired.

2.3.2. High Voltage Splitter. Ideally, the Hybrid would offer good isolation, and as little loss as theoretically possible (3dB). Due to the complexity of high isolation splitters at high voltages a different concept was selected. The splitting is achieved via resistances. This increases the loss, thus reduced the E-Field strengths achievable, but it simplifies the design. Further, it allows achieving sufficient isolation. The isolation is needed as the probe will connect both ports of the splitter with each other, allowing circulating pulses. If those circulating pulses would not be attenuated the DUT would see a string of pulses. Two splitter designs have been implemented:

- A 6 dB splitter using 3x16 Ohm resistors
- A 10 dB splitter having a somewhat more complex resistor network.

Both splitters have similar S11 and S21 performance but the 10dB splitter allows a stronger reduction of the circulating pulses.

Figure 2.47 shows the structure of the 6 dB splitter, the 3 resistors used in our case are all 18 Ω resistors. Figure 2.48 is the photo of the splitter after adding further layers of insulation (for high voltage) and return path control. Figure 2.49 shows the internal structure of the 10 dB splitter before adding further layers of insulation for high

voltage and return path impedance control. After closing the splitter its performance is shown below.
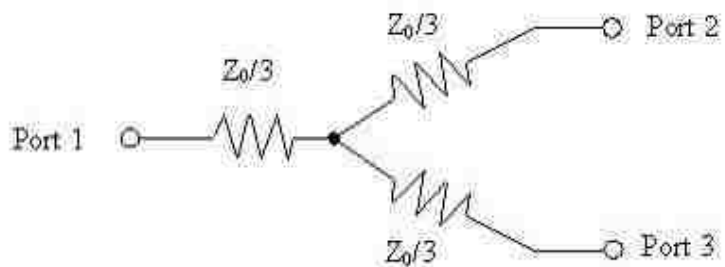
Figure 2.47. Structure of the 6-dB Splitter

Figure 2.48. Photo of 6 dB Splitter

Figure 2.49. Photo of the 10-dB Splitter

2.3.3. Polarity Inverter. The objective of the polarity inverter is made to change the polarity of one output signal from the splitter. In this case, one can add up the two signals coming out of the splitter by adding the inverter to one output port.

Figure 2.50 shows that the two signals coming out from the two output ports are very similar to each other. The splitter can be used up to 2 GHz, and the attenuation is between 9.5 and 10.5 dB up to 2 GHz. The phase differences are small, and are not shown here. Figure 2.51 is the photo of the inverter.
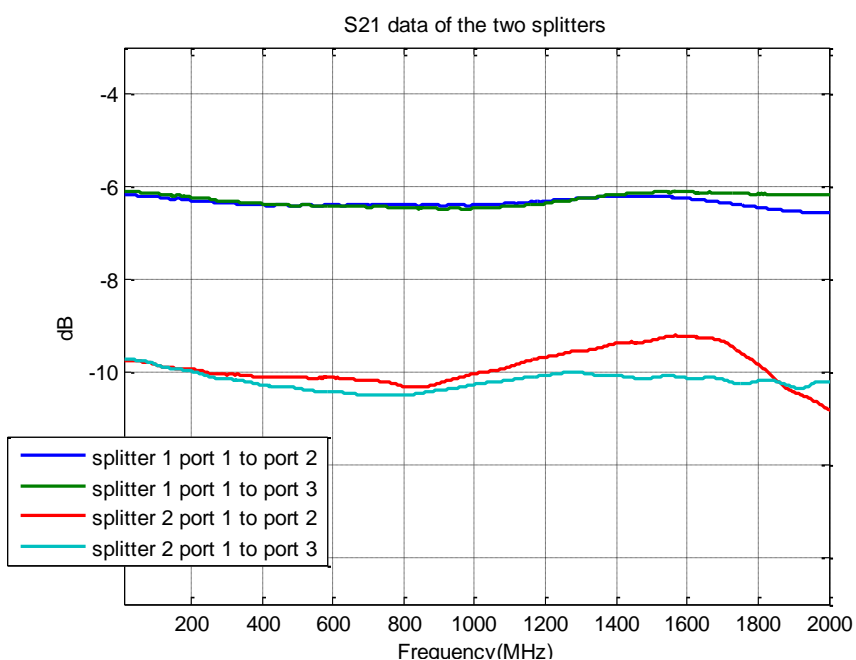
Figure 2.50. The S21 from Input Port to Output Ports of the Two Splitters

Figure 2.51. Photo of the Inverter

Figure 2.52 shows the structure of the inverter. The inner and outer conductors of one coax cable are exchanged within the inverter to change the polarity of the signal. The outer conductors are reconnected at the two ends. For DC components this is a short, the ferrites inside provide a high impedance path, in this way the higher frequencies are not shorted.
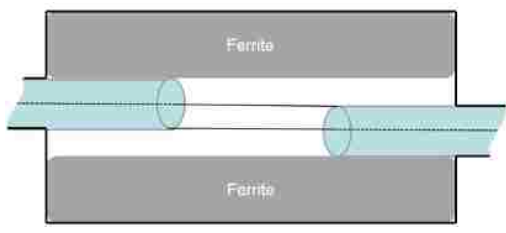
Figure 2.52. Polarity Inverter

Figure 2.53 shows the phase shifting data using the inverter measured by a Network Analyzer.
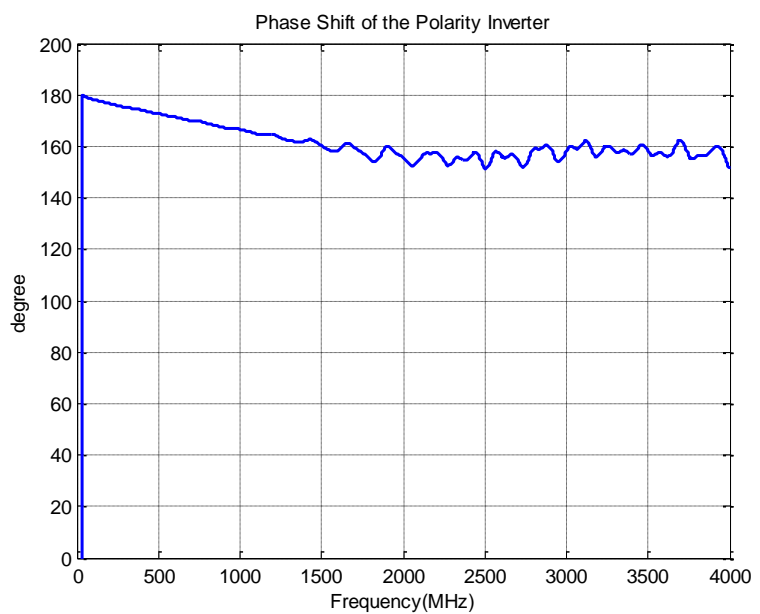
Figure 2.53. Phase Shift Using the Inverter

During the measurement, one end of the inverter is connected to a cable, and then to port 1 of NWA, the other end is connected to port 2 of the NWA. S21 phase in frequency domain is measured. The phase shift of the two ports is about 160 to 180 degrees up to 4 GHz.

2.3.4. Spice Model of the ΣΔ Probe. The SPICE model (shown in Figure 2.54) is to understand the suppression of circulating pulses by the splitter design and to use the model as reference for better analysis of test results. The SPICE model includes the splitter, inverter and main coaxial connectors. The coupling to the test trace is modeled as a small capacitor for the case in which the probe is used as a summing probe (E-field). Table 2.3 shows the meanings of the components in the model.
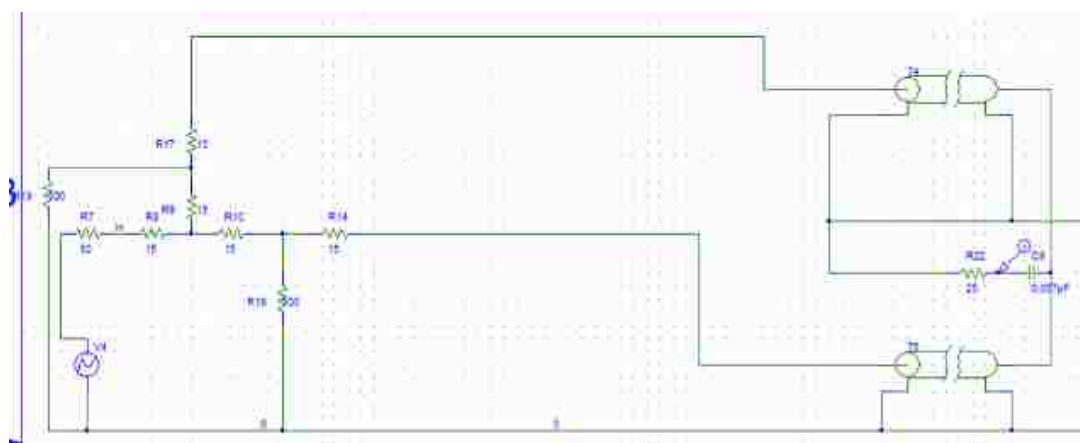
Figure 2.54. Spice Model for the E-field Coupling

Table 2.3. Components of the Spice Model

Components	Physical Meaning
R8 R9 R10 R14 R17 R18 R19	splitter
T4 T5	Probe cable
C9	Capacitive coupling from probe to trace
R22	Load
V4/R7	Source voltage/ impedance of the source

The capacitance is calculated by

$$C = \varepsilon_r \varepsilon_o \frac{A}{d}$$

(6)

The dielectric constant of scotch tape which is used as spacer between trace and probe is about 3.2, the area is about 2 mm^2, and the distance between the two is about 1 mm. So the capacitance between the two is about 0.057 pF (C9 in the Spice model). Figure 2.55 shows the results from the SPICE simulation.
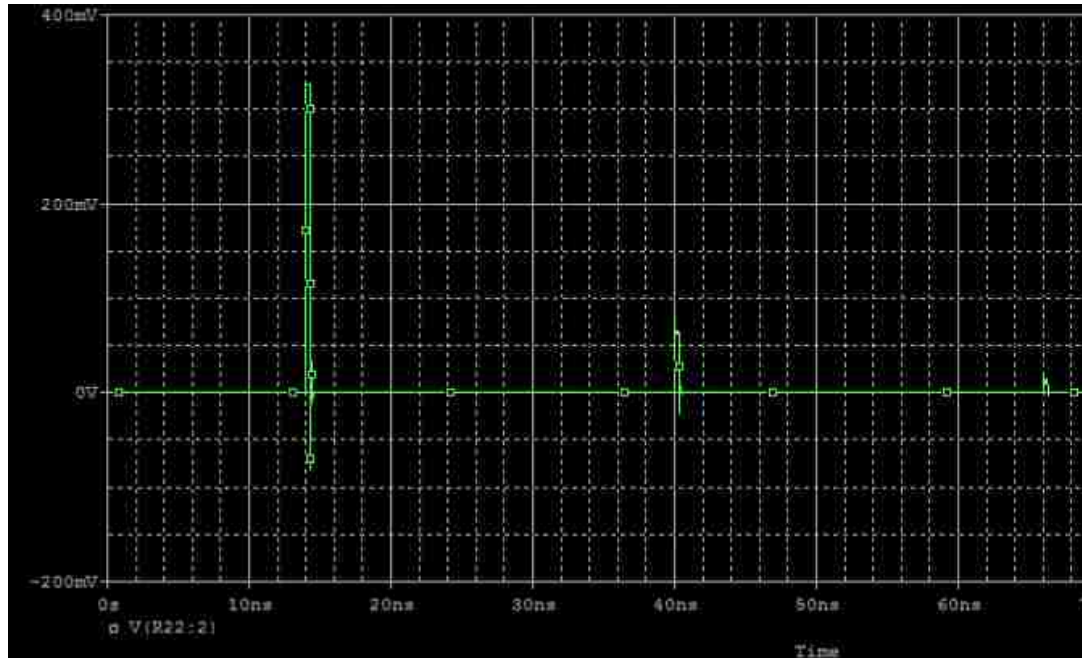
Figure 2.55. Spice Simulation Result in Time Domain

The simulation shows that the amplitude of the pulse is about 350 mV, and time interval between the repeated pulses is about 26 ns. The source voltage is 210 V, as when the charge voltage of the TLP is set to be 500 V, the output voltage the test subject see is about 210 V. Figure 2.56 shows the SPICE model for the H-field coupling. Figure 2.57 is the simulation result. Table 2.4 shows the measurement of the components.
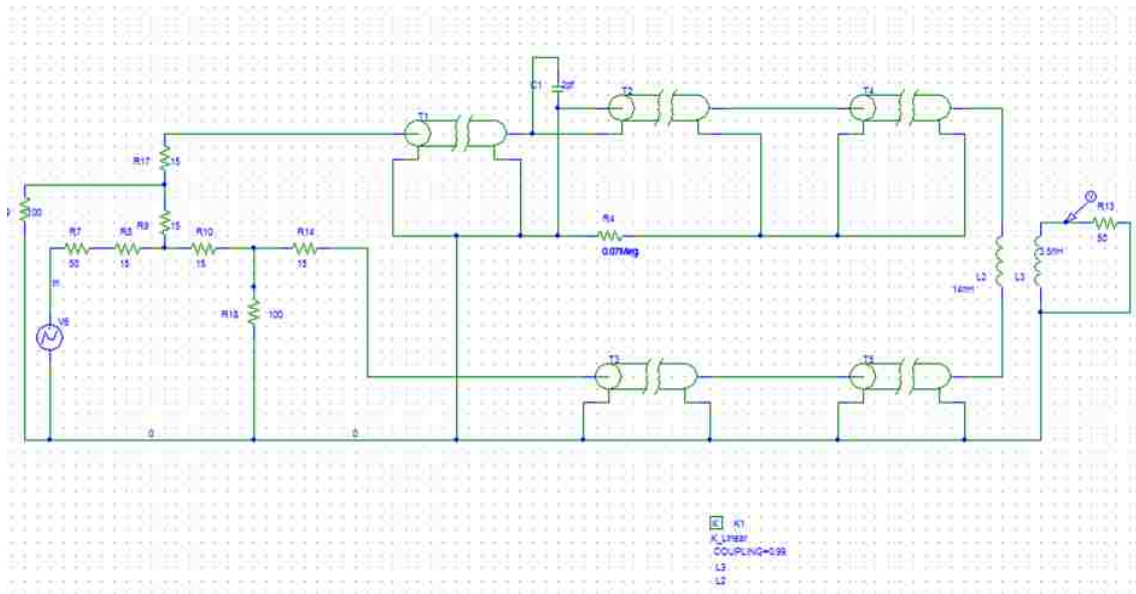
Figure 2.56. PSPICE Model for the H-field Coupling

Table 2.4. Components of the Spice Model

Components	Physical Meaning
R8 R9 R10 R14 R17 R18 R19	splitter
T1 T2	inverter
T3 T4 T5	cable
L2 L3	inductive coupling from probe to trace
R 13	load
V4/R7	source voltage/ impedance of the source
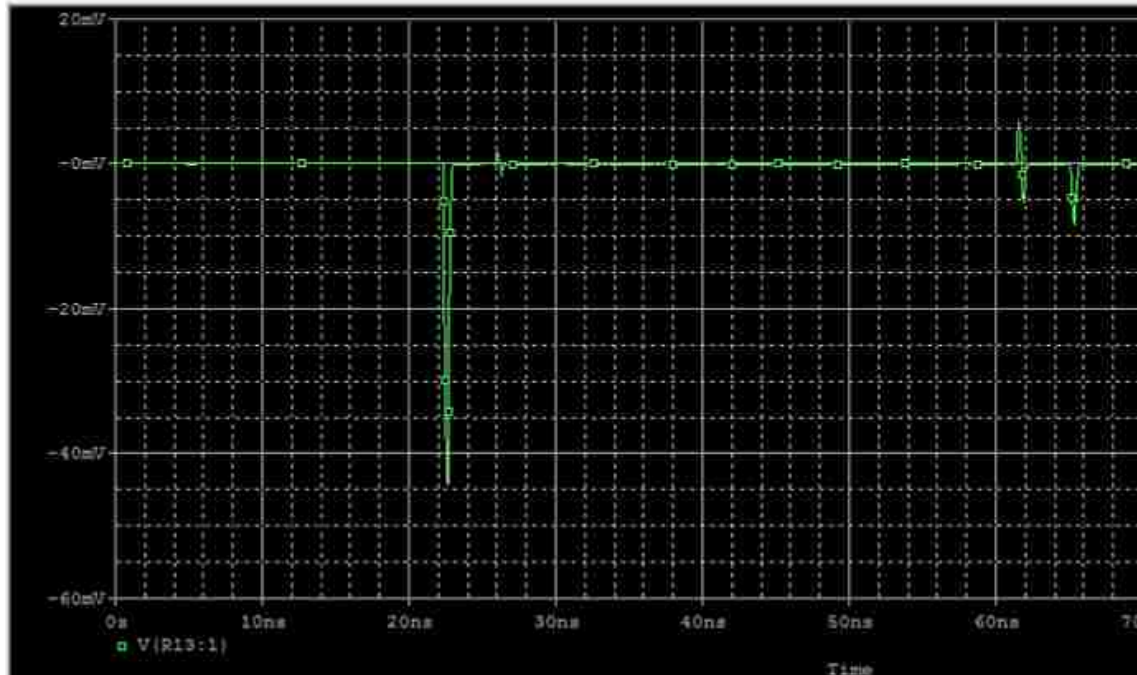
Figure 2.57. PSPICE Simulation Result of the Model

The simulation result shows that the amplitude of the signal is about -45 mV with 500 V charge voltage, and the interval between the repeated pulses is 40 ns.

2.3.5. Suppression of Undesired Field Components. The objective is to measure the H-field suppression in E-field mode of the $\sum\Delta$ Probe, as well as the E-field suppression in H-field mode of the $\sum\Delta$ Probe. The test setup is shown below.

Figure 2.58 shows the setups for the measurement in both modes. In the E-field mode, the inverter is not added, when the hybrid is set to be 0 deg, the two signals with the same phase are added. In this case, the expected E-field in E-field mode is measured. On the other hand, when the hybrid is set to be 180 deg, the two signals are with the same phase will be canceled.   In this case, the unwanted H-field in E-field mode is measured. The test setup in Figure 2.59 used the same method but with the inverter added. Figure 2.60 is the S21 result showing the suppression of undesired fields.

Hybrid 0 deg without inverter

Hybrid 180 deg without inverter
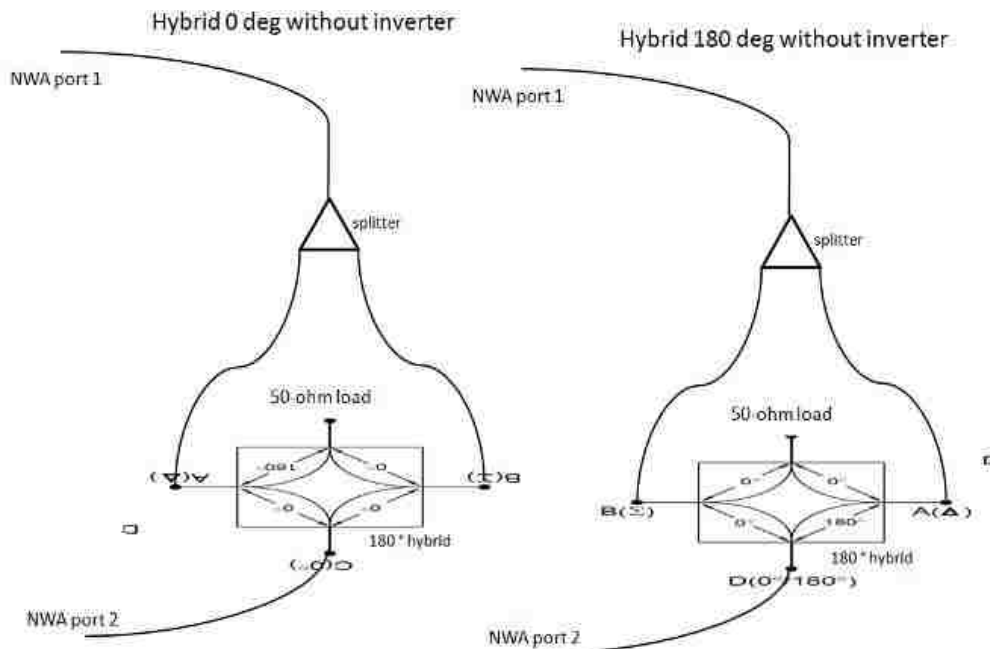
Figure 2.58. Test Setup to Measure the H-field Suppression in E-field Mode

Hybrid 180 deg with inverter

Hybrid 0 deg with inverter
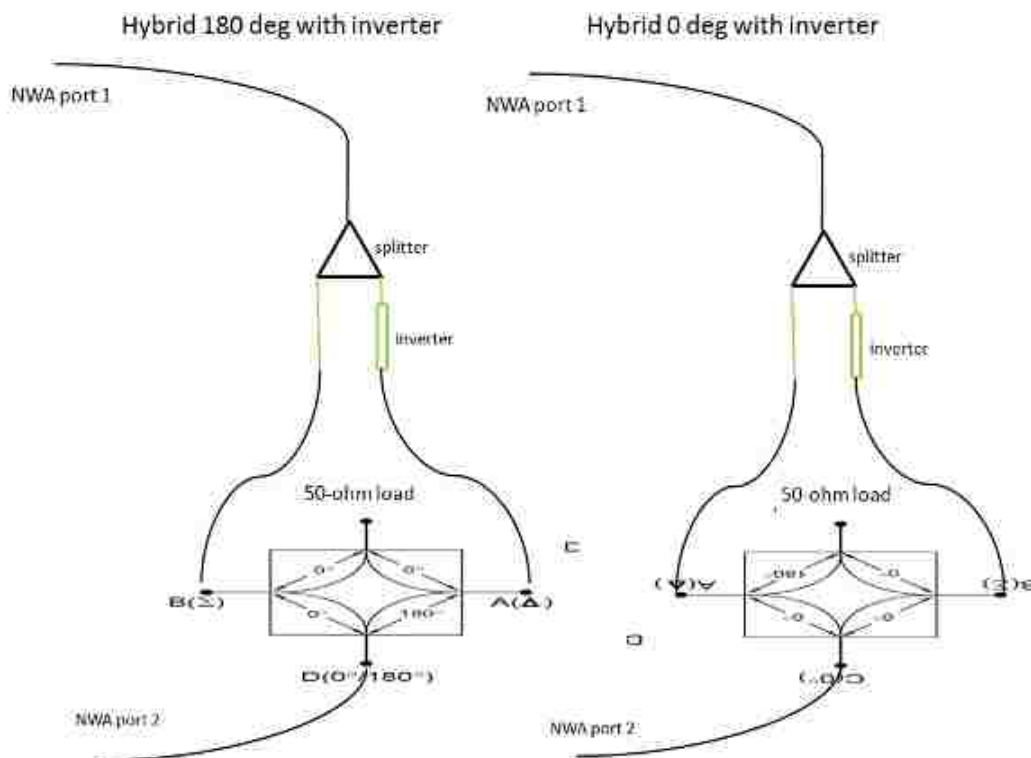
Figure 2.59. Test Setup to Measure the E-field Suppression in H-field Mode

H-field suppression in E-field mode and E-field suppression in H-field mode
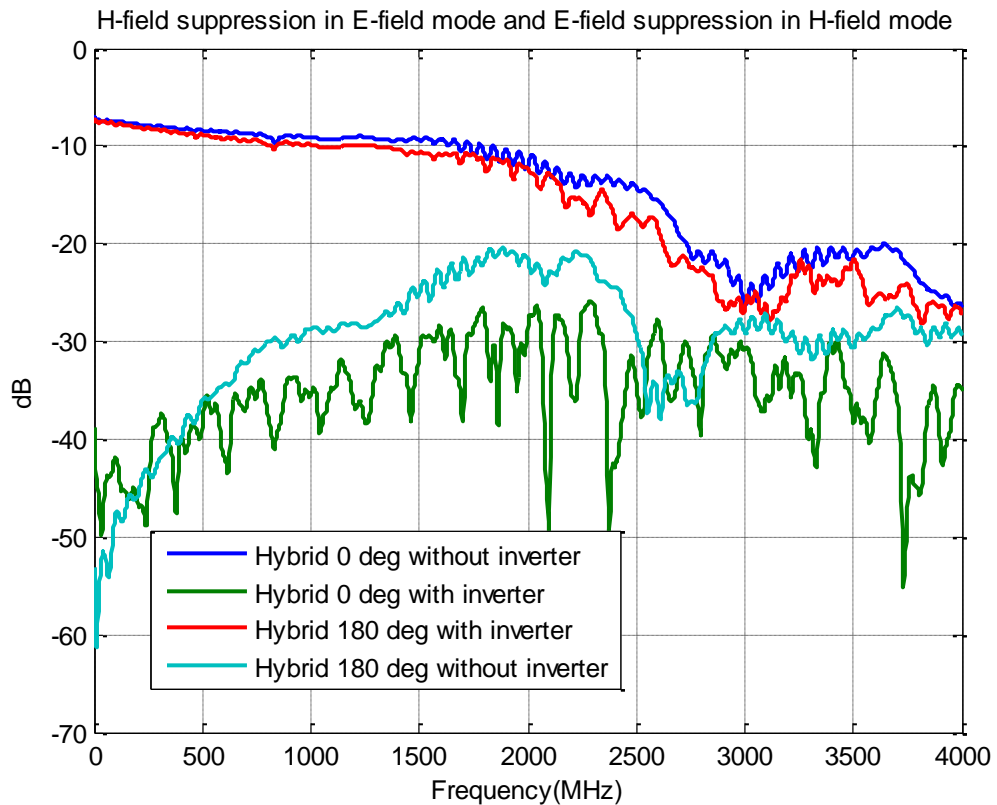
Figure 2.60. S21 Result for the Suppression Measurement

The above figure shows that the unwanted H-field in E-field mode is 20 to 30 dB less than the E-field. And the unwanted E-field in H-field mode is 10-30 dB less than the H-field. The suppression is sufficient, and fields in both modes are very homogeneous.

2.3.6. Characterization of the ΣΔ Probe. Figure 2.61 and Figure 2.62 are the frequency domain and time domain characterization setup.

In the test setup shown in Figure 2.61, the two orange cables have the same length; the green cable and the inverter cable also have the same length. This means the cables from two output ports of the splitter to the two input ports of the hybrid have the same total length. S21 is measured from 1 MHz to 3 GHz. The excitation power is 10 dBm. Inverter is only used in the H-field coupling mode.
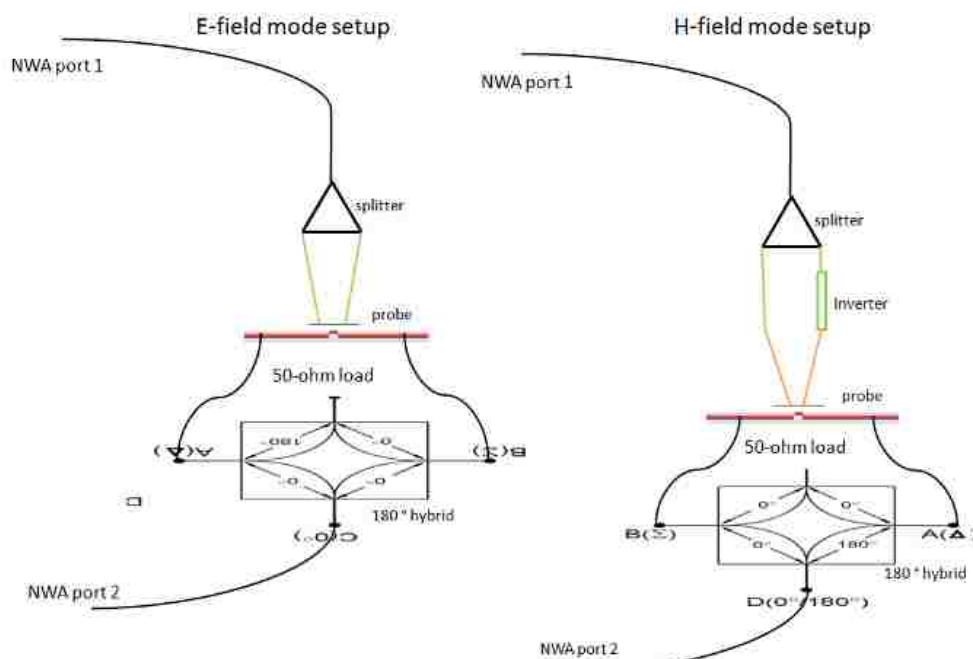
Figure 2.61. Frequency Domain S-parameter Measurement Setup in Both Modes
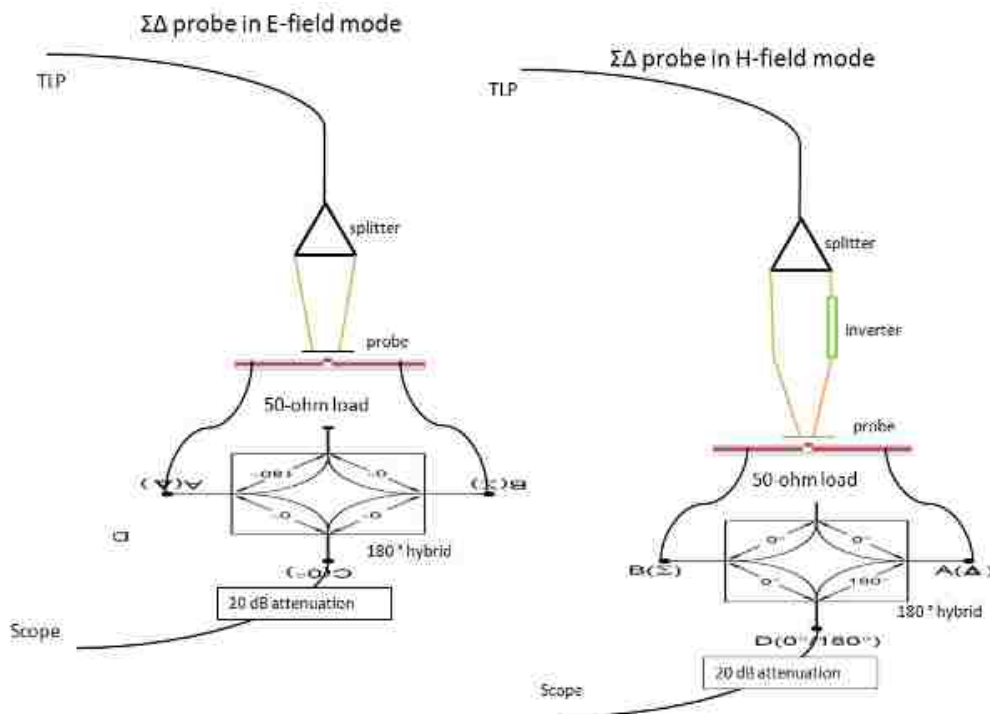
Figure 2.62. Time Domain Induced Voltage Measurement Setup in Both Modes

In the measurement showing in Figure 2.62, the TLP charge voltage is set at 500 volt. A 10 dB attenuator is added to protect the scope. Inverter is only used in the H-field coupling mode. The cables from two output ports of the splitter to the two input ports of the hybrid have the same total length.

Figure 2.63 shows that the S21 follows 20 dB per decade capacitive coupling from the probe to the trace. The resonance formed in the system is about 2 dB.
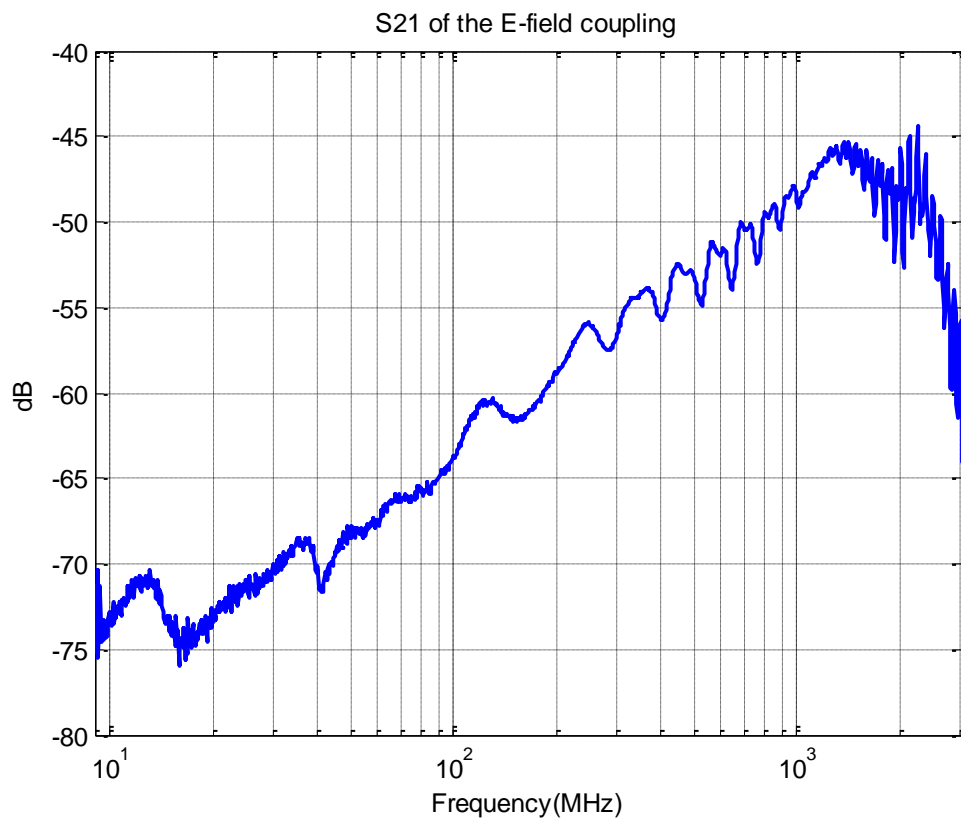
Figure 2.63. S21 of the Probe in E-field Mode

Figure 2.64 is the measured waveform for E-field coupling, when the probe is charged with 500 V from the TLP. Figure 2.65 shows the comparison between the measurement results and simulation results.
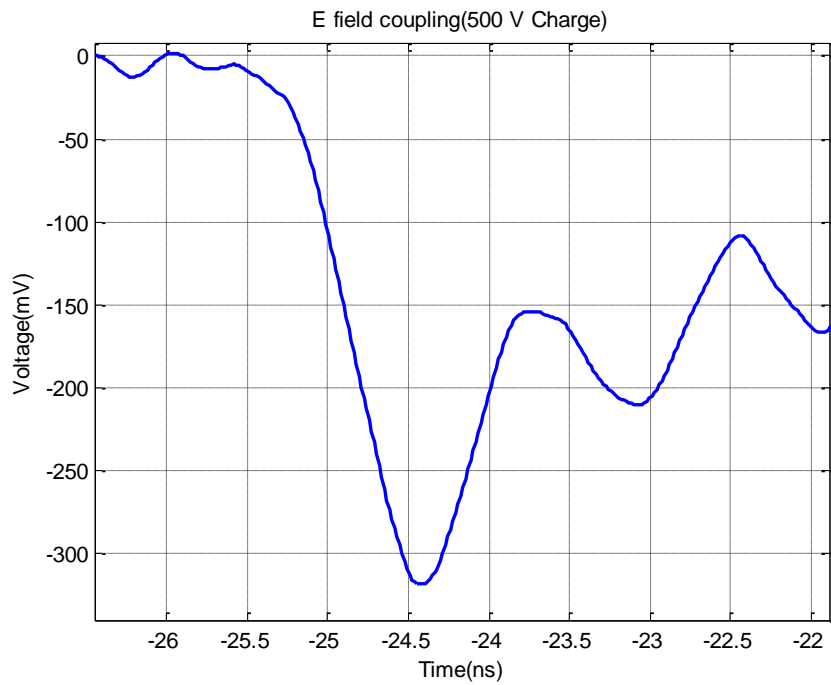
Figure 2.64. Induced Voltage from Probe to Trace at 500 V (zoomed in)
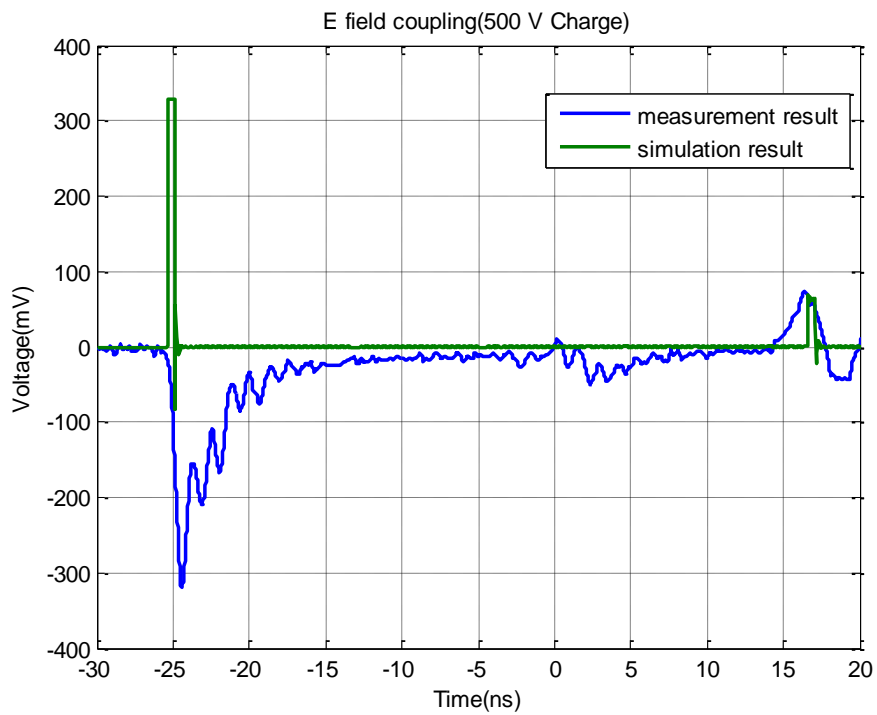
Figure 2.65. Induced Voltage from Probe to Trace at 500 V

From the above figures, one can see that the amplitude of the induced voltage from E-field coupling is about 325 mV, the rise time is about 700 ps, and the time interval between the pulses is about 42 ns. The measurement result is very similar to the SPICE simulation result. Figure 2.66 shows the S21 of the probe in H-field mode coupled to a 4 mm trace. It's mainly the inductive coupling from probe to trace following a 20 dB per decade slope.
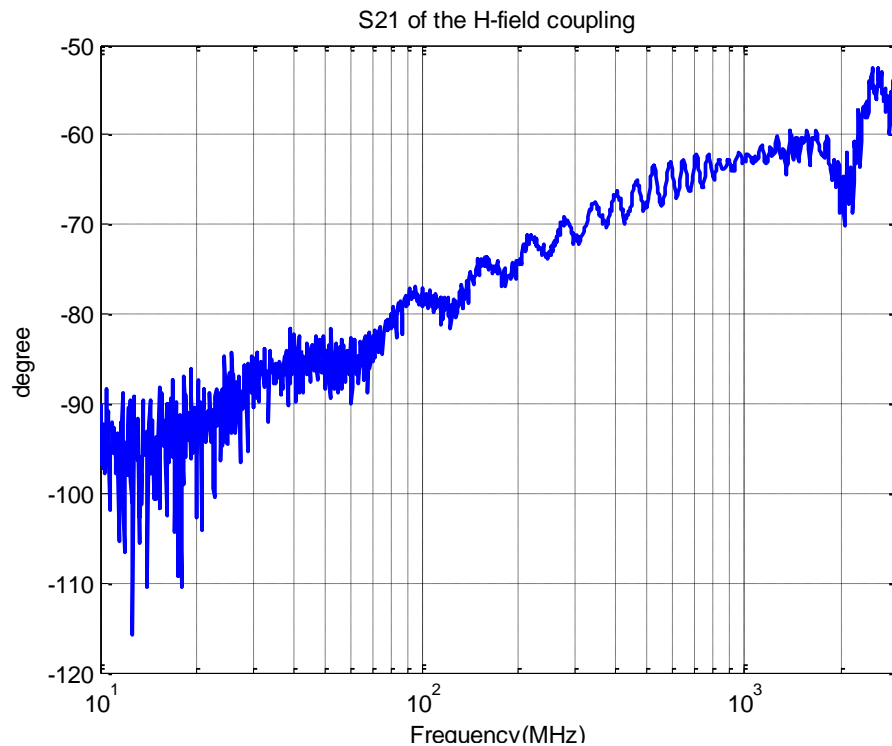
Figure 2.66. S21 of the H-field Coupling

Figure 2.67 shows the amplitude of the induced voltage from probe to trace in the H-field mode is around 45 mV, and the time interval between repeated pulses is about 43 ns. The measurement result and the simulation result are similar with respect to rise time and maximal value.
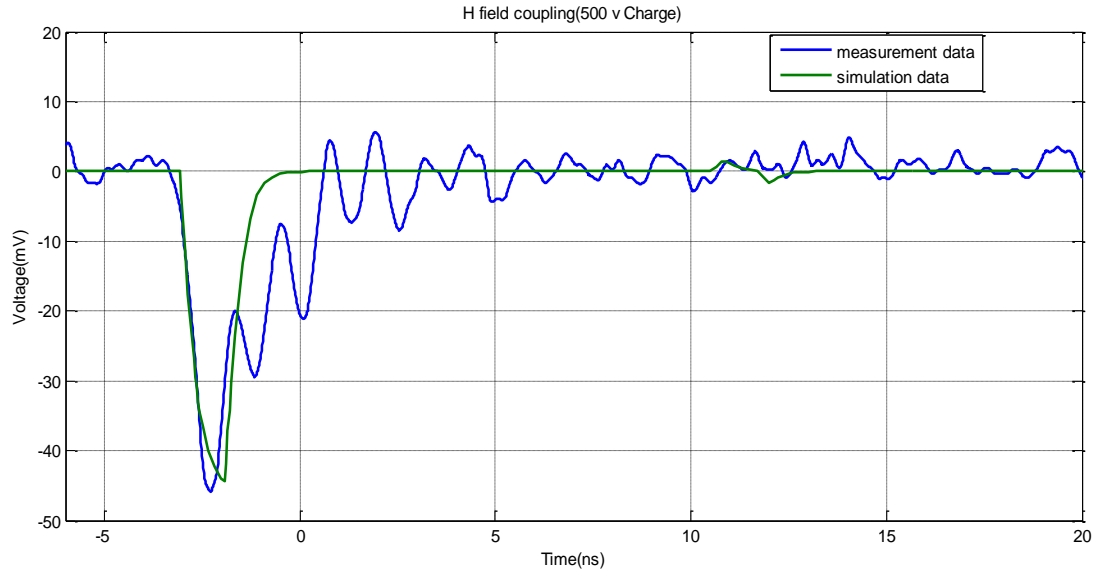
Figure 2.67. H-Field Coupling in Time Domain at 500 V

Figure 2.68 shows the model of the ΣΔ probe in E-field mode coupling to a trace. The two ports are driven in common mode simultaneously, each trace end is terminated with a 50-ohm lumped element. The probe is placed on top of the trace, and the probe trace is in parallel with the receiver trace.
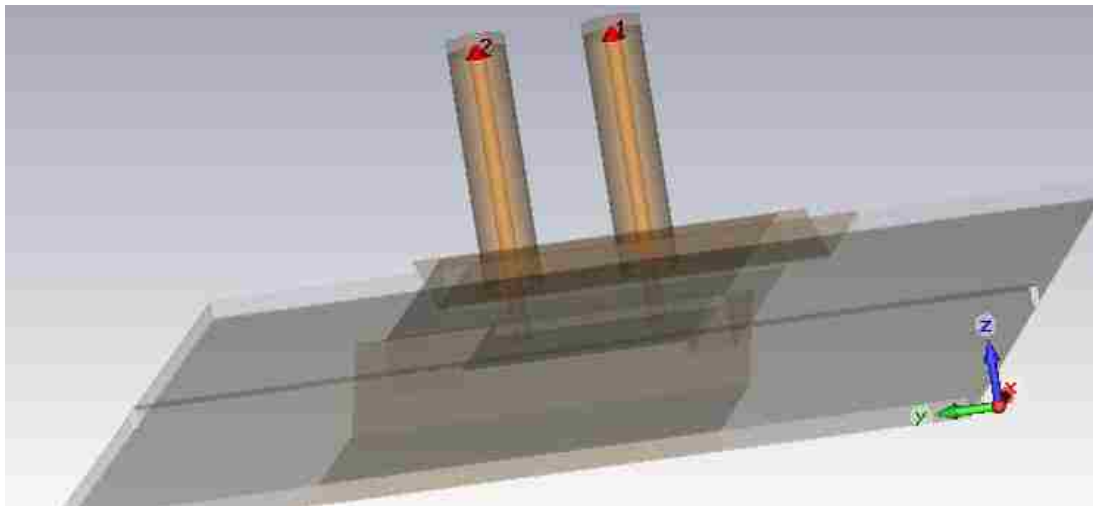
Figure 2.68. Model of the Induced Voltage to a Trace in E-field Mode

2.3.7. Measurement of the Induced Voltage in E-field Mode. Table 2.5 shows the configurations of the setup, and Figure 2.69 shows the test setup of the measurement.

Table 2.5. Configurations of the Measurement

Trace angle	Inverter	Load condition	Dominating field
In parallel with trace	No	50-ohm at one end	E-field

Figure 2.69. Measurement Setup

Figure 2.70 is the comparison of the simulation result and the measurement result. The two waveforms are very similar, but the simulation is about 7.5 V higher than the measurement result.
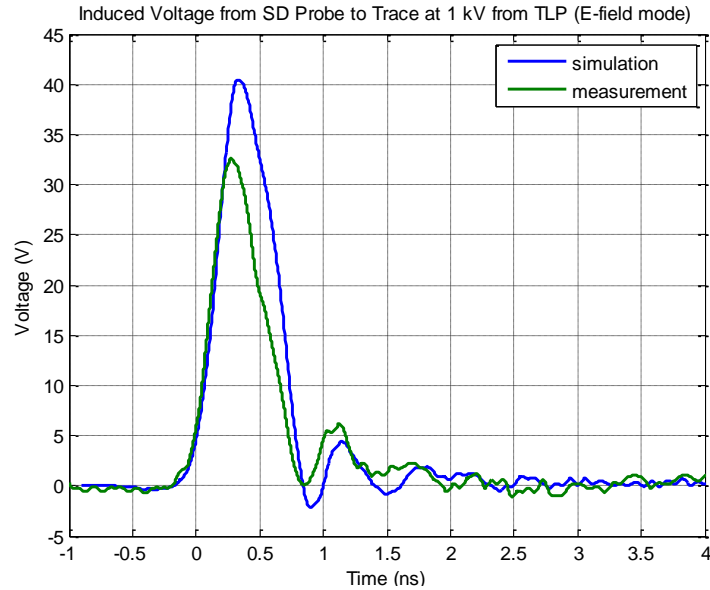
Figure 2.70. Comparison of the Simulation and Measurement

2.3.8. Simulation and Measurement in H-field Mode. Figure 2.71 shows the model of the ΣΔ probe in E-field mode using a trace. The two ports are driven in differential mode simultaneously; each trace end is terminated with a 50-ohm lumped element. The probe is placed on top of the trace, and the probe trace is in parallel with the receiver trace.
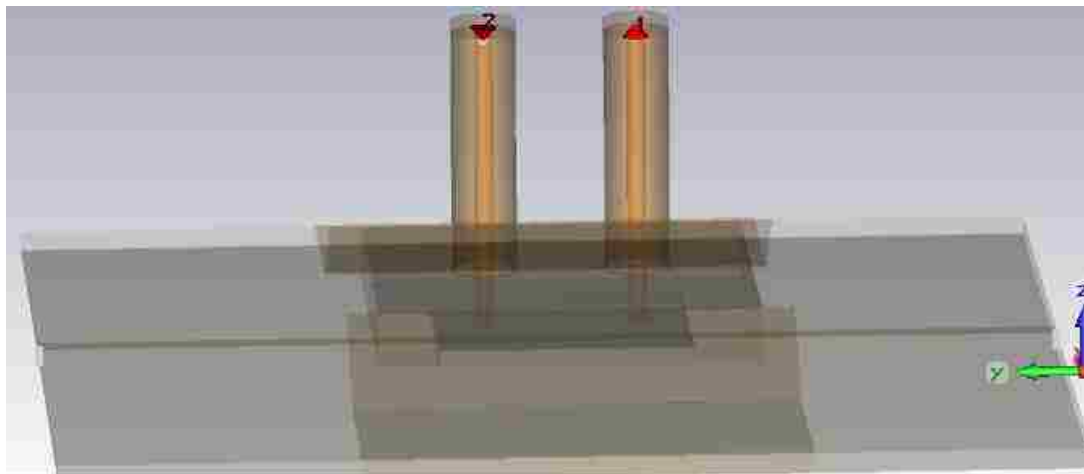
Figure 2.71. Simulation Model of the ΣΔ Probe in H-field Mode

Table 2.6 shows the configurations of the setup, and Figure 2.72 shows the test setup of the measurement.

Table 2.6. Configuration of the Measurement

Trace angle	Inverter	Load condition	Dominating field
In parallel with trace	Yes	50-ohm at one end	H-field
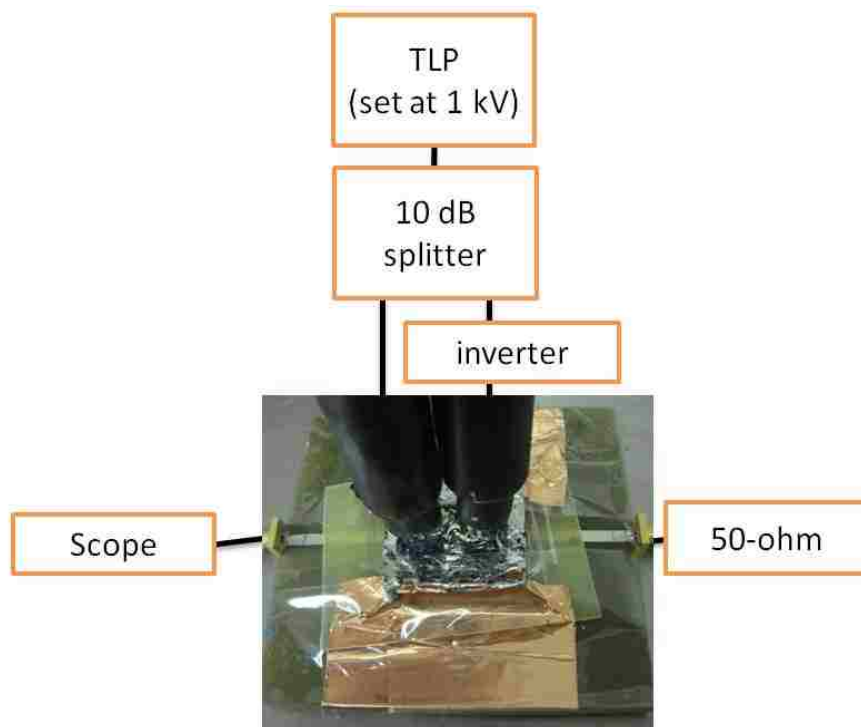
Figure 2.72. Test Setup in H-field Mode

Figure 2.73 is the comparison of the simulation result and measurement result of the induced voltage in H-field mode. The two waveforms are very close, and the difference between the two peaks is only about 0.5 V, which is less than 10%.
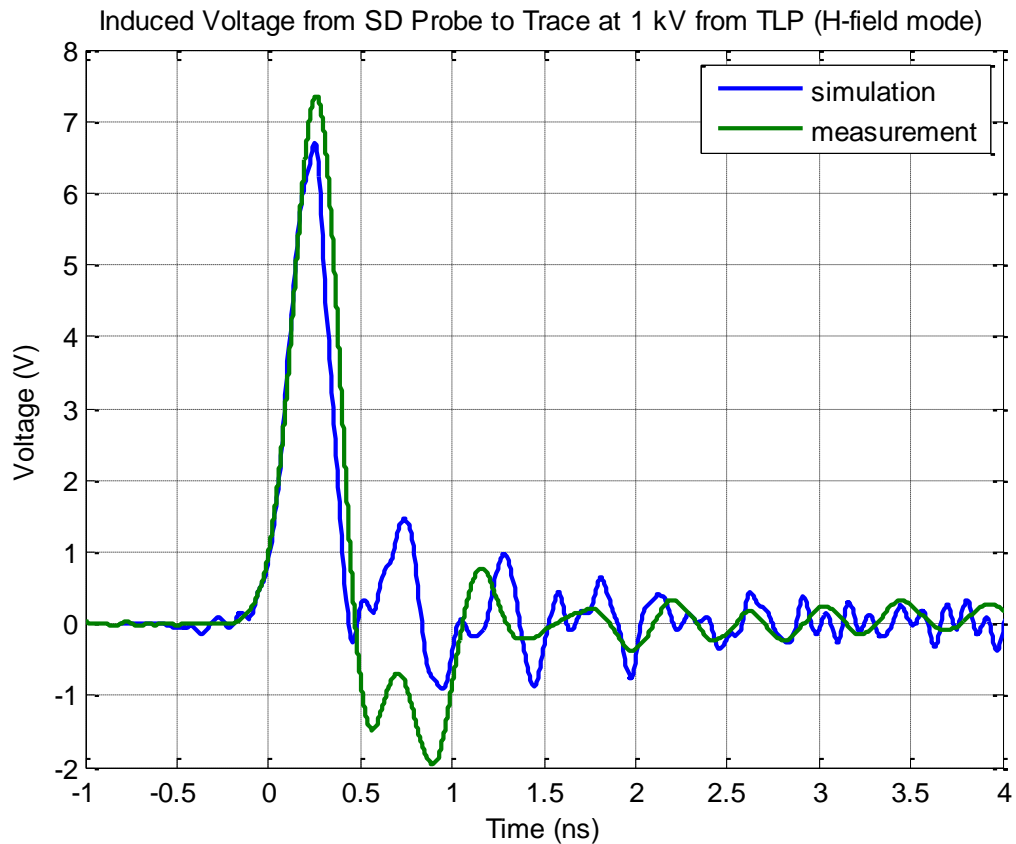
Figure 2.73. Comparison of the Simulation and Measurement

2.3.9. Measurement of the Induced Voltage in H-field Mode. One impedance adjustment line (874-Lk20L constant impedance adjustment line 20 cm) is used to adjust the difference of the two cables to make them highly equal. Figure 2.74 is the photo of the test setup. The TLP is set at 1 kV, and the 10 dB self-built splitter is used to split the signal. Instead of using the paired reference cable, a longer cable is used as the reference, since the length of the impedance adjustment line will add certain length to the inverter. The outputs of the trace ends are connected directly to channel 1 and channel 3 of the Oscilloscope.
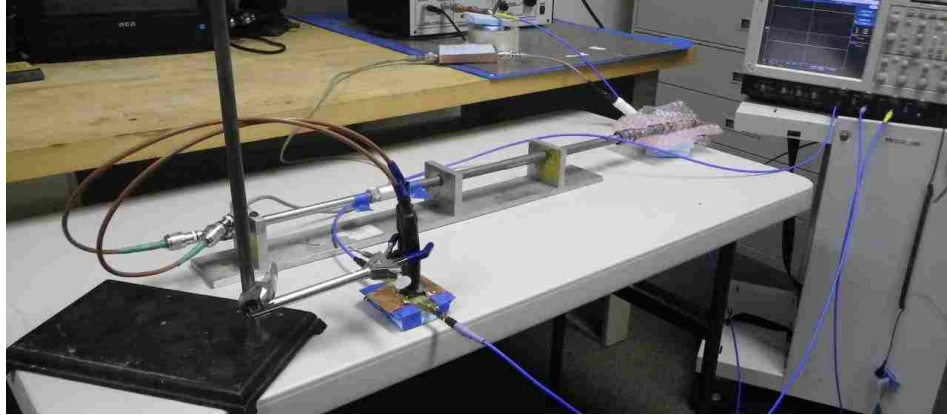
Figure 2.74. Test Setup for the Induced Voltage with the Impedance Adjust Line

First, the waveforms at the two channels are compared. The two cables in the simulation are always identical and balanced; it is necessary to ensure balanced measurement results, in order to compare the results of simulation and measurement.

Figure 2.75 and Figure 2.76 are the results from the two ends of the trace with and without the extra ground connection. One can see that the initial pulses of from the two trace ends are identical after the impedance adjustment line is added.
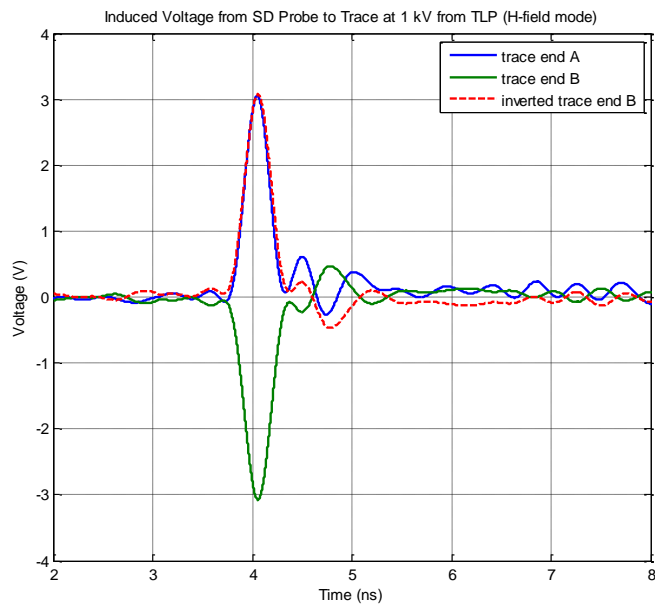
Figure 2.75. Comparison of the Two Channels of Probe in H-field Mode
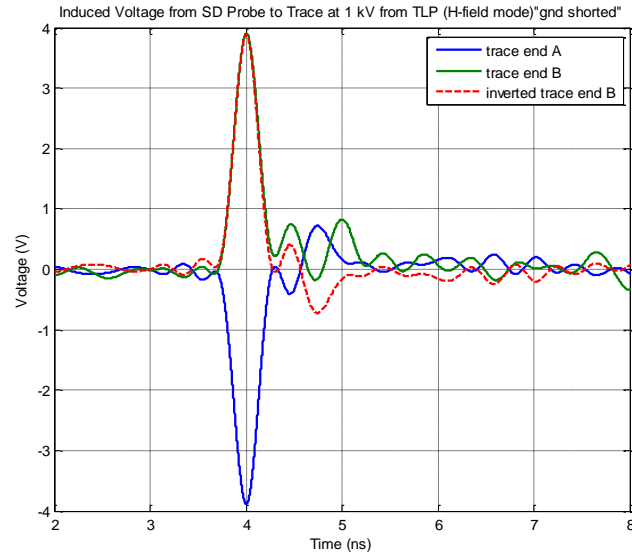
Figure 2.76. Comparison of the Two Channels of Probe in H-field Mode

2.3.10. Comparison of the Waveforms with or without Extra Ground Connection. To minimize the influence of the common mode impedance which is difficult to model, an extra connection is added to create a path for the common mode current to flow.

Figure 2.77 is the photo of the probe on the trace board with and without the extra ground connection. The rest of the test setup stays the same as shown in Figure 2.74.
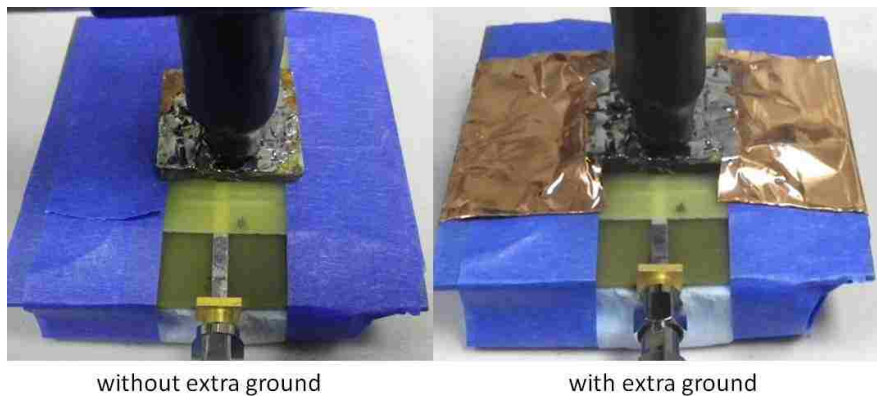
Figure 2.77. Photo of the Extra Ground Connection

Figure 2.78 shows the results comparison of the induced voltage waveforms with and without the extra ground connection. With the ground connection, the peak value is 4 volts, which is 1 volt higher than the value when it's not added. The difference is smaller than assumption that the inverter is sufficiently balanced.

Comparison of the Induced Voltage with and without the Extra Ground (H-field mode)
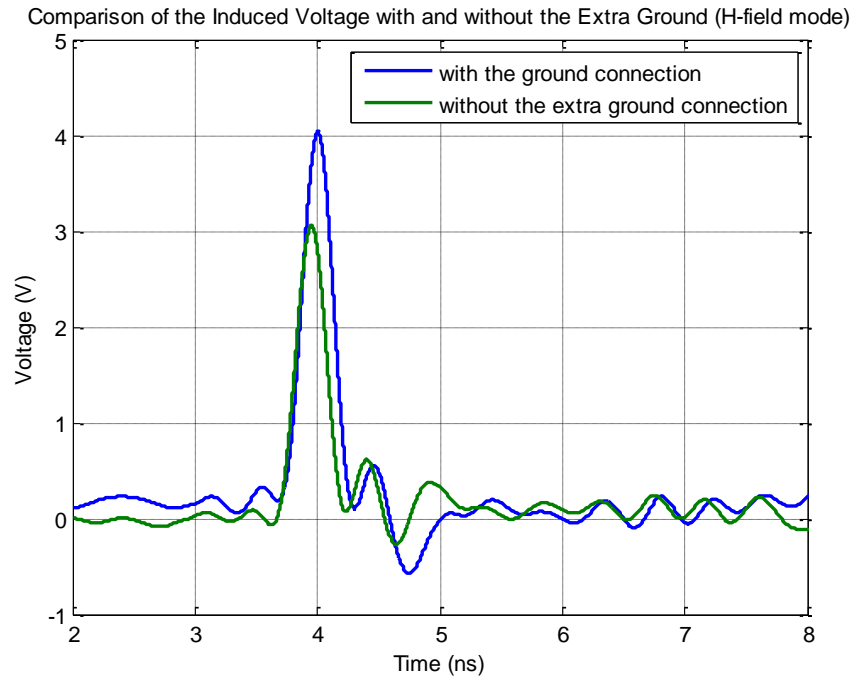
Figure 2.78. Comparison of the Induced Voltages

2.3.11. Comparison of the CST Simulation and Measurement. The simulation results and measurement results are compared after the impedance adjustment is added to the setup. Now, the two channels have the exactly the same amplitude, same as the case in the simulation.

Figure 2.79 is the simulation model of the probe driven in H-field mode, coupling to a 50-ohm trace.
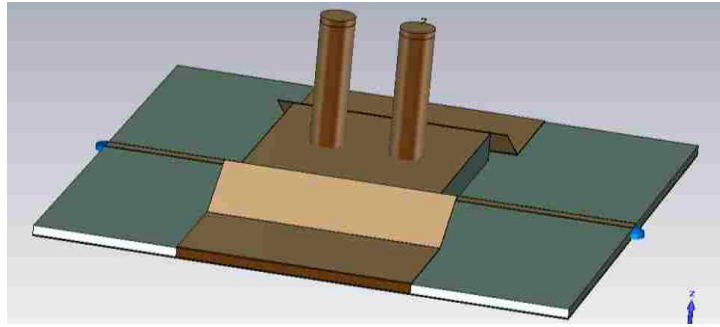
Figure 2.79. Simulation Model of the ∑Δ Probe in H-field Mode

Figure 2.80 shows the comparison of the simulation and measurement results. The two waveforms have similar shape and rise time. But the peak value of the simulation is much higher than the measurement. There are many possible reasons for getting a lower value in the measurement results, as described in the above table. Those expected difference can all be minimized, but hard to avoid in the measurement. The possible contributions of each of these reasons can be added up, and cause a big difference in the comparison.
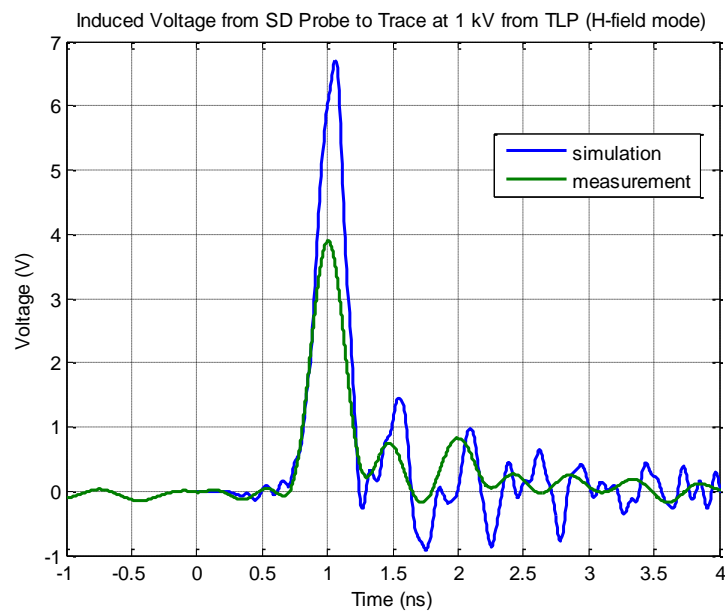
Figure 2.80. Comparison of the Simulation and Measurement in H-field Mode

2.3.12. Magnetic Field Strength and Field Derivative of the ΣΔ Probe. The objective of the calibration is to scale the induced voltages of the crash level to field strength and field strength. Then one can use the results scaled in field and field derivative, and compare it to the block level simulations. The test object of this week is the ΣΔ probe in H-field mode.

One shielded H-field probe is selected as the reference probe, and its effective area is calculated using TEM cell. The first step is to determine the effective area of the reference probe, and the second step is to determine the field strength of ΣΔ probe in H-field mode using the reference probe as a receiver.

In the test setup, a TEM cell is used to excite the reference probe. The loop size of the probe is 1 mm². The vertical H-field components are measured by the reference loop probe. During the measurement, a 10 cm ×10 cm board with a slot is used to cover the top wall of the cell, and the probe is inserted into the cell through the slot. The excitation from the Network Analyzer is set to 10 dBm. The effective area 1.59 mm² as calculated.

The test setup of step 2 is shown in Figure 2.81. A TLP is used as the source to inject pulse to the H-field probes. The charge voltage of the TLP is 1000 V during the measurement. And the reference probe is placed vertically to the reference probe to measure the field generated from the ΣΔ probe.
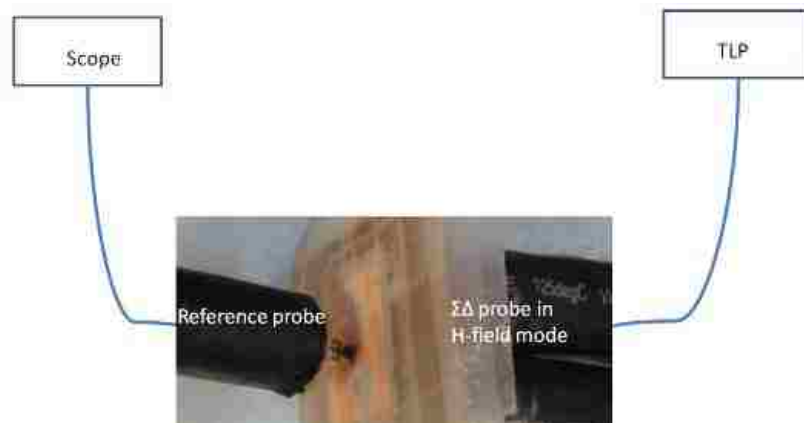
Figure 2.81. Test Setup

Two distances between the probes are selected during the test, one is 0, and the other is 1 mm. A piece of foam which has a thickness of 1 mm is used as the spacer between the two probes. The equation we used is to calculate the field strength and field strength derivative is:

$$\frac{dH}{dt} = \frac{V}{A\mu}$$

(7)

And then the field strength is calculated by integrating the field derivative. The measured and calculated waveforms are shown from Figure 2.82 to Figure 2.84.
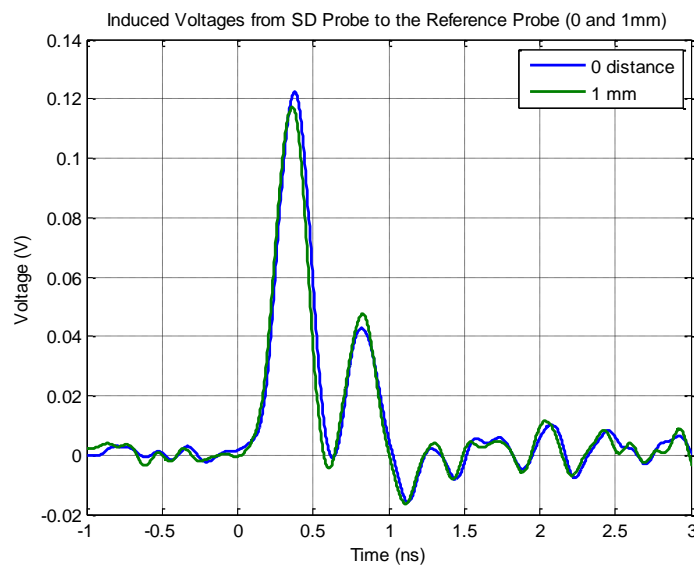
Figure 2.82. Induced Voltage from $\Sigma\Delta$ Probe to the Reference Probe
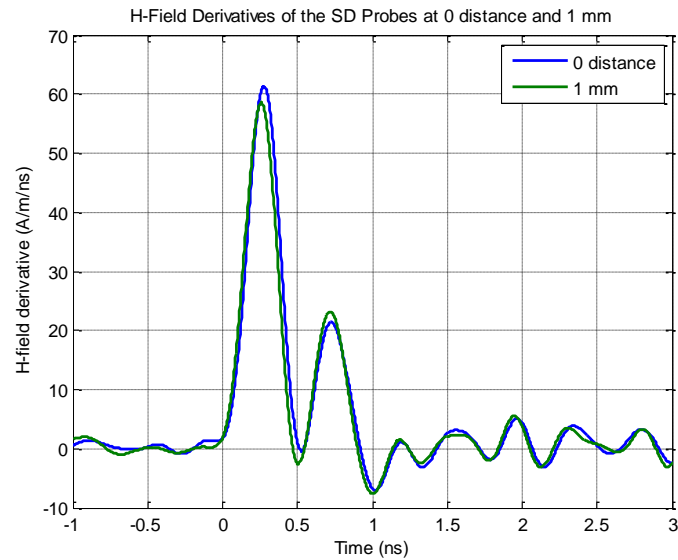
Figure 2.83. Field Derivative of the ΣΔ Probe in H-field Mode at 1000 V
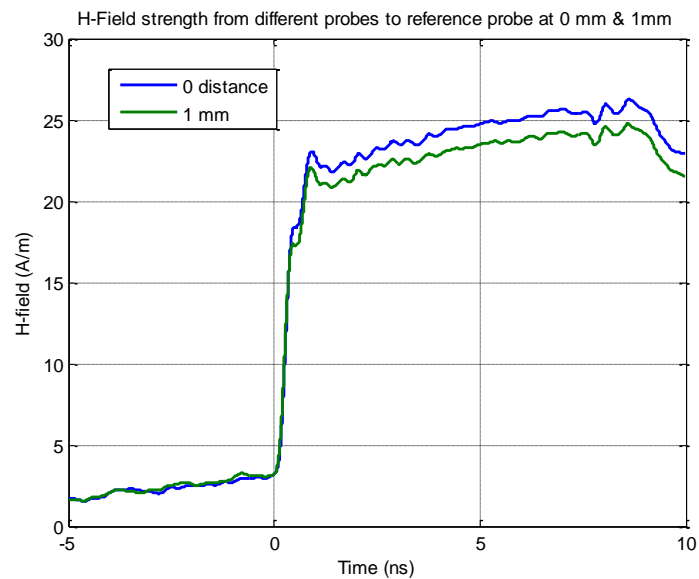
Figure 2.84. Magnetic Field Strength of the Probe at Two Distances at 1000 V

2.3.13. Field Injection to ICs with the ΣΔ Probe. Figure 2.85 shows the structure of probe on a test IC in the E-Field injection measurement, lossy material is added to create a current return path for the high frequency components, low frequency

components will return through the outer conductor of the coax cable and somehow then through the grounding of the test equipments and the device under test.
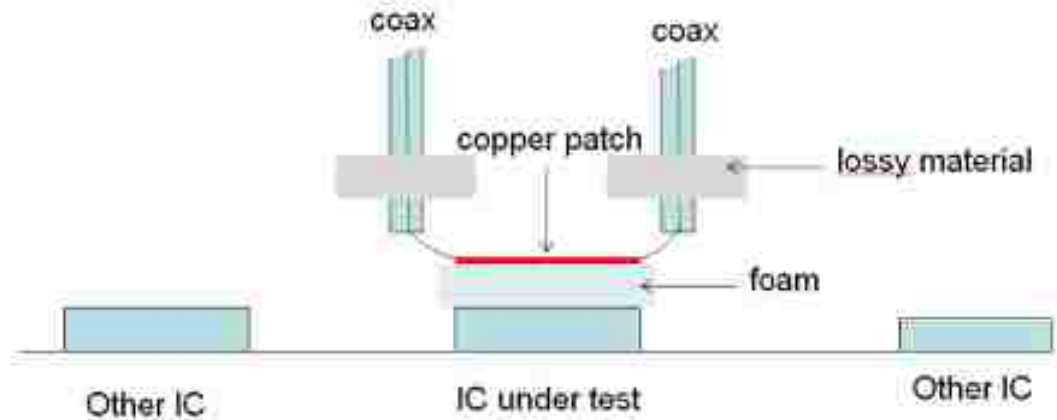
Figure 2.85. Probe on a Test IC

Figure 2.86 shows the E-Field injection setup for both E-field and H-field injection. For H-field injection, the polarity inverter will be added to change the direction of the signal in one coax cable. The signals in two cables are then in phase. In this case, the current will flow from one side of the patch to another side, which creates magnetic field.

For E-Field injection polarity inverter will be removed. The two signals coming out of the splitter will be out of phase. No current will flow on the patch, but potential difference between the patch and the IC will create an E-field coupling.
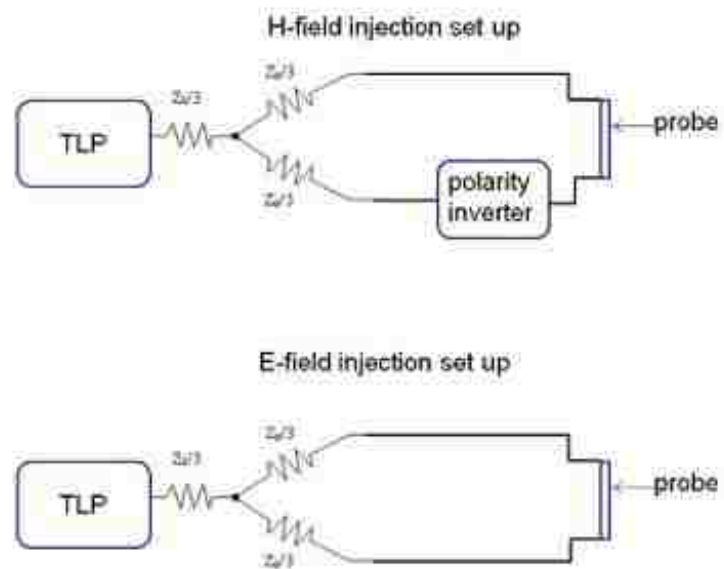
Figure 2.86. Field Injection Setup

3. TEM CELL AND IC STRIPLINE

3.1. TEM CELL FOR HIGH VOLTAGE IMMUNITY TESTING

3.1.1. Limitations of Standard TEM Cells. The standard TEM cell is well suited for emissions measurement. It holds a 10x10cm board. It is only useful up to 1GHz due to higher order resonances. The standard IEC 62132-2 [8] describes procedures for evaluating the radiated emissions and electromagnetic immunity of integrated circuits (ICs) using a TEM cell up to 1 GHz. For improved high frequency performance a TEM cell with higher order mode suppression was designed [12] .

One important requirement for the using the cell as an immunity test cell is that the field strength needs to be strong enough. The commercial version of the cell has a distance of 50 mm from the IC to the septum. The connectors limit the voltage to about 4kV. Thus, the highest achievable E-Field strength is about 8kV/m. This is often not sufficient to cause crashes in ICs.

The short example below illustrates this. If assuming a memory IC having a lead frame to PCB ground distance of 1 mm, and the PIN to PIN distance of 10 mm, then a loop of 10^{-5} m^2 has been created within and underneath the IC. Further, if assume the E-Field strength is 8kV/m, a 377 Ohm TEM field and a rise time of 1 ns.

The magnetic field is about 21 A/m, leading to magnetic field derivative of 21×10^9 A/ (m·s). The magnetic flux is $4\pi \times 10^{-7} \times 21 \times 10^9 \approx 2.6 \times 10^4$ Wb. Using the loop area of 10^{-5} m^2, we obtain a peak voltage of 0.26 V. This is most likely not sufficient to crash the IC.

There are two ways to increase the E-Field strength, one is increasing the voltage, and the other is reducing the distance to the septum. The voltage is limited by the N-type connectors and the PCB transition; this is difficult to improve if N-type connectors are used. Another limitation arises from the transmission line pulses available. However, the septum distance can be reduced. In this design the distance of the septum has been reduced to 1cm, thus the E-Field strength increases four times. This should be sufficient to reproduce most ESD related coupling situations as they occur in products.

3.1.2. Structure of the Cell. The cell design needs to take RF and high voltage into account. It contains multiple transitions from different modal structures, starting at the connector with a circular field, then transitioning to the microstrip field and further into the TEM cell mode. Each transition has been designed by 2D and 3D analysis and then experimentally optimized. Besides these features, some of the methods for higher order mode suppression [12] have been implemented to extend the frequency range.

The septum of the TEM cell is made of a two-layer PCB. The photos of the PCB and the complete cell are shown in the figures below. Figure 3.1 shows the top layer of the septum. It starts from a microstrip structure which has the ground on the second layer, and extends to coplanar region and then follows with a TEM region. Figure 3.2 shows the second layer of the TEM cell. It extends the ground from the N type connector and to the ground walls on both sides of the cell.
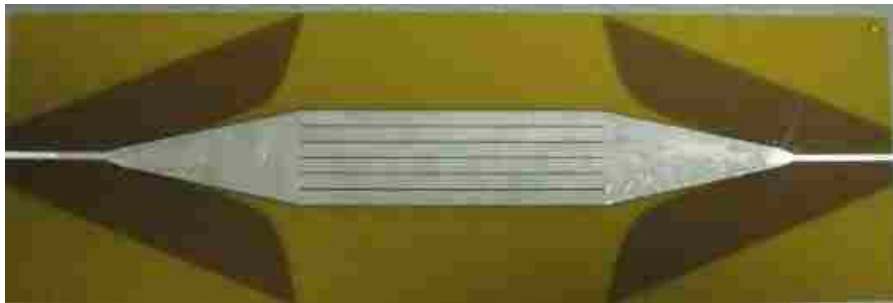
Figure 3.1. The First Layer of the TEM Cell Septum

Figure 3.2. The Second Layer of the TEM Cell Septum

To avoid sparking when using the cell for high voltage, a small slot with 1 mm width is cut at the end of the second layer in Figure 3.3.
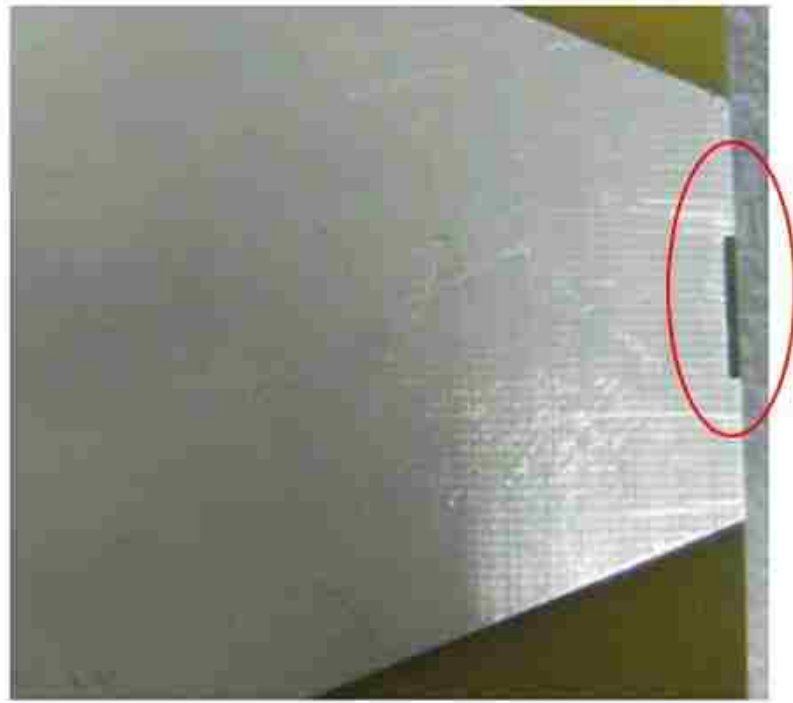
Figure 3.3. Cutout Region for High Voltage Protection

Figure 3.4 shows the overview photo of the cell without the top wall. The PCB was bended with 15 degrees on both sides. Five 75 Ω resistors are mounted between the slots in the center of the septum to reduce high order mode. Slots are cut in the septum in order to form parallel traces in the longitudinal direction and suppress any currents flowing in the transverse direction. Currents flowing in transverse plane are additionally attenuated by these resisters

Figure 3.4. Photo of the Cell without Top Wall

As shown in Figure 3.5, Copper tapes are added to smooth the transition region, fast transition would cause reflections. This was not foreseeable in the 2D cross-sectional analysis, as each slice taken assumes that there are no changes in the Z-direction.

Copper tape is added at the corners to smooth the transition region
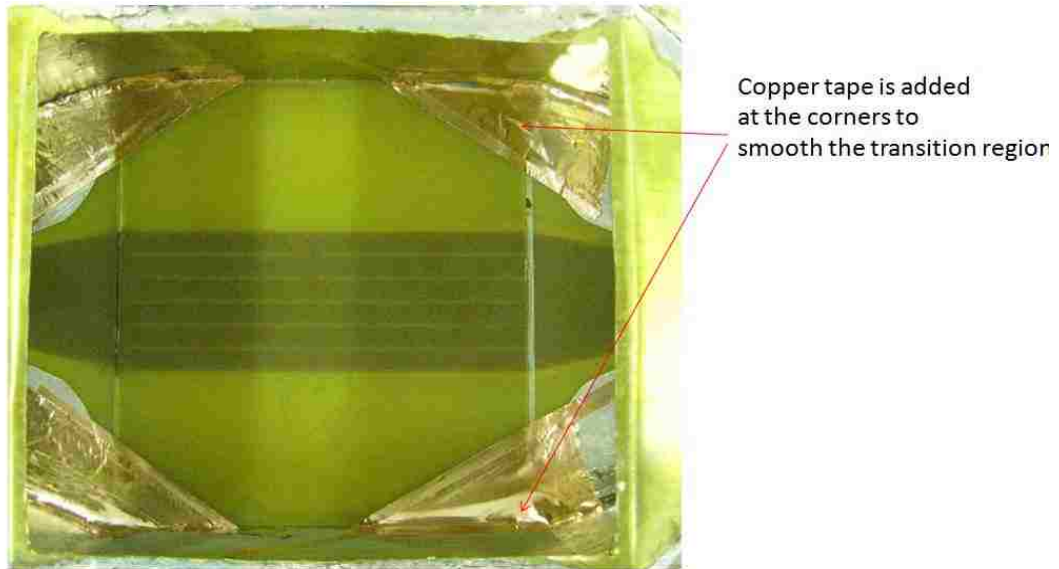
Figure 3.5. Photo of the Cell from Bottom with Extended Ground

RF absorbing materials are placed inside the cell to dampen the high-frequency higher order mode resonances (shown in Figure 3.6).

Figure 3.6. Photo of Cell from Bottom with Absorbing Material Added

Figure 3.7 shows the S11 of the cell is less than -16 dB up to 1.5 GHz. The higher order modes are not strongly suppressed.
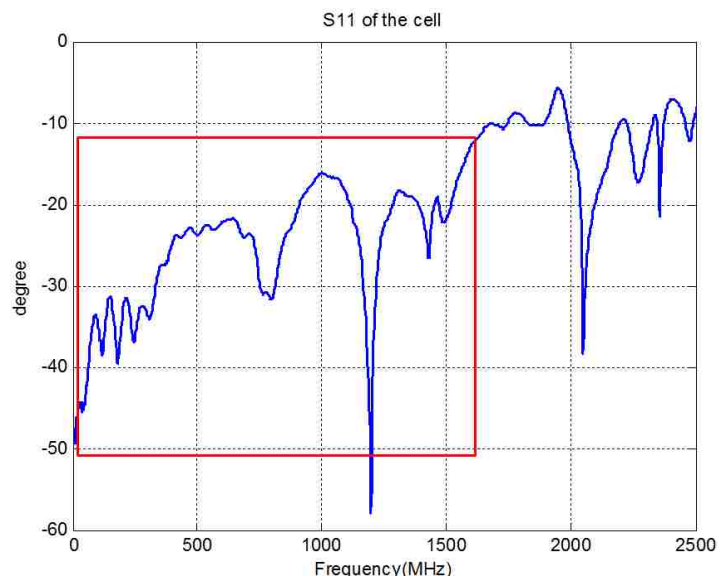
Figure 3.7. S11 of the Cell

The TEM cell design shown in [5] does not bend the septum up and uses a multi-wall structure increasing its complexity significantly. For ESD like pulses a frequency range of up to 1.5 GHz should cover most practical cases. It still has to be verified that at the onset of the higher order mode not strong resonance enhancement of the E-Field takes place. This might cause unrealistic results.

Figure 3.8 is the S21 result; it shows that the loss is 2.5 dB up to 1.5 GHz. The result shows the modifications can extend the useful frequency range of the TEM cell for the high voltage immunity testing from 1 GHz to 1.5 GHz. The first resonance starts around 1.7 GHz, which is caused by TE mode.
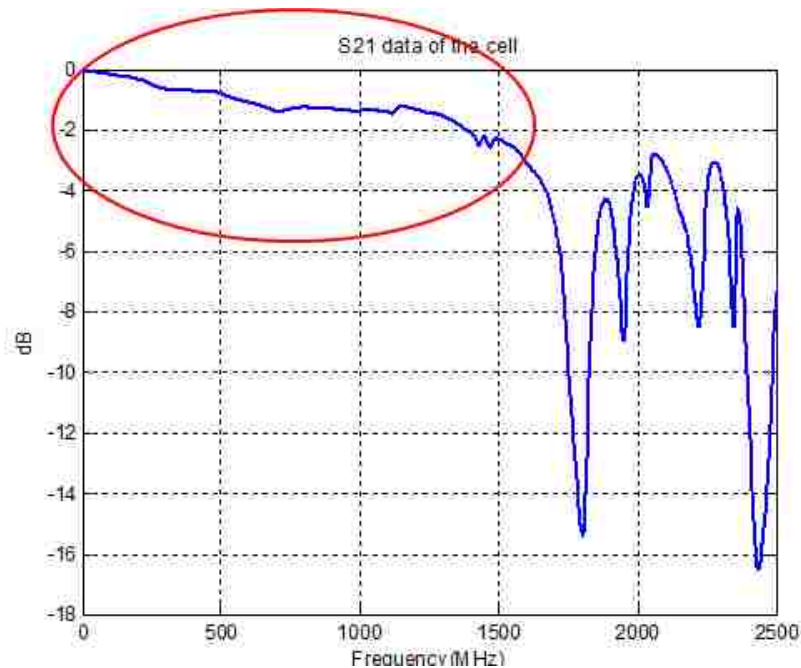
Figure 3.8. S21 of the Cell

3.1.3. Summary of the Cell Design. The TEM cell allows creating well controlled field strengths up to 32kV/m in a frequency range from DC to 1.5 GHz.

3.2. IC STRIPLINE FOR IC IMMUNITY TESTING

3.2.1. Design of the IC Stripline. This section lists some pictures and characteristics of the TEM cell. Figure 3.9 and Figure 3.10 are the photos of the cell.
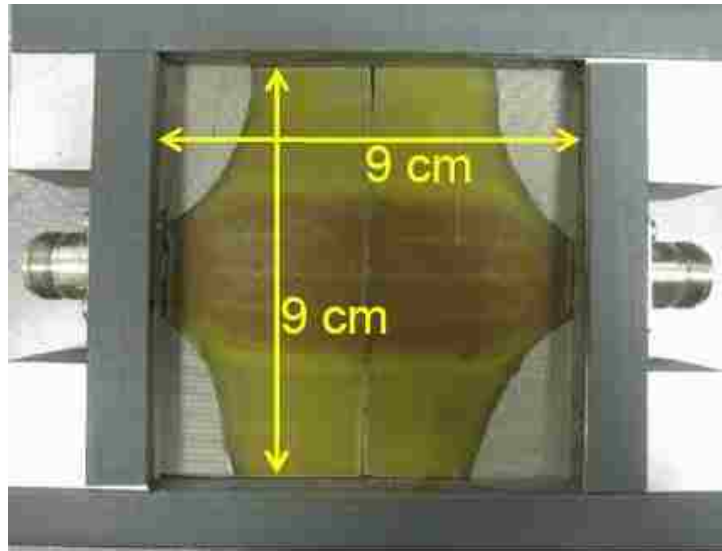
Figure 3.9. Top View of the IC Stripline
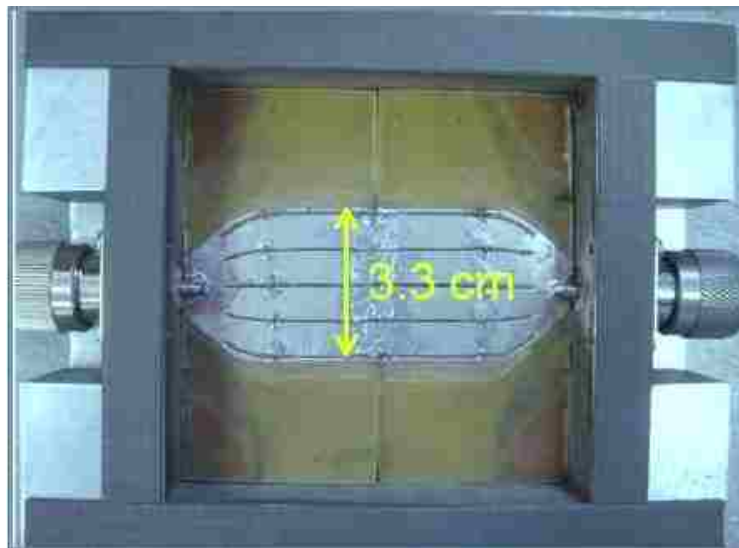
Figure 3.10. Bottom View of the TEM Cell

Some of the features in the TEM cell are as follows,

- Reduced distance between IC and septum (9 mm)
- N type connectors
- Slots on the traces
- Resistors across the slots

3.2.2. Characterization of the IC Stripline. The TEM cell is characterized by the S11 and S21 parameters. Figure 3.11 shows the measurement setup to determine the S11 and S21 of the cell. Figure 3.12 and Figure 3.13 are the S11 & S21 data of the IC stripline.
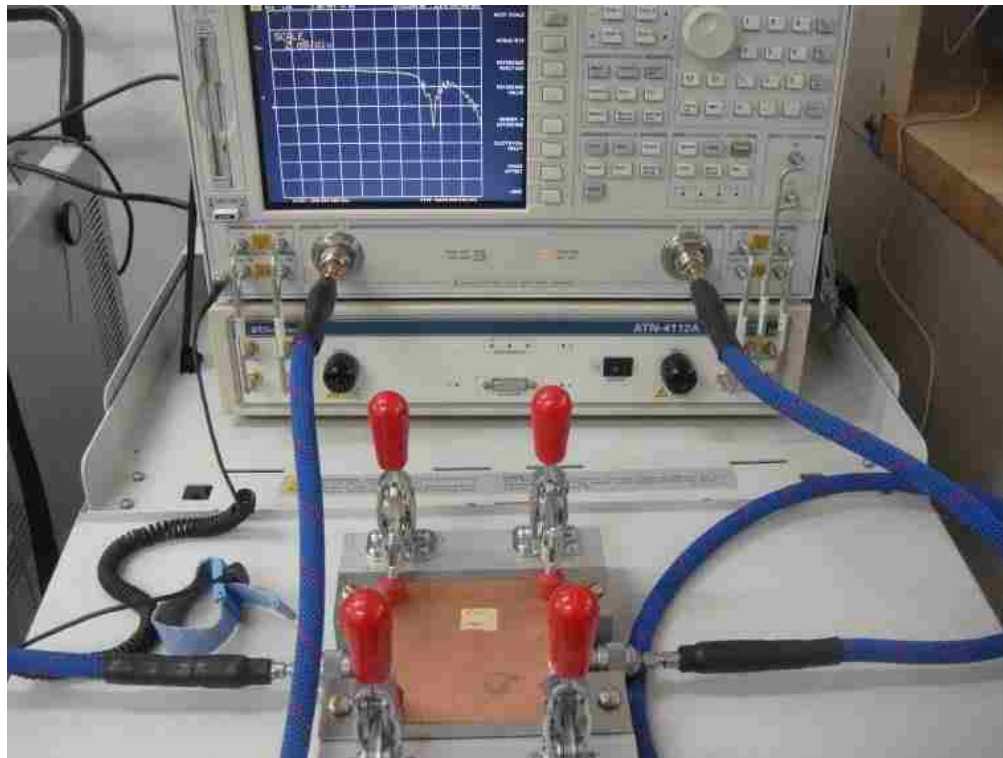
Figure 3.11. Experimental Setup for Measurement of S-parameters
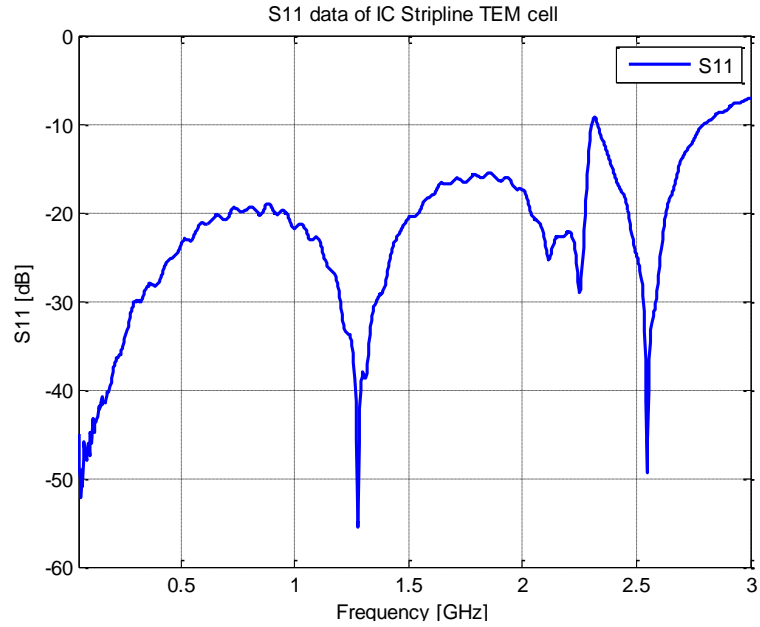
Figure 3.12. S11 of the IC Stripline
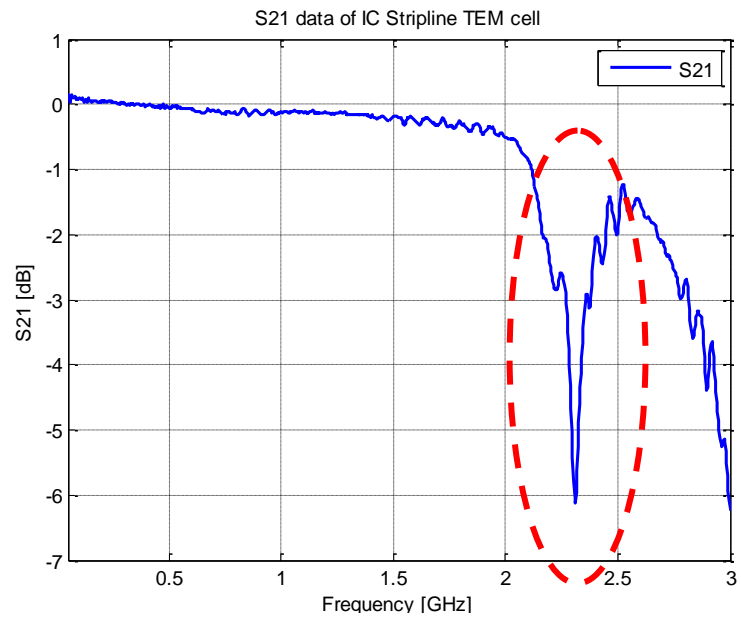
Figure 3.13. S21 of the IC Stripline

The first resonance caused by higher order modes occur at around 2.3 GHz. The useful frequency range of the IC stripline is up to 2 GHz.

4. MEASUREMENT RESULTS FOR THE DATABASE

4.1. INTRODUCTION

This section of the thesis shows the measurement results for the database. The first part presents and discusses the results for one of the tested ICs; the second part of the section discusses results from the measurement data of all ICs. And the last part illustrates how the data can be used. There are 37 real ICs which are included in the database. Not every IC was able to be tested with all the scenarios explained in the next section due to crowded board design (Probes cannot be landed correctly) , IC damage and etc.

4.2. TEST SETUP AND SCENARIOS USING DIFFERENT PROBES

4.2.1. Test Setup for Different Probes Figure 4.1 shows the test scenarios for the individual E-field probes. The three scenarios shown are all tested with both positive and negative voltage.
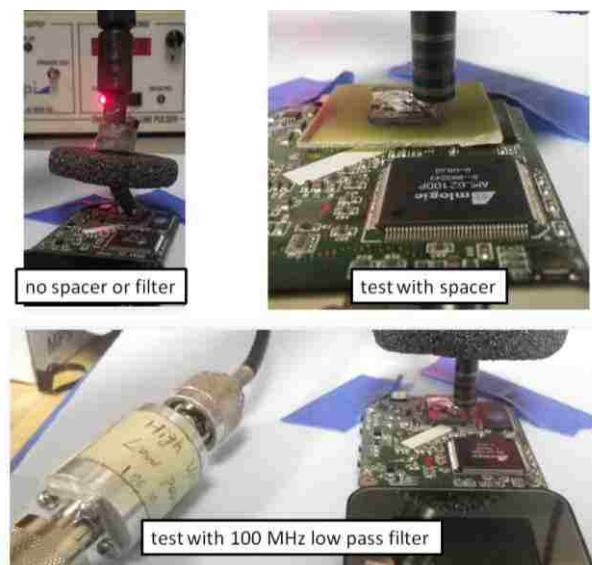
Figure 4.1. Scenarios using E-field Probe

Figure 4.2 shows the test scenarios for the individual H-field probe. The probe used is H14B. For H-field, both 0° and 90° orientation are used for the IC testing.
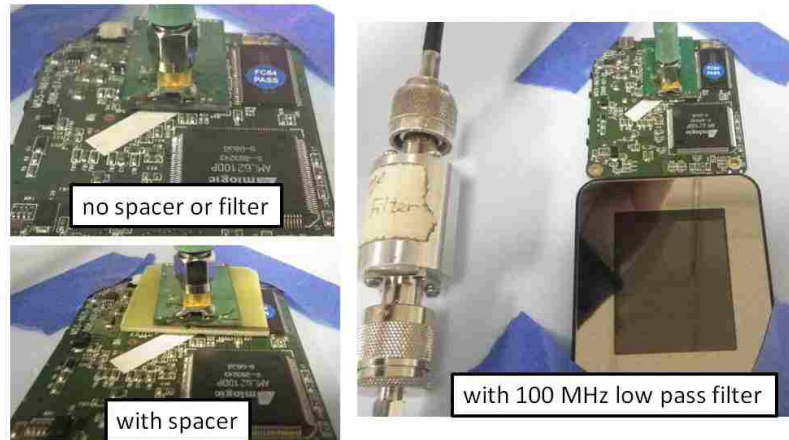
Figure 4.2. Test Scenarios for H-field Probe (for one direction)

Figure 4.3 shows the scenarios for the $\sum\Delta$ probe. The probe can be used for both E-field testing and H-field testing.   The pulse inverter is inserted to achieve H-field injection.
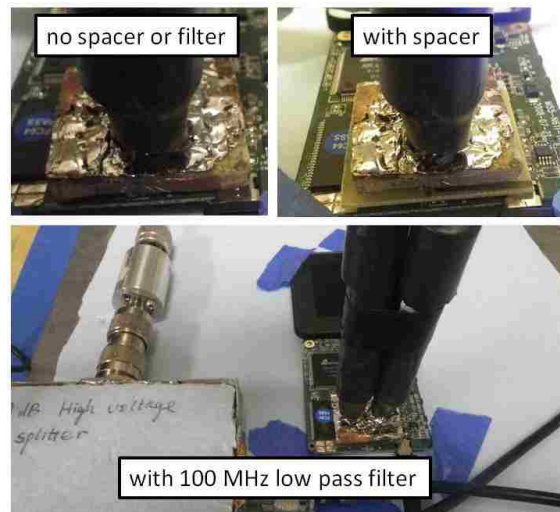
Figure 4.3. Test Scenarios for $\sum\Delta$ Probe

4.2.2. Effect of Adding a Spacer on the Crash Level. The stacks ups structures of the measurement setup with and without a spacer are shown in Figure 4.4 and Figure 4.5.
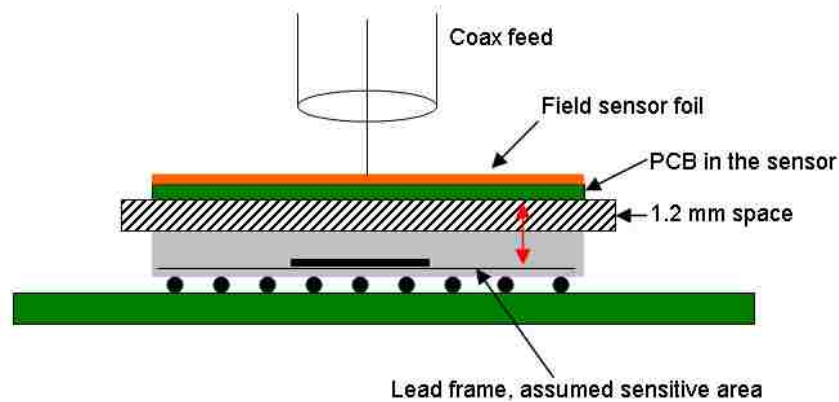
Figure 4.4. Illustration of the E-field Coupling and Critical Distance
for an IC Tested Using a Spacer
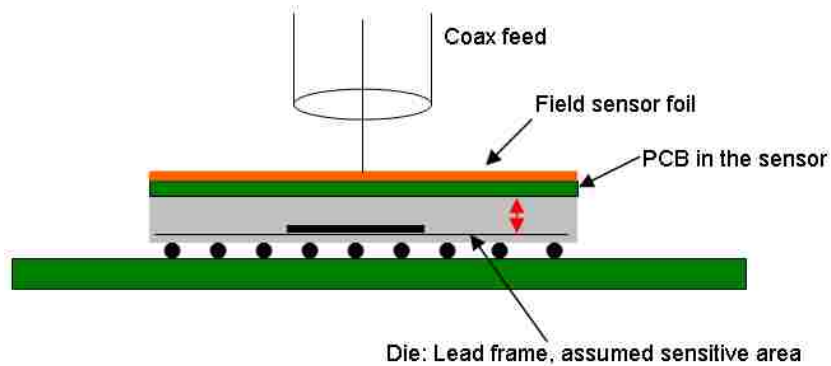
Figure 4.5. Illustration of the E-field Coupling and Critical Distance
for an IC Tested without a Spacer

The current injected by the E-field is a function of the coupling capacitance between the probe and the sensitive area inside the IC. In first approximation, this capacitance is proportional to the distance. If a spacer is added, the field strength is reduced, thus, the needed TLP voltages need to increase. The ratio of field strength

reduction is determined by the distance between the sensitive area in the IC and the metallic foil of the IC.

For Magnetic field coupling, the field should not decay very rapidly under the probe, thus, adding a spacer should lead to only a small reduction of the field strength. The magnetic field probes have been designed to have only a small decay in their magnetic field close to the probe. This is a consequence of having wide conductor that carries the current. Other effects, like edge effects which cause an Hz component might change more rapidly with increased distance.

4.2.3. Effect of a Low Pass Filter on the Crash Levels. For the low pass filter, one approximate approach to determine the effect of the low pass filter on the TLP levels is to look at the dE/dt and the dH/dt values.

Figure 4.6 shows the effect of low pass filter to the E-field pulse. The rise time is about 200 ps without the filter, and 350 ps with the filtering. The ratio of dE/dt between not adding and adding the filter is about 4.7.
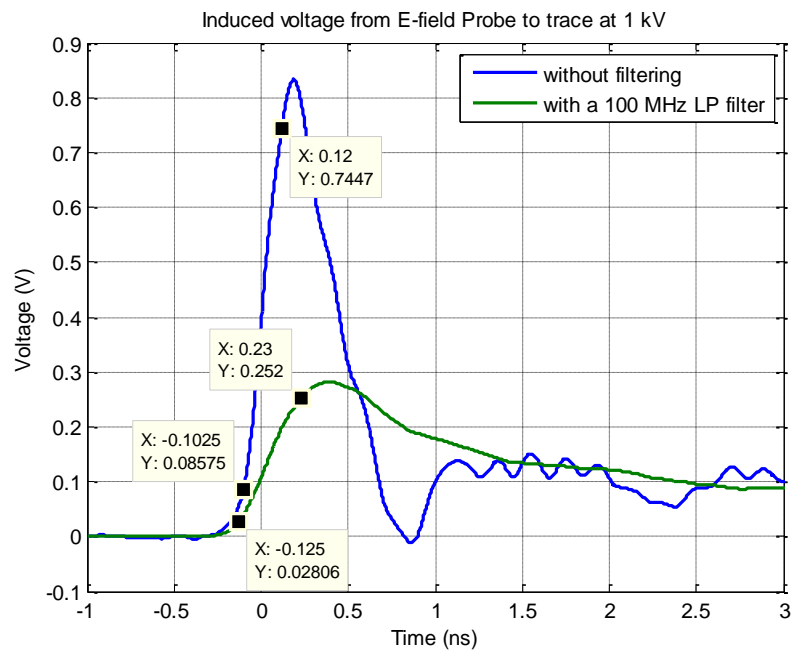
Figure 4.6. Effect of the Low Passing Filtering of the E-field Pulse

Figure 4.7 shows the effect of low pass filter to the H-field pulse. Without the filter, the rise time of the pulse is about 150 ps, and with the filter, the rise time decrease to about 200 ps. And the ratio of dH/dt between not adding the low pass filter and adding the low pass filter is about 8. In first approximation one may assume that the crash level is directly related to dH/dt or dE/dt, thus, the needed TLP voltage would then go up by the amount needed to have the same derivative values after adding the low pass. But the IC may have internal integrating effects or non linear effects thus, the measured data might deviate from this expectation.
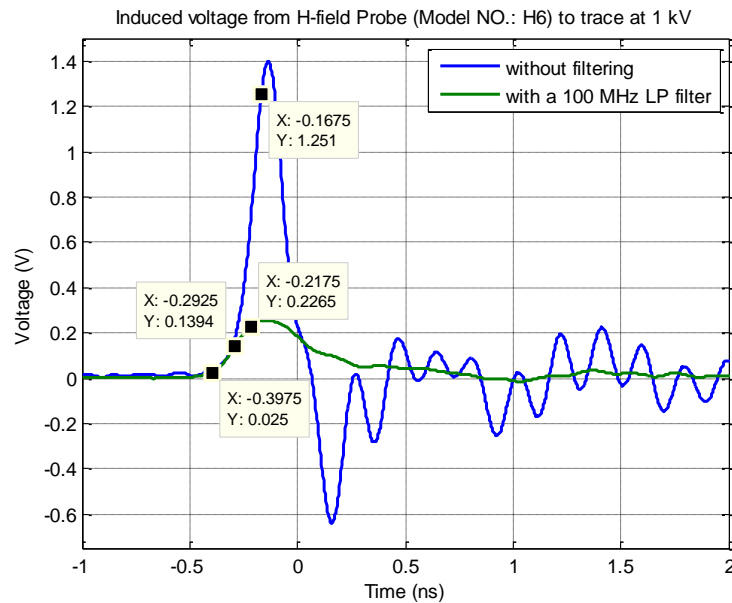
Figure 4.7. Effect of the Low Passing Filtering of the H-field Pulse

4.2.4. Effect of Probe Rotation and Using Different Probes. When rotating the E-field probe, the crash level does not change, if the field components underneath the E-field probes are homogenous Ez components and no edge effects influence the IC crash. For H-field, it's the difference causing by rotating the probe is not possible to predict, without knowing the circuitry inside the IC.

4.3. MEASUREMENT RESULTS FROM ONE EXAMPLE IC

This section presents and discusses the test results from one example IC to illustrate typical results and to provide insight into the measures taken to ensure consistency within the database. The DUT is a mini digital photo frame (as shown in Figure 4.8) with 3 ICs on board, and the IC tested is labeled as MX TD83620.

Figure 4.8. Photo of the IC under Test

The part has been tested with the E-field probe, H-field probe and the $\sum\Delta$ probe respectively. Several symptoms of soft errors have been observed, such as reset, white screen, etc. Sometimes, the resolution of the display decreased as a consequence of ESD injection (as shown in Figure 4.9).

no error   error
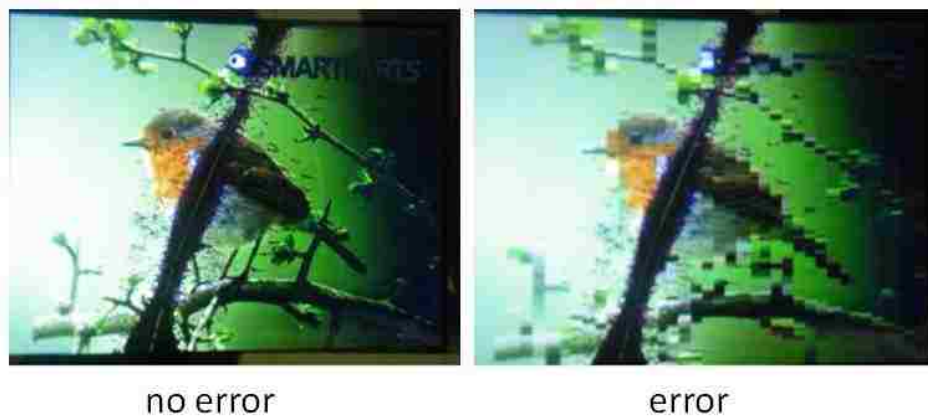
Figure 4.9. An Example of Soft Error Caused by the Field Injection

Table 4.1 to Table 4.3 present the test results using the three probes. It is shown that by adding the spacer, the voltage ratios are about 1.2 for both the positive and negative voltages for both the E-field and H-field. When adding the filter, the ratios are different; the ratio is 1.75 for positive voltages, and 3 for negative voltages in the E-field results. For H-field disturbances, the ratio is between 1.1 to 2.2.

Table 4.2 shows the results when using the H-field probe. The positive failure levels are higher when we used the probe in 0°, the difference between the angles are totally IC dependant. If comparing the results for adding or not adding the spacer, it can be found that the difference is constant, and always around 1.2. The field does not decay very rapidly under the probe, thus, adding a spacer should lead to only a small reduction of the field strength, if the edge of the IC is close to the lead PINs. But after adding the filter, the ratio varies from 1.1 to 2.1. A first order approximation of adding the low pass filter is that the IC is only sensitive to the dH/dt or dE/dt. In this case the TLP voltage needs to be increased to compensate for the reduced dE/dt and dH/dt.

Table 4.1. Test Results for E-field Probe

	no spacer, no filter	with spacer	with filter
Positive	400 V	500 V	700 V
Negative	-600 V	-700V	-1800 V

Table 4.2. Test Results for H-field Probe

	no spacer, no filter	with spacer	with filter
Positive (0°)	4700 V	5300 V	5800 V
Negative (0°)	-2700 V	-3300 V	-4500 V
Positive (0°)	1900 V	2300 V	4100 V
Negative (90°)	-2900 V	-3200 V	-3200 V

Table 4.3. shows the results for the ∑Δ probe. No failure observed when the probe is used in H-field mode for this chip. For E-field, crash levels are about 4 to 5 times higher than for the individual E-field probe. The ratio between adding and not adding the spacer is 1.2 and 1.3 for positive and negative voltages. With the low pass filtering, the ratio is 2.2 and 2.3. The effect of adding the filter is hard to predict, as it's not for sure that dH/dt is the only predictor for the IC response.

Table 4.3. Test Results for ∑Δ Probe (E-field)

	no spacer, no filter	with spacer	with filter
Positive	1900 V	2300 V	4100 V
Negative	-2400 V	-3200 V	-5500 V

Table 4.4 shows the conversion factors for the E-field and H-field probes which have been used for the IC testing, the methodology of the conversion are discussed in the probe calibration part in section two.

Table 4.4.Conversion Factors for Probes Used in the Study

Probe Model Name	Photo	Conversion factor for 1 V from TLP
E-field Probe		30.6 V/m
ΣΔ probe in E-field mode		10.2 V/m

Table 4.4. Conversion Factors for Probes Used in the Study (cont.)

H6		0.1671 A/m
H7		0.2875 A/m
H8		0.2751 A/m
H1		0.3014 A/m
H14B		0.0337 A/m
H16B		0.1461 A/m
ΣΔ probe in H-field mode		0.0263 A/m

4.4. DATABASE RESULTS

The products that have tested are USB hub, mp3 players, Ethernet integrated switch, desktop switch, DVD player, webcam, Ethernet hub, digital photo frame, wireless router, DVD player, digital SLR cameras and etc, the photo of some of the DUTs are shown in Figure 4.10.

As failure criteria is that: any observable change in the behavior was considered a failure. Examples are: Reset, stop of music, changes in displays, inability to control the system by its user interface, stop of USB data transfer etc.

Figure 4.10. Photo of Some DUTs

4.4.1. IC Selection Method. The IC selection method was as follows: A typical consumer electronic system like a picture frame, CD player, MP3 player, camera etc. was purchased. The main ICs where selected for testing. These are typically the microcontrollers, the DSPs etc. Physically small ICs, like power supply controllers,

simple logic; motor drivers have not been selected. This biases the data into the direction of highly complex VLSI IC that combine multiple functions. In most cases the IC selected has been also the physically largest IC on the board.

4.4.2. Data Analysis. The highest TLP voltage that the TLP system can provide is 8 kV (charge voltage), there are scenarios where the IC was not disturbed during the test, especially when the spacer or filter are added. Data from 30 ICs have been used for the database. There are some differences in the upset field strength results when using different probes. Possible reasons are the effect of other field components on the probes, especially at the edge and the feed, mismatch between the probe and IC size, and calibration inaccuracy. The ICs which have been tested with both the individual E-field/H-field probe and the $\Sigma\Delta$ probe are processed as two virtual ICs in the database. The magnetic field coupling results are tested with two different angles, results from the two angles are also been processed as two different virtual ICs. Figure 4.11 illustrate how the virtual ICs are created from real ICs. Another assumption is that the positive and negative results are independent from each other, thus creating more virtual ICs. Thus, one IC can lead to a set of data points in the probability distributions shown in Figure 4.12 to Figure 4.15.
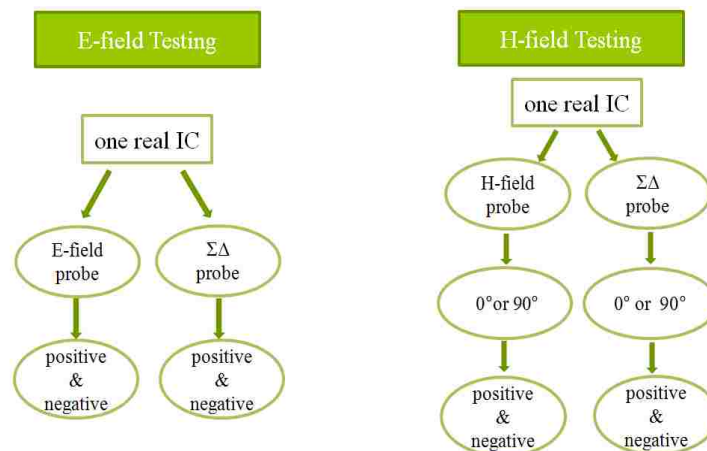
Figure 4.11. Real ICs and Virtual ICs

For E-field results, 94 virtual IC are created from results of 37 real ICs, 115 virtual ICs were created from the results from 31 real ICs, for H-field results. Figure 4.11 is the illustration on how the virtual ICs were generated from the real ICs' results. For the real IC that are not crashed during the measurement, the average number of virtual ICs created from either the E-field (2.5) or H-field results (3.7) are subtracted from the total number of virtual ICs respectively.

4.4.3. Crash Level Results. Figure 4.12 to Figure 4.15 are the crash levels in terms of field strength and field derivative values converted from the TLP measurements results. With a known value of field strength and for a somewhat similar pulse, users can roughly estimate whether the IC will be disturbed by ESD according to the statistics in the tables.

Figure 4.12 shows that the most robust IC crashed at around 200 kV/m, among all the ICs which have been disturbed in the measurements And the most sensitive one crashed at about 6 kV/m. With a field strength value at about 100 kV/m, about 80% of the ICs have been interrupted during the tests. There are 94 virtual ICs included in this data set.
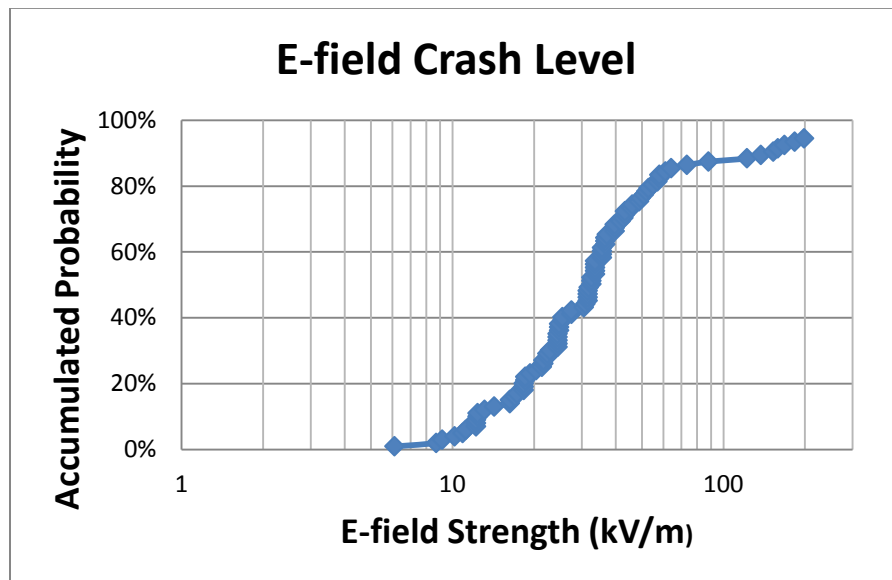
Figure 4.12. Probability of Failure in Terms of E-field

Figure 4.13 shows the probability of the failure for H-field injection, in terms of H-field strength. For magnetic field coupling, the crash levels are recorded and compared with both 0° and 90° probe orientation, but only the lower crash values are included in the database. There are 96 virtual ICs included in this data set. The most sensitive chip was disturbed at 23 A/m, and highest crash level is about 1800 A/m, among all the ICs which have been disturbed in the study. With field strength of 482 A/m, 90% of the ICs had failed during the ESD testing.
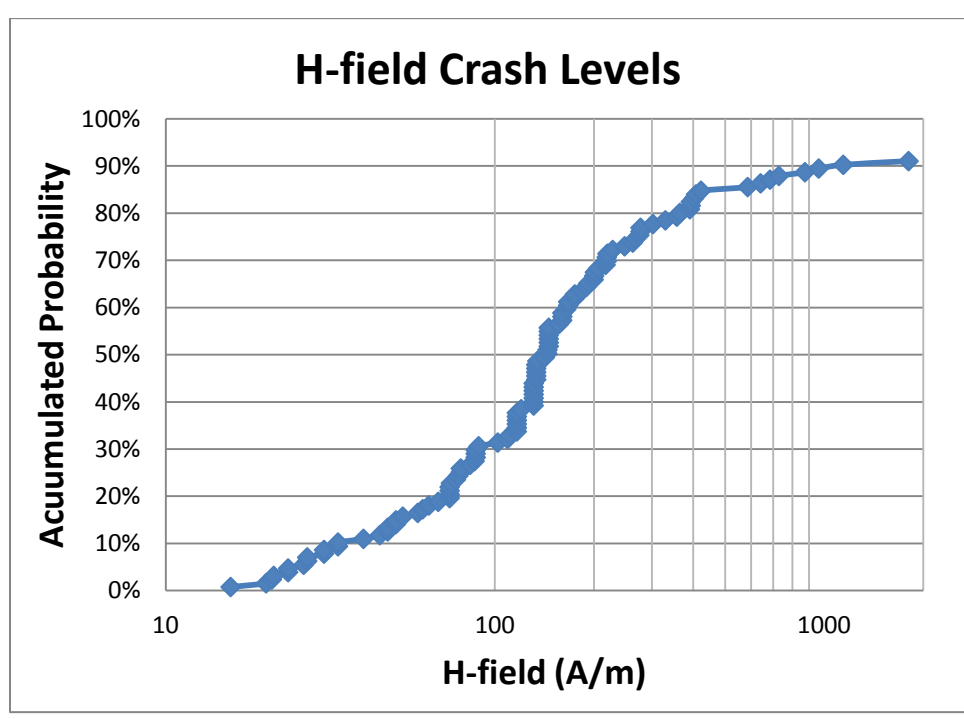
Figure 4.13. Probability of Failure in Terms of H-field Strength

Figure 4.14 shows the crash levels in terms of the E-field derivative values, for the ICs that have been tested. The most robust chip can be operated without soft errors up to 600 kV/m/ns, but the most sensitive chip failed at only about 40 kV/m/ns. 86% of the ICs can be disturbed when the field derivative is less than 350 kV/m/ns. Figure 4.15 shows the H-field derivative crash level results.
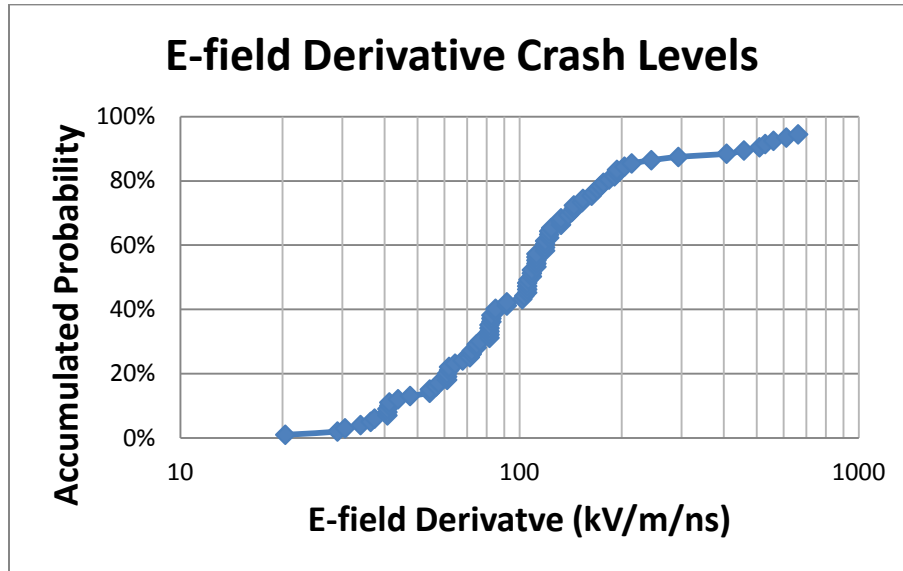
Figure 4.14. Probability of Failure in Terms of E-field Derivative
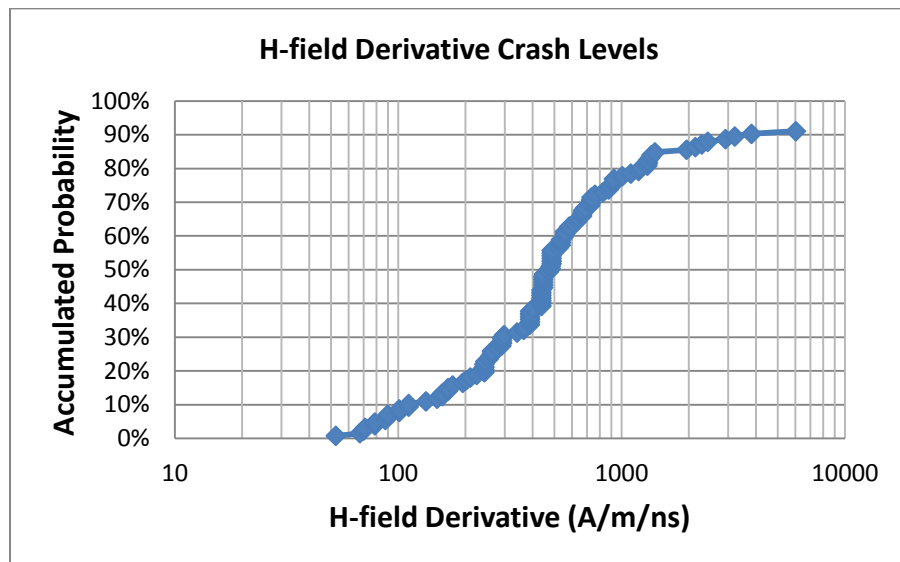
Figure 4.15. Probability of Failure in Terms of H-field Derivative

Assume only coupling to a pin on the lead frame. The area is about 5 mm × 0.8 mm. Then one can use the following equation to estimate the induced current for a given field derivative value [26]. Since the height of the IC is very small, only the field

incident on the horizontal portion of the pin is important in this case. Where Ez is the vertical electrical field, is permittivity, and is the differential surface area of the pin. Since the field varies slowly over the IC, the current may be approximated as

$$I_s = \iint (\frac{dE_z}{dt}\varepsilon)dS \ = \ \frac{dE}{dt} \ \varepsilon \cdot S \tag{8}$$

Also the voltage at the input can be also approximately calculated, if simply assume that this input is connected to a trace having 60 Ohm impedance (a typical PCB value) and the trace is long enough that the reflection does not reach the IC before the pulse is over.

Table 4.5 is a table showing the calculated induced current and the voltage at the input, with different field derivative values in the database. 20 kV/m/ns is the lowest crash level, and 660 kV/m/ns is the highest crash level; and with a field derivative of 112 kV/m, this part of the data base is based on testing 31 ICs, and 115 virtual ICs were created.

Table 4.5. Calculated Induced Current with Different E-Field Derivative Levels

	Lowest crash level	Crash level of 50% of the ICs	Highest crash level
	20 kV/m	112 kV/m	660 kV/m
Induced current	0.003 A	0.02 A	0.09
Voltage at the input	0.2 V	1.2 V	5.4 V

Crash levels of the ICs, in terms of the H-field derivative are shown in Figure 4.15. About 80% of the ICs had soft errors detected at about 830A/m/ns, although the most robust IC survived at about 5000 A/m/ns. The most sensitive IC crashed at about 70 A/m/ns.

The induced voltage can be approximately calculated from the field derivative from the following equation.

$$V_{ind} = \frac{dH}{dt}\mu \cdot A_{eff} \tag{8}$$

For example if the IC has a height of 0.5 mm, and a 2 mm length inside the package. A small loop assumption would be 0.5 x 0.5mm and a large loop assumption would be 15 x 1 mm (like full IC width PCB ground to internal structure).

For estimating the induced voltage into loops formed by the PCB ground and the internal IC structure three different cases are considered. The small loop assumption is the case where the field is mainly coupled into a bond wire, assuming the bond wire has a loop size of 0.5x0.5mm. For the large loop case, the loop is defined as being formed diagonally across the entire IC; and here the loop size is about 15x1 mm loop size.

If assume quasi-static induction, and no effect of the currents within the loop on the magnetic field penetrating the loop, an induced voltage proportional to both the loop area and the magnetic field derivative can be obtained. Table 4.6 shows the calculated voltage values with different loop areas.

Table 4.6. Calculated Induced Voltages with Different Loop Areas

Magnetic field strength derivative	Small loop 0.5x0.5mm	Middle size loop 0.5x1mm	Large size loop 15x1mm
70A/m/ns	0.022 V	0.045V	1.3V
5000A/m/ns	1.6V	3.2V	92.8V

4.4.4. Effect of Adding a Spacer on the Crash Levels. As discussed earlier, theoretically adding a spacer or low pass filter will increase TLP voltages needed to upset the IC. Table 4.7 shows the measurement results showing the effect of adding the spacer and the 100 MHz low pass filter when different probes were used in the

measurements. By adding the spacer, the average increase of the crash levels are about 30% for both E-field and H-field coupling. When adding the 100 MHz filter, the average increase is not very stable, and it is between 48% and 80%. Figure 4.16 & Figure 4.17 are the histograms of the ratios showing the effects of the spacer and the filter in the results.

Table 4.7. The Effect of Adding the Spacer and Filter on Crash Levels

	E-field probe (14 ICs)	H-field probe (19 ICs)	$\Sigma\Delta$ (E-field) (11 ICs)	$\Sigma\Delta$ (H-field) (12 ICs)
with spacer	35%	30%	25%	25%
with LPF	68%	80%	48%	77%
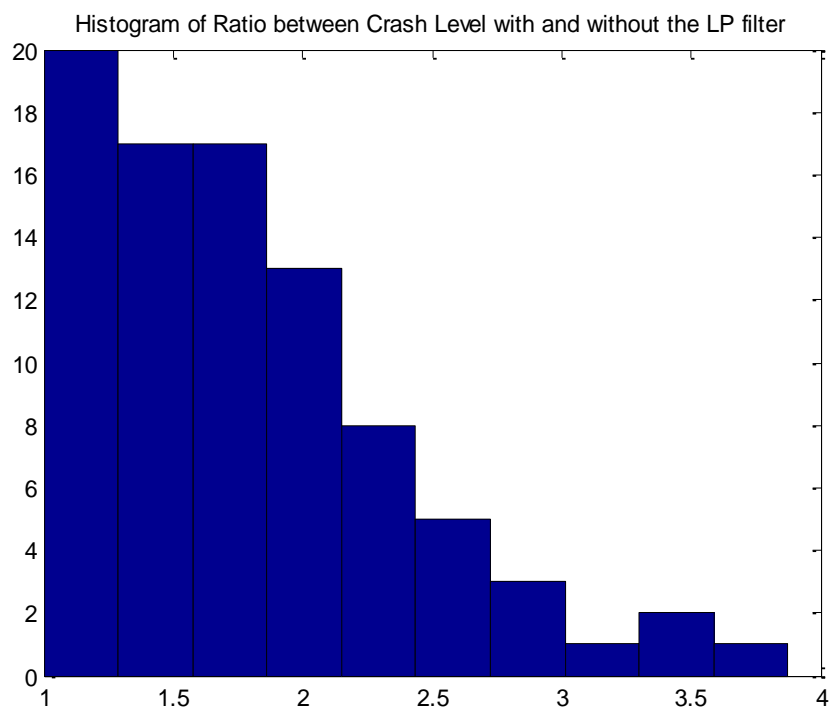
Figure 4.16. Histogram of the Ratio Between Adding and not Adding the LPF

Histogram of Ratio between Crash Level with and without the Spacer
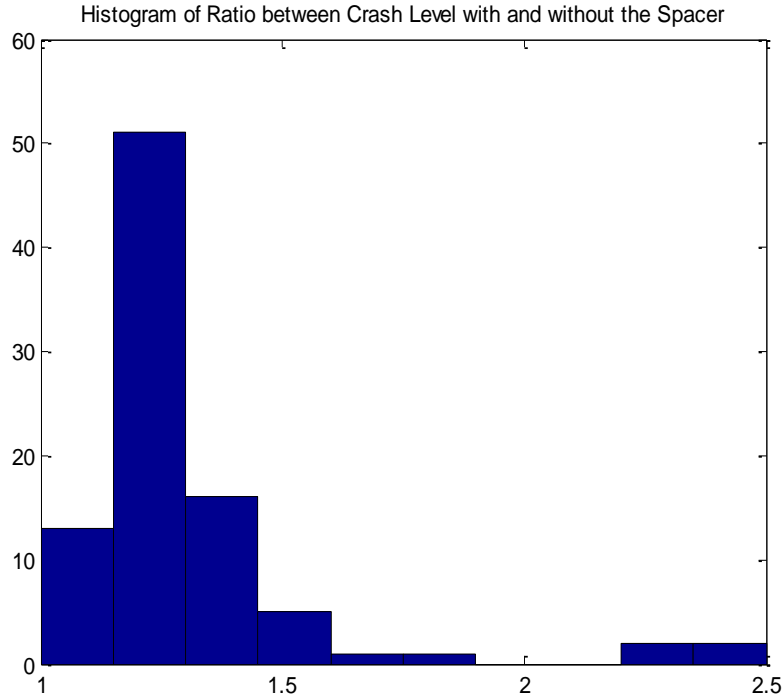
Figure 4.17. Histogram of Ratio Between Adding and not Adding the Spacer

4.4.5. Comparison of Results from Using Different Probing Systems. Some of the ICs are tested using different probing systems. The results using the individual probes and the $\Sigma\Delta$ probe are compared. The average field strength ratio between using the E-field probe and the $\Sigma\Delta$ probe is 1.18, based on the results from 20 virtual ICs. And the field strength ratio between using the H-field probe and the $\Sigma\Delta$ probe is 1.07, based on the results from 22 virtual ICs.

5. CONCLUSION

An ESD sensitivity database for ICs is established to estimate the occurrence of soft error of typical electronics. Different injection hardware has been developed to establish the ESD sensitivity for ICs. For the field coupling probes, they can be used for used for immunity testing up to about 3 GHz, with a relatively constant and homogenous field above the subject IC. For the modified TEM cell, the useful frequency range of the cell is increased to 1.5 GHz by the high order mode suppression techniques, which is sufficient to cover most of the practical case in IC immunity testing. The distance between septum to ICs has been increased to obtain higher field coupling. And the IC stripline can be used up to 2 GHz without higher mode resonances.

The test results on ICs are repeatable in multiple injections using the probes. In most cases, the field strengths are sufficient enough to disturb most of ICs, and determine the crash levels of the ICs. Adding a low-pass filter will generally increase the crash levels, the increase of the crash level is mainly IC dependent, and the average ratio is between 48% to 80%, depends on which probe is used, and which field components is injected. The increase of the crash level varies a lot, and is difficult to estimate, without knowing the circuitry inside the IC. By adding a FR4 spacer, the crash levels are generally 20% higher for both the E-field and H-field injection. Most of the ICs are tested using two different probing systems. The average difference is within 20% of E-field results, and within 10% between the H-field results. The results from the two systems are both included in the database, and the difference between the two probing systems could be caused by the non homogenous field components between the probe and the IC or calibration errors.

APPENDIX

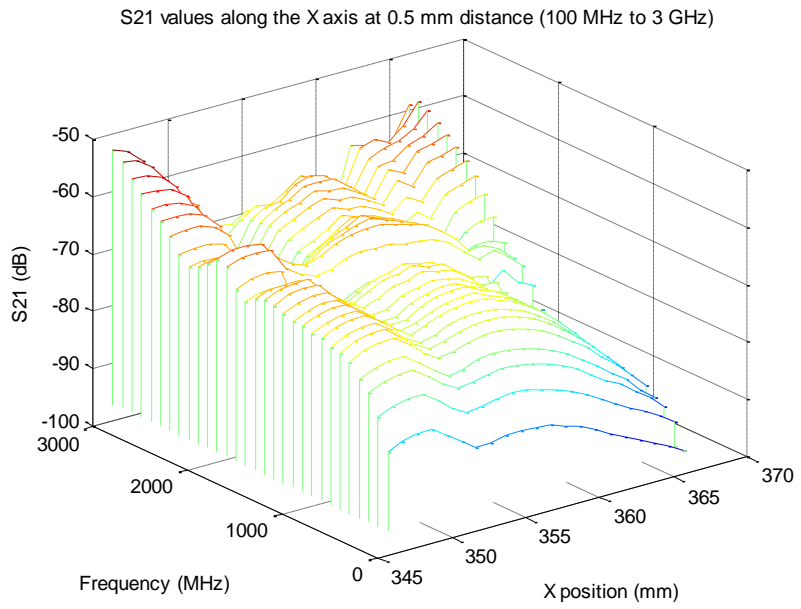**S21 SCANNING OF THE H-FIELD PROBE AT DIFFERENT HEIGHT**

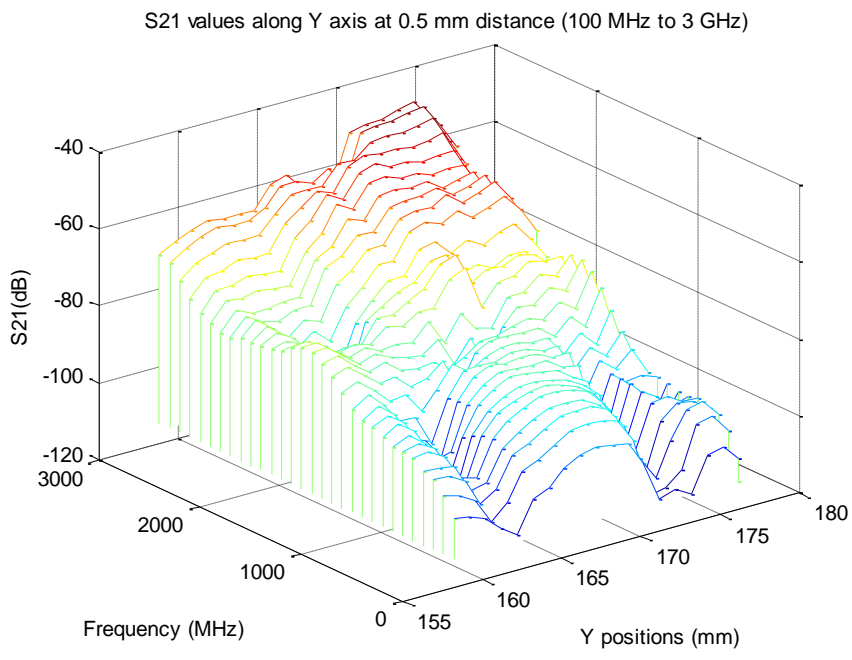Figure A.1. S21 Values along the X Axis at Y Center (0.5 mm above the trace)

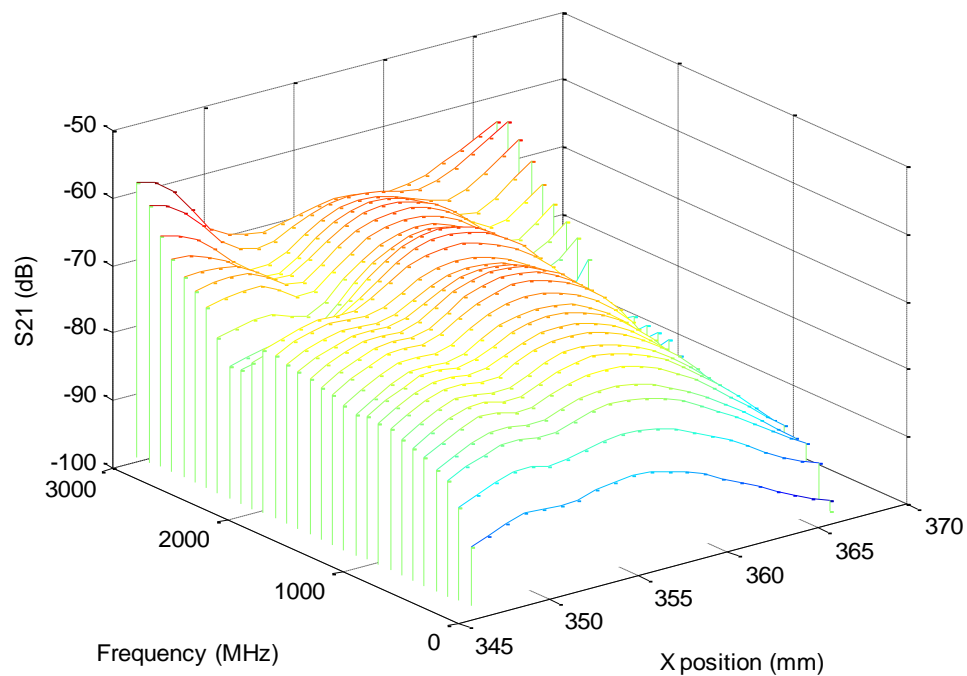Figure A.2. S21 Values along the Y Axis at X Center

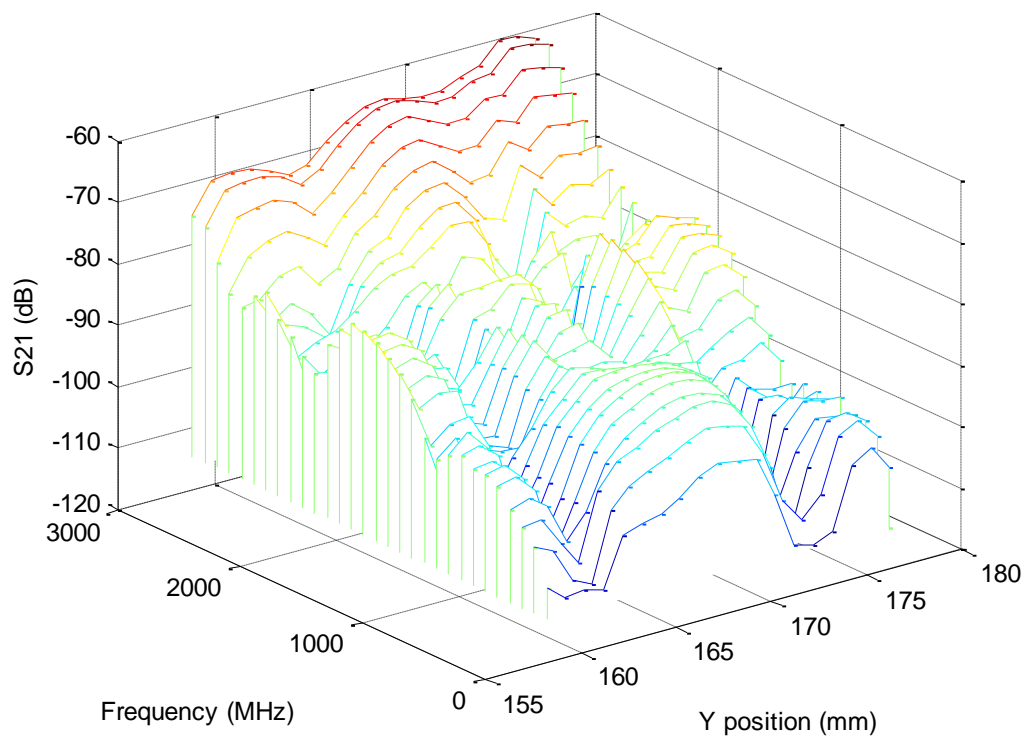Figure A.3. S21 Values along the X axis at Y Center (1 mm above the Trace)

Figure A.4. S21 Values along the Y Axis at X Center (1 mm above the Trace)

BIBLIOGRAPHY

[1] Ki Hyuk Kim; Yongsup Kim, "Systematic Analysis Methodology for Mobile Phone's Electrostatic Discharge Soft Failures," Electromagnetic Compatibility, IEEE Transactions on , vol.53, no.3, pp.611-618, Aug. 2011

[2] Heinrich, R.; Mullerwiebus, V.; Lange, A.; Deutschmann, B.; Karsten, U.; Klotz, F., "Application of GTEM cells for IC EMC testing," Electromagnetic Compatibility and 19th International Zurich Symposium on Electromagnetic Compatibility, 2008. pp.263-266, 19-23 May 2008

[3] IEC 62132-8, "Integrated circuits-Measurement of electromagnetic immunity – Part 8: Measurement of radiated immunity-IC stripline method," Ed. 1.0, 2009-01-30

[4] Crawford, M.L., "Generation of Standard EM Fields Using TEM Transmission Cells," IEEE Transactions on Electromagnetic Compatibility, vol.EMC-16, no.4, pp.189-195, Nov. 1974

[5] No-Weon Kang; Jin-Seob Kang; Dae-Chan Kim; Jeong-Hwan Kim; Joo-Gwang Lee, "Characterization Method of Electric Field Probe by Using Transfer Standard in GTEM Cell," IEEE Transactions on Instrumentation and Measurement, vol.58, no.4, pp.1109-1113, April 2009

[6] Lijun Han; Jayong Koo; Pommerenke, D.; Beetner, D.; Carlton, R., "Experimental Investigation of the ESD Sensitivity of an 8-Bit Microcontroller," IEEE International Symposium on Electromagnetic Compatibility, vol., no., pp.1-6, 9-13 July 2007

[7] IEC 61967-3, "Integrated circuits-Measurement of electromagnetic emissions, 150 kHz to 1 GHz,- Part 2: Bulk Current Injection (BCI), 10 kHz to 1 GHz ," 2005

[8] IEC 62132-2, "Integrated Circuits, Measurement of Electromagnetic Immunity, 150 kHz to 1 GHz - Part 2: Measurement of Radiated Immunity TEM-Cell and Wideband TEM-Cell Method ," 2009

[9] IEC 62132-4, "Integrated Circuits, Measurement of Electromagnetic Immunity, 150 kHz to 1 GHz - Part 4: Direct RF Power Injection Method," 2001.

[10] K.Wang, J. Koo, G. Muchaidze, and D. Pommerenke, "ESD susceptibility characterization of an EUT by using 3D ESD scanning system," IEEE transactions on Electromagnetic Compatibility, vol. 49, pp. 504-511, Aug. 2007

[11] D. Pommerenke, J. Koo, G. Muchaidze, "Finding the root cause of an ESD upset event", DesignCom2006, Santa Clara, Feb. 2006

[12] S. Deng, D. Pommerenke, T. Hubing, "An Experimental Investigation of Higher Order Mode Suppression," IEEE transactions on Electromagnetic Compatibility, vol. 50, pp. 416-419, May. 2008

[13] B. Körber1, M. Trebeck1, N.Müller1, F. Klotz, V. Müllerwiebus, "IC-Stripline: A New Proposal for Susceptibility and Emission Testing of ICs," EMC COMPO, pp.125-129, Torino, 2007

[14] Zhou, F.; Pommerenke, D.; Feng, G., "Correlating ESD scanning results to circuit behavior," EMC Compo 09, Toulouse, 2009

[15] Lacrampe, N.; Caignet, F.; Bafleur, M.; Nolhier, N.; Mauran, N., "Characterization and modeling methodology for IC's ESD susceptibility at system level using VF-TLP tester," 29th Electrical Overstress/Electrostatic Discharge Symposium, 2007. EOS/ESD , vol., no., pp.5B.1-1-5B.1-7, 16-21 Sept. 2007

[16] Lacrampe, N.; Alaeldine, A.; Caignet, F.; Perdriau, R., "Investigation on ESD Transient Immunity of Integrated Circuits," IEEE International Symposium on Electromagnetic Compatibility, 2007 , vol., no., pp.1-5, 9-13 July 2007

[17] Jui-Chu Lee; Young, R.; Liou, J.J.; Croft, G.D.; Bernier, J.C., "An improved experimental setup for electrostatic discharge (ESD) measurements based on transmission line pulsing technique," IEEE Transactions on Instrumentation and Measurement, vol.50, no.6, pp.1808-1814, Dec 2001

[18] Boyer, A.; Bendhia, S.; Sicard, E., "Characterisation of electromagnetic susceptibility of integrated circuits using near-field scan," Electronics Letters , vol.43, no.1, pp.15-16, Jan. 4 2007

[19] Baffreau, S.; Akue-Boulingui, S.; Dupoux, C.; Sicard, E.; Bouvier, N.; Vrignon, B.; Boyer, A., "A new methodology to measure electromagnetic interferences in 3G mobile platform," 2010 Asia-Pacific Symposium on Electromagnetic Compatibility (APEMC), vol., no., pp.1076-1079, 12-16 April 2010

[20] Ramdani, M.; Sicard, E.; Boyer, A.; Ben Dhia, S.; Whalen, J.J.; Hubing, T.H.; Coenen, M.; Wada, O., "The Electromagnetic Compatibility of Integrated Circuits—Past, Present, and Future," Electromagnetic Compatibility, IEEE Transactions on , vol.51, no.1, pp.78-100, Feb. 2009

[21] Tankielun, A.; Garbe, H.; Werner, J., "Calibration of electric probes for post-processing of near-field scanning data," 2006 IEEE International Symposium on Electromagnetic Compatibility, vol.1, no., pp.119-124, 14-18 Aug. 2006

[22] Gieser, H.; Haunschild, M., "Very-fast transmission line pulsing of integrated structures and the charged device model," *Electrical Overstress/Electrostatic Discharge Symposium, 1996. Proceedings* , pp. 85- 94, 10-12 Sept. 1996

[23] Pozzolo, V.; Tenti, P.; Fiori, F.; Spiazzi, G.; and Buso, S., "Susceptibility of integrated circuits to RFI", *Proc. CPES Annu. Semin.*, vol. 1, p.10 , 2002

[24] Camp, M.; Garbe, H.; Nitsch, D., "UWB and EMP susceptibility of modern electronics," *Electromagnetic Compatibility, 2001. EMC. 2001 IEEE International Symposium on* , vol.2, no., pp.1015-1020, 2001

[25] Nitsch, D.; Camp, M.; Sabath, F.; ter Haseborg, J.L.; Garbe, H., "Susceptibility of some electronic equipment to HPEM threats," *Electromagnetic Compatibility, IEEE Transactions on* , vol.46, no.3, pp. 380- 389, Aug. 2004

[26] Zhang, J.; Beetner, D.G.; Moseley, R.; Herrin, S.; Pommerenke, D., "Modelling electromagnetic field coupling from an ESD gun to an IC," *Electromagnetic Compatibility (EMC), 2011 IEEE International Symposium on* , vol., no., pp.553-558, 14-19 Aug. 2011

[27] Aurand, T.; Dawson, J.F.; Robinson, M.P.; Marvin, A.C., "Defining a measure for the immunity of analogue to digital converters exposed to electric fields," *Electromagnetic Compatibility, 2008. EMC 2008. IEEE International Symposium on* , vol., no., pp.1-4, 18-22 Aug. 2008

VITA

Zhen Li was born on June 18th, 1983 in Changsha, China. She completed her Bachelor's degree in English at Hunan University of Commerce in 2005, and her Master's degree in Technical Communication at Missouri University of Science and Technology in May 2009. She joined the Electromagnetic Compatibility Laboratory at the Missouri S&T in 2009 as a graduate research assistant.